Spatial and Temporal Variabilities of Climate Extremes over Canada in a Changing Climate

by

Yang Yang

A thesis submitted in partial fulfillment of the requirements for the degree of

Doctor of Philosophy

in

Water Resources Engineering

Department of Civil and Environmental Engineering
University of Alberta

Abstract

In the past few decades, there have been more extreme climate events occurring worldwide, constituting a growing risk for our societies. For example, Canada has experienced several extreme precipitation events that resulted in billions of dollars of damage, such as the flood events of Calgary and Toronto in 2013. Meanwhile, the 2001–2002 drought in the Canadian Prairies (CP) swept almost the entire southern part of the country, which was recorded as one of the top ten worst droughts observed over the instrumental period.

However, most past studies have focused on changes in the mean climate (such as precipitation and temperature). This dissertation aims to address the spatial and temporal variabilities of climate extremes in Canada under the possible impact of a changing climate, which will improve our understanding of the changing hydroclimate extremes in Canada. Therefore, the objectives of this dissertation are: (1) to characterize spatiotemporal changes of climate extremes under the possible impacts of climate change; (2) to identify how atmospheric convection, temperature, and humidity have contributed to climate extremes; (3) to detect the influences of large-scale climate patterns on climate extremes in Canada.

Chapter 2 investigates the spatial and temporal changes in precipitation extremes over Canada, as well as their teleconnections to large-scale climate patterns by using trend analysis, principal component analysis, and wavelet analysis. The results show that extreme precipitation defined from 10 extreme precipitation indices of Canada has generally become more severe since the mid-twentieth century. Meanwhile, strong teleconnections are found between extreme precipitation and climate indices, but the effects of climate patterns differ from region to region.

Chapter 3 analyses the relationship between Convective Available Potential Energy (CAPE) and extreme precipitation event, which indicates a positive correlation over much of the eastern US and some parts of the Canadian prairies. In addition, increasing temperature and surface specific humidity could potentially lead to an overall increase in CAPE and extreme precipitation observed over these regions.

Chapter 4 studies the variations in drought characteristics in terms of duration, frequency, area, and severity in Canada using the Standardized Precipitation Evapotranspiration Index (SPEI) at seasonal and annual time scales. The results suggest that droughts in Canada have generally become less severe over 1950-2016, and the relationships between climate patterns and drought variability have changed over time.

Chapter 5 evaluates the non-stationary behavior of dry and wet spells in Canada using the generalized extreme value (GEV) distribution and Bayesian quantile regression. This analysis shows that dry spells have aggravated in the southern Canadian Prairie from 1979 to 2018, and the stationarity has been compromised as more grids are found to be non-stationary under the impacts of El Niño–Southern Oscillation (ENSO) and Pacific-North American pattern (PNA).

Conclusions and future research are provided in Chapter 6.

Preface

This thesis is based on four major chapters, and it is organized in an article format: each chapter is written as an integrated paper with independent introduction and conclusion.

Chapter 2 of the thesis has been published as Yang, Y., Gan, T.Y., Tan, X., 2019. Spatiotemporal changes in precipitation extremes over Canada and their teleconnections to large-scale climate patterns. J. Hydrometeorol. 275–296. https://doi.org/10.1175/jhm-d-18-0004.1 (©American Meteorological Society, used with permission). Chapter 4 has been submitted to Atmospheric research, and we have just submitted our revised manuscript to the journal (Yang, Y., Gan, T.Y., Tan, X.). The work on Chapter 3 has been submitted to the International Journal of Climatology and is currently under review, and it was accomplished principally in collaboration with Dr. Mesgana Seyoum Gizaw from Golder Associates. For the work done in Chapter 2, 4, and 5, I was responsible for the design of the research topic, data collection, data analysis, and the manuscript composition. In addition, I am planning to submit the work on Chapter 5 (Yang, Y., Gan, T.Y., Tan, X.) to a scientific journal.

An aggregated bibliography is provided for the entire thesis to avoid reference repetition.

Dedication

This thesis is dedicated to my wife (Lea Wang) who has always been a constant source of support and encouragement during the challenges of my Ph.D. study. This work is also dedicated to my parents, parents-in-law, brother, and sister who have always loved me unconditionally.

Acknowledgments

First, I would like to express my sincere gratitude to my supervisor Professor Thian Yew Gan for his continuous support and encouragement of my Ph.D. research, for his patience, motivation, and immense knowledge. His guidance helped me in all the time of research and writing of this thesis. My sincere thanks also go to Dr. Amin Elshorbagy, Dr. Daniel S. Alessi, Dr. Yuntong She, Dr. Jeff Birchall, Dr. Wenming Zhang, Dr. Debra Davidson, and Dr. Yang Liu for their valuable comments and suggestions.

I am grateful to all my friends and fellow graduate students in the Water Resources Engineering group for their support throughout my stay in Canada. Last but not least, I would like to acknowledge the China Scholarship Council (CSC), the University of Alberta, and the Alberta Innovates for financial assistance throughout the course of my research.

Table of Contents

List of Tables

List of Figures

List of Abbreviations

20CRv2	Twentieth century reanalysis
ACP2	Adjusted Daily Precipitation dataset
AHCCD	Adjusted and Homogenized Canadian Climate Dataset
AIC	Akaike information criterion
AMO	Atlantic Multi-decadal Oscillation
AO	Arctic Oscillation
AP	Apparent temperature
AR5	Fifth assessment report
BDL	Bayesian dynamic linear model
BM	Block maxima method
BSTQR	Bayesian spatiotemporal quantile model
CAPE	Convective available potential energy
C-C	Clausius-Clapeyron equation
CDD	Consecutive dry days
CMI	Crop moisture index
COI	Cone of influence
CP	Canadian Prairies
CPC	Climate Prediction Center
CRCM	Canadian Regional Climate Model
CRU	Climatic Research Unit
CWD	Consecutive wet days
DA	Drought area

DD	Drought duration
DF	Drought frequency
DS	Drought severity
DSD	Dry spell duration
DSN	Number of dry spells
ENSO	El Niño–Southern Oscillation
EOF	Empirical orthogonal function
ETCCDI	Expert Team on Climate Change Detection and Indices
FDR	False discovery rate
GCMs	General circulation models
GEV	Generalized extreme value distribution
GHCN	Global Historical Climatology Network
GLM	Generalized linear model
IDF	Intensity-Duration-Frequency curves
IPCC	Intergovernmental Panel on Climate Change
IVT	Integrated water vapor transport
KS	Kolmogorov-Smirnov test
LSMPs	Large-scale meteorological patterns
MEI	Multivariate ENSO index
MK	Mann-Kendall
MLE	Maximum likelihood estimation
NA	North America
NAO	North Atlantic Oscillation

NARR	North America Regional Reanalysis
NCEP	National Center for Environmental Prediction
NLDAS-2	North American Land Data Assimilation System-phase 2
NOAA	National Oceanic and Atmospheric Administration
NPGO	North Pacific Gyre Oscillation
PC	Principal component
PCA	Principal component analysis
PDF	Probability distribution function
PDO	Pacific Decadal Oscillation
PDSI	Palmer drought severity index
PET	Potential evapotranspiration
PNA	Pacific-North American
RCP	Representative concentration pathway
RDI	Reconnaissance drought index
sc_PDSI	Self-calibrating PDSI
SPEI	Standardized precipitation evapotranspiration index
SPI	Standardized precipitation index
SSH	Sea surface height
SST	Sea surface temperature
SVD	Singular value decomposition
SYR	Synthesis report
US	The United States
WMO	World Meteorological Organization

WSD	Wet spell duration
WSN	Number of wet spells
WSVI	Water surplus variability index
WTC	Wavelet transform coherence

Chapter 1. Introduction

1.1 Background and Problem Statement

In recent decades, climate change is one of the most significant, global-scale challenge to mankind in the 21st century given climatic extremes such as floods and droughts have been occurring more frequently and in greater severity across the world, resulting in significant impacts to both our society and the natural environment. The recent assessment and special report of the Intergovernmental Panel on Climate Change (IPCC) affirmed that the radiative forcing of rising concentration of greenhouse gases such as CO_2, methane, and nitrous oxide due to anthropogenic activities have caused the earth to warm by about 1°C above pre-industrial levels (with a range between 0.8°C and 1.2°C) globally since the beginning of the twentieth century. Further, according to the climate projections of climate models, under the current warming trend, global warming is likely to reach by 1.5°C in 2030-2052 (IPCC, 2018).

Our climate has been changing, especially climatic extremes which are expected to become more severe with more significant impacts over the 21st century (Easterling, 2000). Rising temperature at a global scale is likely to affect the global water cycle with major consequences, and sea level rise due to worldwide melting of sea ice and glaciers. According to the Clausius-Clapeyron equation, the water-holding capacity of the atmosphere will increase at about 7% per K in temperature, which could increase the occurrences of precipitation extremes (Allan and Soden, 2008). Therefore, as the atmospheric water holding capacity increases with rising temperature, a warmer world is expected to experience more extreme rainfall events, as has been observed in many parts of the worldwide in recent decades (Hansen et al., 2012). For example, the increase in the frequency or intensity of precipitation extremes have also been reported in southern China

(Zhai et al., 2005), Japan (Duan et al., 2015), Denmark (Gregersen et al., 2013), Sweden (Gregersen et al., 2015), the United States (Dhakal and Tharu, 2018; Huang et al., 2017), and Brazil (Zilli et al., 2017).

Canada has also been impacted by several extreme precipitation events which resulted in billions of dollars of damage, such as the flood events of Calgary and Toronto in 2013 which, as the respective worst natural disaster of Alberta and Ontario, are also ranked the first and the third largest natural insured disasters in the Canadian history, respectively (Milrad et al., 2015; X. Wang et al., 2014). In southern Alberta of Canada, Gizaw and Gan (2016) projected an overall increase in its future extreme precipitation in the mid and late 21st century, while Kunkel et al. (1999) detected increasing trends in extreme precipitation of 1-7 day durations over 1951-1993 in Canada.

In addition to extreme precipitation, drought is another form of climatic extreme due to a prolonged period of abnormally dry weather, often resulting in severe water shortages and acute hydrological imbalance (Pachauri et al., 2014). Even though increased heating due to global warming may not directly cause droughts, it is expected that when droughts occur they tend to be more intensive (Trenberth et al., 2014), and the warming-induced drying from increased evaporation will likely be the largest over northern mid-high regions (Dai, 2011a). For example, the severe drought across northern China in 1997 resulted in 226 days of zero flow in the lower reach of the Yellow River (Cong et al., 2009), and another drought in 2000 damaged more than 40 million hectares of crops (Yu et al., 2014). From the trend analysis, Joshi *et al.* (2016) found that the occurrence of droughts had increased significantly in northeastern and central India over the second half of the 20th century. In Mexico, Escalante-Sandoval and Nuñez-Garcia (2017) projected that under RCP 4.5

and 8.5 climate scenarios of IPCC (2013), the duration and intensity of droughts would increase significantly. Meanwhile, an analysis of the spatial and temporal characteristics of droughts in the continental United States (US) also revealed that drought duration, severity, and intensity have increased in the western and eastern US over the past century (Ge et al., 2016). On the whole, the global percentage of dry areas has increased by about 1.74% per decade over 1950-2008 (Dai, 2011a).

In Canada, droughts have been identified as one of the most damaging natural disasters with enormous impacts on agriculture, industry, municipal services, and human health, among other sectors. The 2001–2002 drought in the Canadian Prairies (CP) that almost affected the entire southern part of Canada, was one of the top ten worst droughts observed over the instrumental period (Bonsal and Regier, 2007). In Alberta, crop producers lost $413 million and $1.33 billion in 2001 and 2002, respectively, while the estimated reduction in crop production in Saskatchewan accounted for losses of $925 million and $1.49 billion in 2001 and 2002, respectively (Wheaton et al., 2008). Furthermore, the spring and summer drought of 2015 was noted for its severity, extent, and impacts. Large areas in southern British Columbia were assigned with the highest drought rating, and the Alberta government designated the province as an Agricultural Disaster Area (Szeto et al., 2016). Moreover, the extreme dry and warm conditions led to one of the most active and persistent wildfire seasons for western Canada, while some rivers experienced their lowest historic flow levels in 100 years (CMOS, 2016). Therefore, as the climate continues to change, the risks and losses coupled with climate extremes could lead to greater impacts.

1.2 Research Objectives

Most previous studies on the extreme precipitation in Canada have either used the generalized extreme value distribution (GEV), or they have only focused on some regions in Canada. Given the positive correlation between convective available potential energy (CAPE), sea surface temperature (SST), and specific humidity (Riemann-Campe et al., 2009; Seeley and Romps, 2015), we would anticipate an increase in CAPE values and precipitation extremes due to the observed and projected warming for the 21st century. Although large-scale climate drivers have been teleconnected to seasonal precipitation in Canada (e.g., Gan et al. (2007)), their influences on precipitation extremes have not received much attention and thus require further investigation.

Studies have been conducted regarding droughts in the CP, but so far limited research has been conducted to investigate drought characteristics across Canada, especially the dynamic and time-varying relationships between large-scale climate signals and Canadian drought characters. In addition, most past studies are based on monthly precipitation; however, relying only on the monthly precipitation amount or frequency can sometimes lead to misleading conclusions. Furthermore, few previous studies have systematically and simultaneously examined dry and wet spell characteristics and performed a comprehensive evaluation with sufficiently long daily precipitation in Canada.

Given the recent extreme climatic events that had incurred significant impacts to both the Canadian government and the general public, the key objective of this thesis is to address the spatial and temporal variabilities of climate extremes in Canada under the impacts of a changing climate. The results of this study can provide a better understanding of the dynamics of climate extremes in

Canada, which is essential for policymakers and practitioners to improve risk management and to implement mitigation strategies.

The objectives of this research are:

(1) To characterize spatiotemporal changes of climate extremes under the possible impacts of climate change;

(2) To identify how atmospheric convection, temperature, and humidity have contributed to climate extremes;

(3) To detect the influences of large-scale climate patterns on climate extremes in Canada.

1.3 Organization of Thesis

The Thesis is organized into six chapters. The background information, problem statement, and research objectives are presented in Chapter 1; the spatial and temporal changes in precipitation extremes over Canada and their teleconnections to large-scale climate patterns in Chapter 2; changes to the summer Convective Available Potential Energy and extreme precipitation of southern Canada and the United States in Chapter 3; the variations of drought characteristics and their dynamic drivers in Chapter 4; and how dry and wet spell characteristics have altered in Canada in Chapter 5. Finally, the overall summary of conclusions and recommendations to future work to variabilities of climate extremes over Canada are given in Chapter 6.

Chapter 2. Spatiotemporal Changes in Precipitation Extremes over Canada and Their Teleconnections to Large-scale Climate Patterns

2.1 Introduction

In recent decades, hydrologic extremes such as floods and droughts have caused more public attention because they have been occurring more frequently and in greater severity worldwide (Easterling et al., 2000; Costa and Soares, 2009; Wang et al., 2014; Chen et al., 2015; Elewa et al., 2016; Zilli et al., 2016). As the Earth warms, a higher temperature likely means that more precipitation will fall over shorter time intervals, thus increasing the frequency and severity of extreme storm events, which could incur significant damage and severe hardship to our society and natural systems (L. Gao et al., 2017; Zhang et al., 2011). Conversely, because of the global warming impact, droughts in semi-arid/arid regions of Africa have worsened in recent years (Gan et al., 2016). A brief review of some related studies is presented below.

Climatic extremes can have devastating impacts on our societies (Hales et al., 2003; Mass et al., 2011). For example, Canada has experienced several climate extremes which resulted in billions of dollars of damage, such as the extreme precipitation events of Calgary and Toronto in 2013 which, as the respective worst natural disaster of Alberta and Ontario, are also ranked the first and the third largest natural insured disasters in Canada, respectively (Milrad et al., 2015; X. Wang et al., 2014). In southern Alberta, Canada, Gizaw and Gan (2016) projected an overall increase in its future extreme precipitation in the mid and late 21st century, while Kunkel et al. (1999) detected increasing trends in extreme precipitation of 1-7 day duration over 1951-1993 in Canada. Meanwhile, the increase in the frequency or intensity of precipitation extremes have also been observed in southern China (Zhai et al., 2005), Japan (Duan et al., 2015), Denmark (Gregersen et

al., 2013), Sweden (Gregersen et al., 2015), the United States (Dhakal and Tharu, 2018; Huang et al., 2017), and Brazil (Zilli et al., 2017).

Flooding may cause an outbreak of cholera, typhoid, and diarrhoeal disease because of environmental pollution resulted from floodwater mixed with human and animal waste. On the other hand, droughts that reduce the amount of water available for sanitation can increase the risk of diseases such as malaria and dengue fever (Hales et al., 2003). Other than damage and hardships caused by floods and famines by droughts, extreme climate events can also have significant impacts on human health. Li et al. (2018) have shown that human perceived temperature or apparent temperature (AP) has increased faster than air temperature over land, and the summer increase in AP-based thermal discomfort is expected to outpace the winter decrease in AP-based thermal discomfort.

Global warming could increase occurrences of precipitation extremes (Allan and Soden, 2008) since according to the Clausius-Clapeyron equation, the water-holding capacity of the atmosphere will increase at about 7% per K in temperature. According to the Synthesis Report (SYR) of the IPCC Fifth Assessment Report (AR5), the surface temperature is projected to increase over the 21st century under all Representative Concentration Pathway (RCP) emission scenarios of IPCC (2013), and extreme precipitation events are projected to become more intensive and frequent in many regions across the world (Pachauri et al., 2014). Located in high-latitude areas, warming and extreme precipitation in Canada are expected to be more pronounced (Lemmen and Warren, 2004; Bush et al., 2014; Fischer and Knutti, 2016). From 1948 to 2012, the air temperature has increased

in most parts of Canada, with the largest warming in winter and spring, and precipitation has also increased, especially in northern Canada (Jiang et al., 2015; Vincent et al., 2015).

Among various climate indices used for research in extreme climate, 27 indices developed by the Expert Team on Climate Change Detection and Indices (ETCCDI, http://etccdi.pacificclimate.org/) have been relatively popular, for they are designed to provide scientifically robust measures of the characteristics of precipitation and temperature, two most important daily climate variables (Zhang et al., 2011), e.g., Miao et al. (2015) and Jiang et al. (2017) used ETCCDI indices to study changing behaviors of precipitation extremes in China.

Past studies on the extreme precipitation in Canada have either used probability distributions such as the generalized extreme value distribution (GEV) (Simonovic et al., 2016; Tan and Gan, 2017), or they have only focused on extreme precipitation of some parts of Canada (Benyahya et al., 2014; Wang et al., 2015). Even though large-scale climate patterns have been teleconnected to precipitation in some parts of Canada (e.g., Gan et al. (2007)), their influences on precipitation extremes have not received much attention and thus require further investigations (Xi et al., 2018; Zhang et al., 2001). Using teleconnection patterns PDO, PNA, and AO as covariates, Asong et al. (2016) built a Generalized Linear Model (GLM) to model seasonal precipitation, temperature, and their extremes in the CP. Based on the Bayesian spatiotemporal quantile (BSTQR) model, Tan et al. (2018a) examined the effects of large-scale climate patterns on Canadian winter precipitation at different quantile levels. They found that the teleconnections of Canadian winter precipitation to climate patterns are stronger at higher than at medium quantiles, implying that large-scale climate patterns likely exert a stronger influence on precipitation extremes.

The primary objectives of this study are: (1) to analyze spatiotemporal changes of historical extreme precipitation over Canada using ten extreme precipitation indices; and (2) to find the influence of large-scale climate patterns on precipitation extremes of Canada. The results of this study will provide a more comprehensive understanding of precipitation extremes and their observed changes in Canada. The datasets are described in Section 2.2, the research methodology in Section 2.3, results and discussions in Sections 2.4, and conclusions in Section 2.5.

2.2 Datasets

2.2.1 Precipitation Time Series

Among 464 stations of daily precipitation data given in the second generation, Adjusted Daily Precipitation dataset (ACP2) for Canada (Mekis and Vincent, 2011), 164 stations across Canada (Figure 2.1) which met the following requirements were selected in this study. The station should have data over the 1950 to 2012 period, and it should have no more than 2 consecutive years of missing values. ACP2 is part of the Adjusted and Homogenized Canadian Climate Dataset (AHCCD), and it is the most homogeneous long-term observed daily precipitation data currently available for Canada (Tan and Gan, 2017). Among the 164 stations selected, only few stations are located in northern Canada. More details about the adjustments and quality control including wind undercatch, evaporation and wetting losses, and trace observation of the dataset have been extensively discussed by Mekis and Vincent (2011).

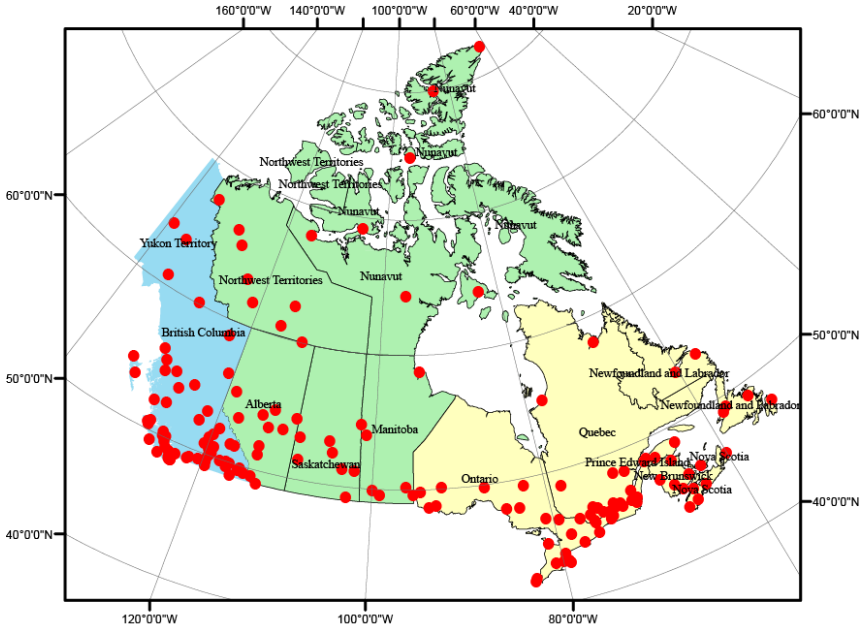

Figure 2.1 Study area and meteorological stations. Abbreviations: Alberta (AB), Saskatchewan (SK), Manitoba (MB), Newfoundland and Labrador (NL), Prince Edward Island (PE), Nova Scotia (NS), Northwest Territories (NT), Nunavut (NU), Ontario (ON), New Brunswick (NB), Yukon Territory (YT), British Columbia (BC), Quebec (QC).

2.2.2 Extreme Precipitation Indices

Out of 27 indices recommended by ETCCDI, we have adopted ten extreme precipitation indices grouped into two types to analyze extreme precipitation data of Canada and made the results comparable internationally (Fu et al., 2014; Lovino et al., 2018; Wang et al., 2013): (1) precipitation amount or intensity, which includes PRCPTOT, SDII, R95p, R99p, Rx1day, and Rx5day; and (2) number of days exceeding certain thresholds in rainfall depth, which are CDD, CWD, R10mm, and R20mm. The definitions and units of these indices in mm, mm/day and days, respectively are described in Table 2.1.

Table 2.1 Definitions of extreme precipitation indices

Index	Definition	Unit
Rx1day	Monthly maximum 1-day precipitation	mm
Rx5day	Monthly maximum consecutive 5-day precipitation	mm
R95p	Annual total precipitation when daily precipitation > 95p	mm
R99p	Annual total precipitation when daily precipitation > 99p	mm
PRCPTOT	Annual total precipitation in wet days (daily precipitation≥1mm)	mm
SDII	Simple precipitation intensity index	mm/day
R10mm	Annual count of days when daily precipitation≥10mm	Day
R20mm	Annual count of days when daily precipitation≥20mm	Day
CDD	Max number of consecutive days with daily precipitation < 1mm	Day
CWD	Max number of consecutive days with daily precipitation≥1mm	Day

2.2.3 Climate Indices

We have selected certain large-scale climate patterns that have contributed to the precipitation variability over Canada (Coulibaly, 2006), such as North Atlantic Oscillation (NAO), Pacific-North American (PNA), North Pacific Gyre Oscillation (NPGO), Pacific Decadal Oscillation (PDO), and El Niño–Southern Oscillation (ENSO). ENSO likely has the most significant inter-annual climate variability and influence on the climate of Northern Hemisphere (Rasmusson and Wallace, 1983), including Africa (e.g., Ntale and Gan, 2004). The Multivariate ENSO Index (MEI) is selected to represent ENSO.

PDO is the leading principal component (PC1) of North Pacific (poleward of 20N) monthly sea surface temperature anomalies since 1900 (Mantua and Hare, 2002). The warm and cold phases of PDO has an influence on the precipitation of North America. For example, winter precipitation in

the western United States (Brown and Comrie, 2004) and western Canada have been found to be affected by PDO (Gan et al., 2007). PNA depicts a quadripole of 500 millibar geopotential height anomalies, with opposite anomalies centered over Hawaii and central Canada, and with similar signals over the south of Aleutian Islands and southeastern USA (ncdc.noaa.gov/teleconnections/pna/). It is one of the most significant modes of low-frequency variability in the extra Tropics of Northern Hemisphere throughout the year except June and July.

NAO represents the climate variability from the east coast of the United States to Siberia, and from the Arctic to the subtropical Atlantic (Hurrell et al., 2001). It is characterized by changes in surface pressure, and it is one of the dominant and prevailing modes of atmospheric behavior in North Atlantic (Hurrell et al., 2001; Coulibaly, 2006). NPGO is the second dominant mode of sea surface height (SSH) variability in the Northeast Pacific correlated with fluctuations of salinity, nutrients, and chlorophyll in the California Current and Gulf of Alaska. It indicates changes in the intensity of central and eastern North Pacific gyre circulations, and it is driven by upwelling and horizontal advection (Di Lorenzo et al., 2008).

MEI is the first un-rotated principal component of six atmosphere-ocean variables over the tropical Pacific: sea-level pressure, zonal and meridional components of the surface wind, sea surface temperature, surface air temperature, and total cloudiness fraction of the sky over the tropical Pacific. It gives a more comprehensive description of the ENSO event than traditional ENSO indices, Nino3 and SOI (Wolter and Timlin, 2011, 1998, 1993).

2.2.4 Convective Available Potential Energy and Specific Humidity

Convective Available Potential Energy (CAPE), a proxy for weather conditions amenable for the occurrence of extreme precipitation events, is the vertical integral of parcel buoyancy between the level of free convection and the level of neutral buoyancy (Ye et al., 1998). CAPE (Joule/kg) has been widely used to measure the onset of convection given high CAPE values represent favorable conditions for the occurrence of severe convective storms and tornado events (Brooks et al., 2007; Dong et al., 2018; Kishtawal et al., 2010; Monkam, 2002; Seeley and Romps, 2015). We used monthly CAPE data of the Twentieth Century Reanalysis (20CRv2) of National Oceanic & Atmospheric Administration (https://www.esrl.noaa.gov/psd/data/gridded/data.20thC_ReanV2.html), which is an international project aimed at producing a high-quality global atmospheric circulation dataset (Compo et al., 2011). The dataset covers from 1871 to 2012, and it is available at 2˚ spatial resolution. Comparisons with satellite data and other reanalysis data show that 20CR is generally of high quality (Compo et al., 2011). Using the CAPE data from 20CR, Krichak et al. (2015) found that heavy precipitating events are associated with an intense intrusion of humid tropical air and the presence of high CAPE values in the Mediterranean region. Further, given precipitation is also related to air temperature and humidity, monthly temperature, and specific humidity, these data were also analyzed in this study.

2.3 Research Methodology

2.3.1 Trend Analysis

The non-parametric Mann-Kendall (MK) trend test (Mann, 1945; Kendall, 1955) recommended by the World Meteorological Organization (WMO) was used for the trend analysis of the precipitation data. The null hypothesis (H_0) is that the data are independent and randomly

distributed, while the alternative hypothesis (H_1) is that a monotonic trend exists (Song et al., 2015). The MK method has been widely used in the trend analysis of hydrologic and climate data (Shadmani et al., 2011; Frazier and Giambelluca, 2016; Pedron et al., 2016). However, the presence of autocorrelation in a time series can affect the detection of trends in the time series. Hamed and Rao (1998) proposed subtracting a non-parametric trend estimator from the original time series to account for the autocorrelation, and a detailed calculation procedure was given by Daufresne et al. (2009). The modified MK test was then applied to the time series of all indices listed in Table 2.1, and trend magnitudes were estimated using the non-parametric Sen's slope estimator (Sen, 1968).

2.3.2 Field Significance and False Discovery Rate

Statistically, an individual test performed at a given significance level α has a α chance of falsely rejecting the null hypothesis. When conducting multiple tests simultaneously on data that are spatially correlated, it is necessary to adjust α to avoid falsely rejecting a large number of the null hypothesis (Ventura et al., 2004). In view of a large number of stations selected in the study, it is necessary to consider the field significance statistically in relation to multiple tests. Here the false discovery rate (FDR) method which controls the expected percentage of falsely rejected null hypotheses is employed to identify the significance of tests conducted in this study (Benjamini and Hochberg, 1995). We applied the FDR method by using the "p.adjust" function in the R language (R Core Team, 2017).

2.3.3 Principal Component Analysis

Principal component analysis (PCA) is a statistical method to reduce the dimensionality of a multivariate time series to several orthogonal principal components (PCs) that explain a large percentage of the variability in the time series (Jolliffe, 2002). For R95p and R99p indices analyzed in this study, the first two leading PCs account for more than 30% of the total variance. Following Cioffi et al. (2015) and for brevity, the leading PC1s are used for subsequent analysis of the time series of R95p and R99p.

2.3.4 Wavelet Analysis

Wavelet transform is an effective tool designed to transform a time series into time and frequency domains simultaneously, revealing temporal and frequency changes of the dominant oscillations of the time series (Torrence and Compo, 1998). Compared to the traditional Fourier transform, wavelet transform is well known for its ability to analyze nonstationary time series (Cazelles et al., 2008), which is particularly useful for climate series that exhibits nonstationary behaviors (Chang et al., 2015; Tan and Gan, 2017).

Another important application of wavelet transform is the wavelet transform coherence (WTC) between two time series, defined as the square of their cross-spectrum normalized by the power spectrum of each time series, which gives us their cross-correlation (between 0 and 1) as a function of frequency (Torrence and Compo, 1998). Wavelet analysis has been extensively used in climate research (Gan et al., 2007; Mwale et al., 2009; Jiang et al., 2014; Okonkwo, 2014). Herein we chose the Morlet wavelet as the mother wavelet because it finds a delicate balance between time and frequency localizations (Grinsted et al., 2004). It should be noted that since we are dealing

with finite-length time series, zeros are padded at the ends of the time series to reduce the edge effects (Torrence and Compo, 1998), and so the wavelet power beyond the cone of influence (COI) should be explained with caution (Gan et al., 2007).

2.4 Results and Discussion

2.4.1 Changes in Extreme Precipitation Amount/Intensity

To present overall changes to extreme precipitation of Canada in 1950-2012, Figure 2.2 shows the average annual time series of Canada for all indices, while Table 2.2 shows the number of individual stations detected with positive or negative trends for the indices analyzed in this study. Overall, in these indices, positive trends dominate over negative trends, which means that extreme precipitation over Canada shows more increasing than decreasing trends in the study period.

Over 1950-2012, both the average time series of RX1day (Figure 2(a)) and RX5day (Figure 2 (b)) of Canada show statistically significant increasing trends at 0.34 and 0.90 mm/decade, respectively. Figures 2(c) and (d) show that the average time series of R95p and R99p also show significant positive trends at 3.13 and 1.52 mm/decade, respectively. However, for individual stations, R99p trends ranged from -8.77 to 21.06 mm/decade (Table 2.2). As for the average time series of PRCPTOT, the trend of 9.44 mm/decade is statistically significant, while the average SDII time series of Canada has a non-significant negative trend.

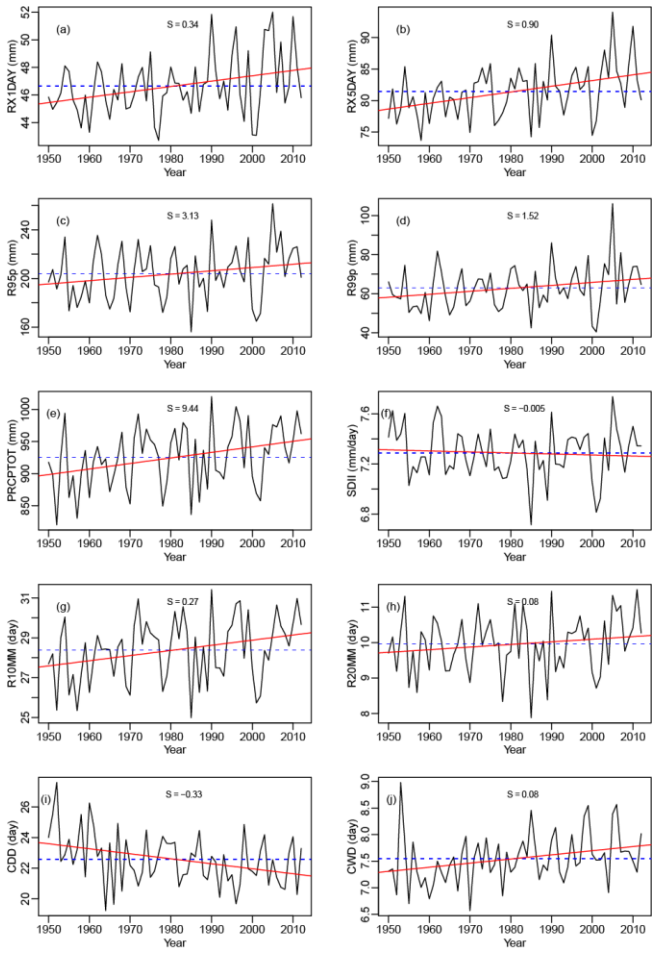

Figure 2.2 Annual series of extreme precipitation indices from 1950 to 2012. The red line is the linear trend; The blue dashed line is the mean. S is the trend per decade by Sen's slope.

There are more stations showing positive than negative trends for RX1day and RX5day (respectively 102 and 107 versus 60 and 55), but only about 10% of positive trends are statistically significant, which agrees with Shephard et al. (2014) who also reported a general lack of significant trend signals. By contrast, no station has shown a significant negative trend in either index. A comparable number of stations show positive and negative trends in R95p and R99p (respectively 108 and 103 versus 54 and 60), but for R99p only 2 stations show statistically significant positive trends. Additionally, a comparable number of stations show positive and negative trends in SDII (88 versus 76), but more positive than negative trends are statistically significant (20 versus 9).

Spatial patterns of these results are presented in Figure 2.3. Generally, stations with positive extreme precipitation amount/intensity trend were located along the southern border of Canada while trends that are more negative are found in the central Canadian Prairies (CP): British Columbia (BC), Alberta (AB), Saskatchewan (SK), and Manitoba (MB). Meanwhile, positive trends dominate the northern part of Canada.

Table 2.2 Trends per decade and number of stations showing positive or negative trends of extreme precipitation indices during 1950-2012

Index	Regional trends (unit/decade)	Range	Positive trend	Significant positive trend	Negative trend	Significant negative trend
Rx1day	**0.34**	-3.19 to 3.46	102	9	60	0
Rx5day	**0.90**	-3.93 to 8.95	107	10	55	0
R95p	**3.13**	-38.25 to 50.91	108	10	54	3
R99p	**1.52**	-8.77 to 21.06	103	2	60	0
PRCPTOT	**9.44**	-65.92 to 89.47	117	32	47	3
SDII	-0.005	-0.54 to 0.34	88	20	76	9
R10mm	**0.27**	-2.67 to 2.63	107	27	56	9
R20mm	0.08	-1.71 to 1.32	101	10	63	7
CDD	**-0.33**	-5.00 to 2.08	62	0	101	3
CWD	**0.08**	-0.77 to 1.25	114	16	50	2

Annual trends that are statistically significant at the 0.05 level are in bold.

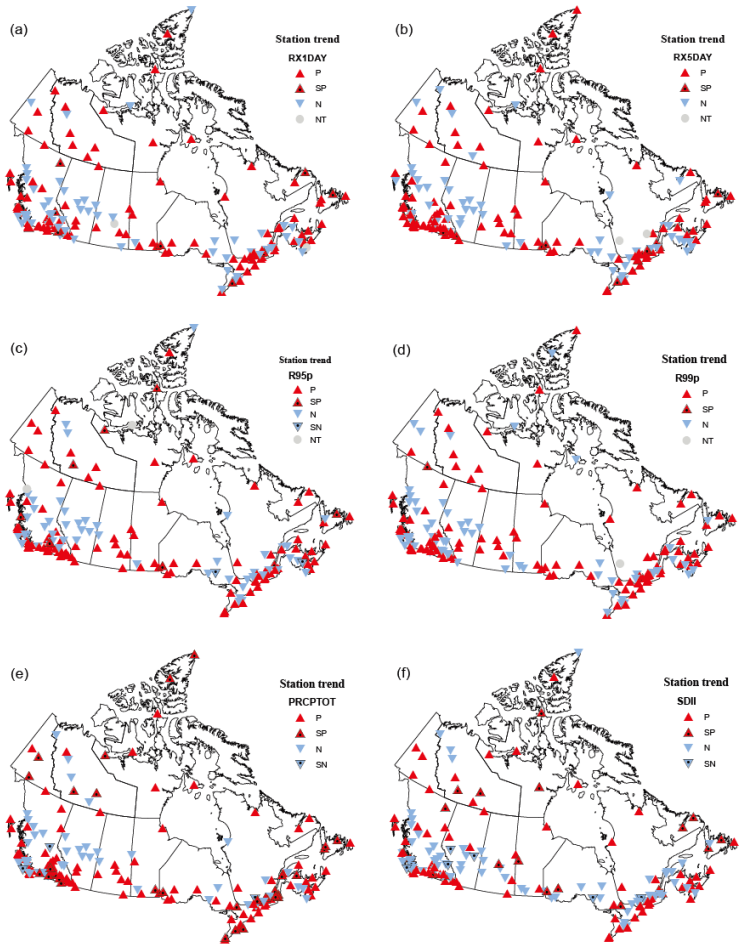

Figure 2.3 Spatial patterns of trends for extreme precipitation amount/intensity indices from 1950 to 2012. The abbreviations are P: positive trend, SP: significant positive trend, N: negative trend, SN: significant negative trend and NT: no trend.

2.4.2 Changes in Number of Days with Extreme Precipitation

About twice as many stations show positive than negative trends in R10mm and R20mm (number of days ≥ 10 and 20mm of precipitation per day, respectively), and more positive trends are statistically significant especially for R10mm (27 versus 9). Therefore, out of 164 stations of R10mm data of Canada analyzed, the average trend estimated was about 0.27 day/decade. For R20mm, a comparable number of negative and positive trends are significant which over 1950 to 2012 range from -1.71 to 1.32 day/decade. It is noted that more stations show negative trends in

Consecutive Dry Days (CDD) than in Consecutive Wet Days (CWD) (101 versus 50), but the reverse number of positive trends between CDD and CWD (62 versus 114). However, most of the detected trends are not statistically significant except for positive trends in CWD. The trend magnitude for the average CDD time series (-0.33 day/decade) is much higher than that of the average CWD time series (0.08 day/decade). The overall results obtained for the above 10 indices show that from 1950 to 2012, Canada has generally become wetter, which is what we would expect from increasing atmospheric moisture as the global climate has become warmer since the mid-20th century.

Figure 2.4 shows spatial distributions of trends for extreme precipitation indices, R10mm, R20mm, CWD, and CDD across Canada, of which the first three indices display analogous spatial distributions with the indices Rx1day, Rx5day, R95p, R99p, SDII, and PRCPTOP discussed in Section 4.1. However, CDD displays a different spatial distribution: negative trends dominated in the north and a mixed pattern in the south, which again shows that Canada had generally become wetter since the 1950s especially in the North.

We have detected decreasing trends in the annual SDII and CDD over Canada and more increasing trend in days with heavy precipitation (R10mm) in 1950–2003, similar to the results of Vincent and Mekis (2006). One consequence of this change could be an increased frequency and severity of flash floods (Limsakul and Singhruck, 2016). From analyzing changes in global precipitation extremes using ETCCDI indices, Alexander et al. (2006) also found a widespread and significant increase in precipitation extremes. Wang et al. (2015) detected decreasing heavy rainfall intensities in eastern and southern Ontario, which is similar to the decreasing SDII of southern Ontario in

Figure 2.3(f). However, using a regional climate model, Wang et al. (2014) projected both the intensity and frequency of extreme rainfall of Ontario would likely increase in the future. Even though hydrologic extremes are generally expected to become more severe in North America (Kunkel, 2003), locally possible changes to future extreme precipitation remain uncertain because of many possible factors involved, such as moisture availability, thermodynamic instability (warming near the surface and cooling in the upper troposphere), effects of large-scale atmospheric circulations, terrain features, and others.

Spatially, these extreme precipitation indices exhibit a mixture of increasing and decreasing trends across Canada in 1950-2012, which is consistent with the relatively low spatial coherence of extreme precipitation shown by Vincent and Mekis (2006). However, other than CDD, all indices exhibit more increasing than decreasing trends in southern Canada, except in central CP where decreasing trends are more dominant. Zhang et al. (2001) found that albeit the temporal distribution of the number of heavy precipitation events in Canada is spatially coherent, it varies considerably between seasons and regions. Tan and Gan (2017) who analyzed the non-stationarity of heavy precipitation events of Canada concluded that stations with increasing trends are mostly located in the southwest and in Quebec while more decreasing trends are detected in the CP.

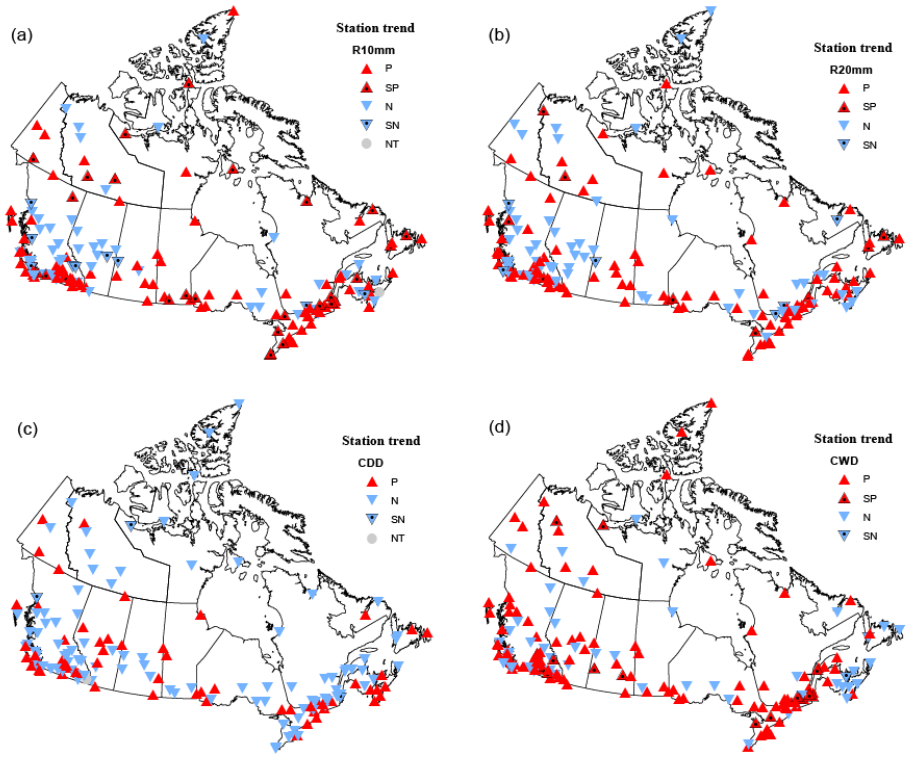

Figure 2.4 Spatial patterns of trends for extreme precipitation day indices from 1950 to 2012. The abbreviations are the same as Figure 2.3.

2.4.3 Relationship between extreme precipitation indices and annual precipitation

To examine if extreme precipitation indices are good indicators of the annual precipitation, their relationships are estimated using the Spearman's rank correlation rho (Spearman, 1904). As Table 2.3 shows, all indices are significantly correlated to the annual precipitation, especially for R95p, PRCPTOT, R10mm, and R20mm whose Spearman rank correlation coefficients exceeded 0.80. CDD is the only index negatively correlated to the annual precipitation, which is expected because CDD represents the number of consecutive dry days. The result demonstrates that these 10 extreme precipitation indices can adequately reflect changes in the annual precipitation of Canada.

Table 2.3 Correlation coefficients between extreme precipitation indices and annual precipitation

	Rx1day	Rx5day	R95p	R99p	PRCPTOT	SDII	R10mm	R20mm	CDD	CWD
AP	**0.571**	**0.657**	**0.847**	**0.723**	**0.989**	**0.583**	**0.946**	**0.832**	**-0.448**	**0.398**

AP stands for annual precipitation. Coefficients that are statistically significant at the 0.05 level are in bold.

2.4.4 Probability Distribution Functions (PDF)

To investigate the temporal variation in extreme precipitation further, all indices were divided into three 20-year sub-periods: 1950-1970, 1971-1991, and 1992-2012 (Figure 2.5). Based on results obtained from the Kolmogorov-Smirnov test, it is noted that distributions of RX5day, PRCPTOT, R10mm, CDD, and CWD of sub-period 1 are statistically different from that of sub-period 3, suggesting a shift in these extreme precipitation indices. Generally, all indices except CDD, tend to shift to the right from sub-periods 1 to 2 and to 3, which demonstrates that probabilistically, extreme precipitation of Canada has been increasing in severity and frequency since the mid-twentieth century. For example, R10mm was less than 32 days in 1950-1970, but it exceeded 32 days in 1971-1991 and 1992-2012.

Moreover, from PDFs of RX1day, RX5day, R99p, PRCPTOT, and R10mm, it seems that the probability of occurrence of moderate extreme precipitation events has decreased since the 1950s. For example, the probability of getting RX1day at 46mm was about 35% in 1950-1970, but the probability decreased to just over 10% in 1992-2012. In contrast, the probability of getting moderate CDD has increased in the 2nd and 3rd sub-periods, while CWD has shifted so that the duration of CWD tends to increase compared to the past. Overall, it seems that extreme precipitation in Canada will tend to occur more frequently in the future, probably leading to more flooding events.

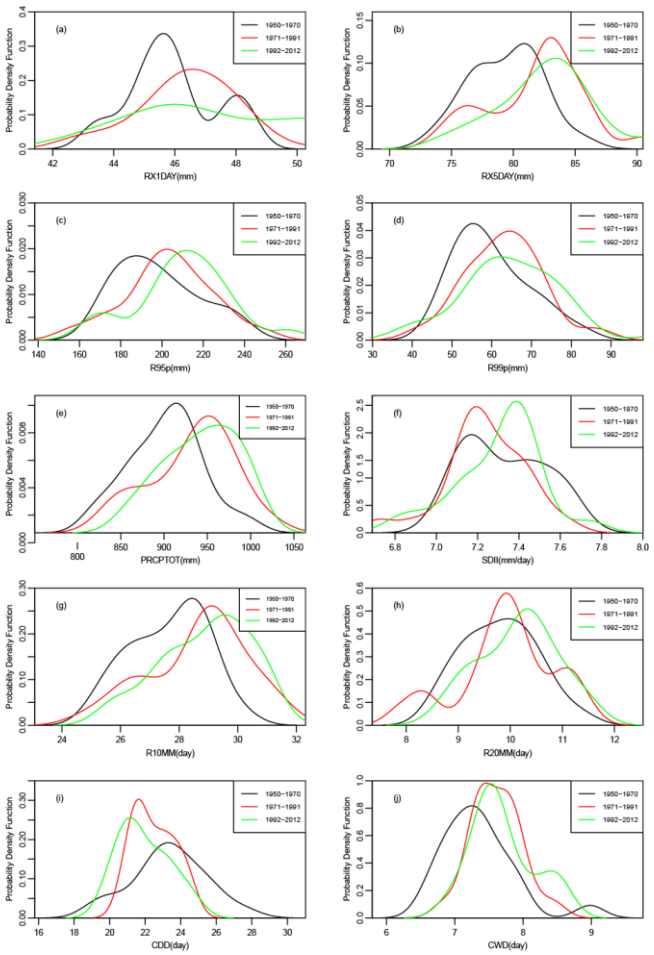

Figure 2.5 Annual probability density functions for extreme precipitation indices from 1950 to 2012 for three time periods: 1950-1970, 1971-1991, and 1992-2012.

2.4.5 Relationship between R95p/R99p and Climate Indices

2.4.5.1 Wavelet Analysis of R95p and R99p

Given the vast landmass and various climatic zones of Canada, we have divided Canada into three regions, eastern, central, and western Canada. A similar regionalization approach has been adopted to analyze synoptic circulation patterns related to heavy precipitation (Tan and Gan, 2017) and seasonal precipitation (Coulibaly, 2006) in Canada. Figure 2.6 shows the wavelet power spectra of PC1 for R95p and R99p of western, central and eastern Canada. The thick black contours represent statistically significant power at 95% significance level against red noise, and the white

sag line is the cone of influence (COI), outside which results may be affected by edge effects of zero paddings.

In general, R95p and R99p showed somewhat similar oscillation patterns in the same regions. However, each region exhibited different oscillation patterns for R95p and R99p. As shown in Figures 2.6(a) and (b), the power spectrum plot of western R95p reveals two distinct bands at 4-8 year and 2-4 year periodicities from 1960 to 1975 and in the 1980s, respectively. Two bands of 2-6 year and 12-16 year periodicities are in the 1980s for the power spectrum plot of western R99p. In contrast, an 8-16 year band and a 1-4 year band dominate the central R95p and R99p power spectrum plots in 1950-1970 and 2000s, respectively. A small band of 1-year in the 1980s, two bands of 2-4 year and 6-8 year periodicities in 2000s are found in eastern R95p and R99p power spectrum plots, respectively.

In investigating heavy precipitation of Canada for 1900-1998, Zhang et al. (2001) also found decadal oscillation as a dominant feature in precipitation extremes, while wavelet analysis of R95p and R99p indices in Figure 2.6 show a combination of significant interannual and decadal oscillations that appeared and disappeared over 1950-2012 in eastern, central, and western Canada without any consistent pattern.

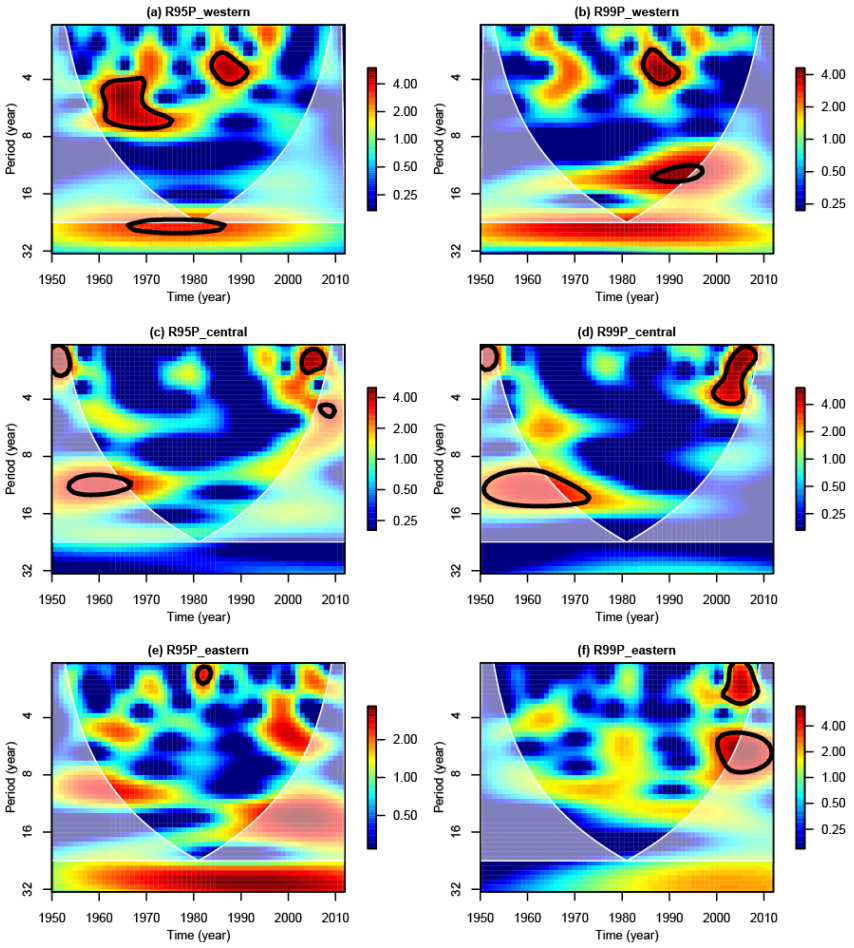

Figure 2.6 Wavelet power spectra of PC1 for R95p and R99p in the eastern, central, and western Canada.

2.4.5.2 Wavelet Transform Coherence (WTC)

The WTC plots between extreme precipitation indices (PC1 of R95p and R99p) and selected climate indices are shown in Figures 2.7-2.9. The arrows indicate the phase difference: arrows pointing to the right (left) mean that two time series are in phase (anti-phase) while arrows pointing up (down) mean that one time series leads (lags) the other by $90°$. Analogous to Figure 2.6, WTC between R95p and climate indices are similar to WTC between R99p and climate anomalies in the same region, and so we only present results of R99p. The coherence spectrum plots between the MEI and R99p show statistically significant power at 2-4 year bands in some years over western Canada (Figure 2.7(a)) and at 2-6 year bands over eastern Canada, respectively. After the 1970s,

there was a consistently strong coherence at 8-16 year bands between R99p and MEI in western and eastern Canada, although parts of the bands are outside the COI. For central Canada, the power of the wavelet coherence between MEI and R99p (Figure 2.7(c)) was relatively weak, which is expected because of the blocking effect of the Canadian Rockies.

There was a strong 8-12 year wavelet coherence since the 1980s between PDO and R99p in western Canada (Figure 2.7(b)), but a weak coherence between PDO and R99p in eastern and central Canada. There was a high 2-8 year coherence between PNA and R99p from the 1950s to 1990s in western Canada (Figure 2.8(a)) and a strong 8-14 year coherence between PNA and R99p during the 1950s and after 1995 in eastern Canada (Figure 2.8(e)). For central Canada, other than a strong 1-4 year coherence that appeared since the 1990s, PNA did not seem to have much effect on R99p. Figure 2.8(b) shows that there are scattered strong interannual (1-4 year) coherence between NAO and R99p in western Canada and a significant coherence band of 6-8 year periodicity in central Canada. The band of high 12-16 year coherence mainly occurred after the 1990s, but it is outside the COI of the wavelet coherence plot (Figure 2.8(f)). The wavelet coherence between NPGO and R99p was active in western Canada, of interannual 2-8 year cycle and 8-16 year cycle for R99p (Figure 2.9(a)). Some scattered coherence between NPGO and R99p of 4-6 year cycle can be found in central Canada, and a strong 8-16 year coherence from the 1990s is detected in eastern Canada (Figure 2.9(c)).

From a non-stationary analysis of the frequency and intensity of heavy Precipitation over Canada using a generalized extreme value distribution (GEV), Tan and Gan (2017) found a strong non-stationary relationship between heavy precipitation and large-scale climate patterns. For example,

annual maximum daily precipitation in southwestern coastal regions and southern CP tend to be larger in El Niño than in La Niña years. In our study, results of the WTC analysis further show that extreme precipitation of western Canada based on R95p/R99p indices are strongly correlated with MEI, PDO, PNA, and NPGO. For extreme precipitation of central Canada, NAO and NPGO exerted more influence than other climate anomalies, while for eastern Canada, extreme precipitation primarily comes under the influence of MEI, PNA, and NPGO. Jiang et al. (2014) also found the seasonal precipitation of Alberta (central Canada) to be strongly influenced by ENSO, PDO, and NPGO, while Gan et al. (2007) showed the influence of ENSO and PDO on the winter precipitation of southwestern Canada.

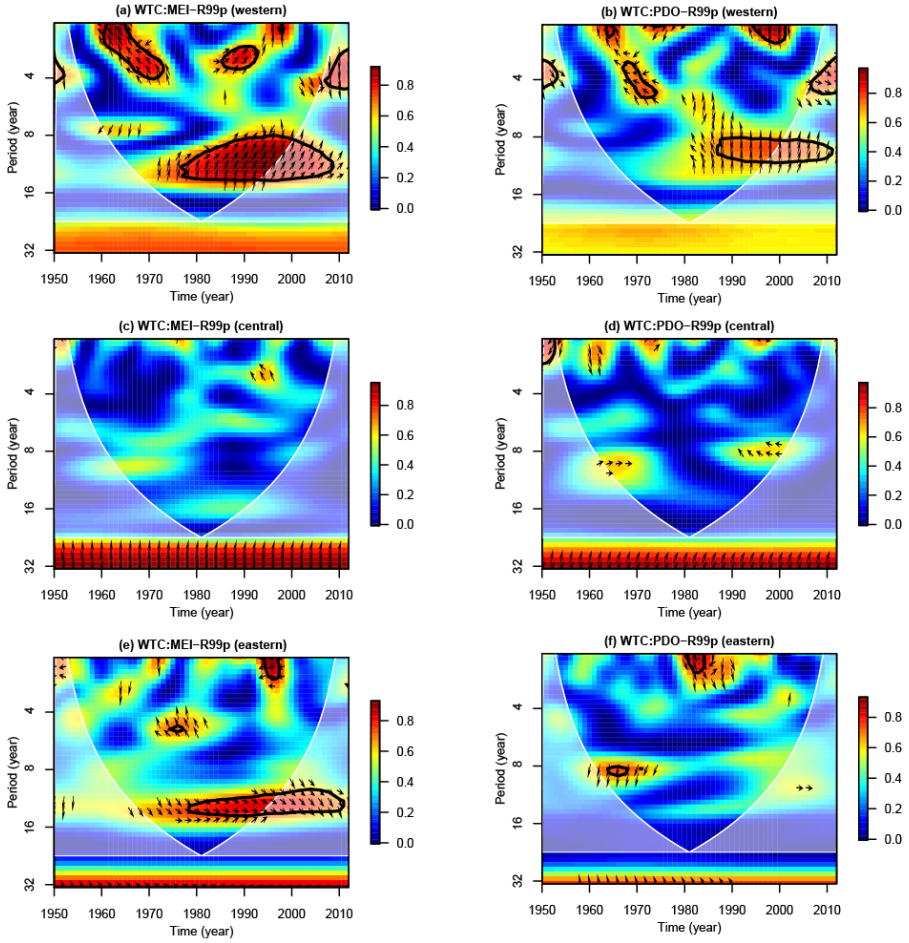

Figure 2.7 Wavelet coherence between the MEI/PDO and R99p for the eastern, central, and western Canada.

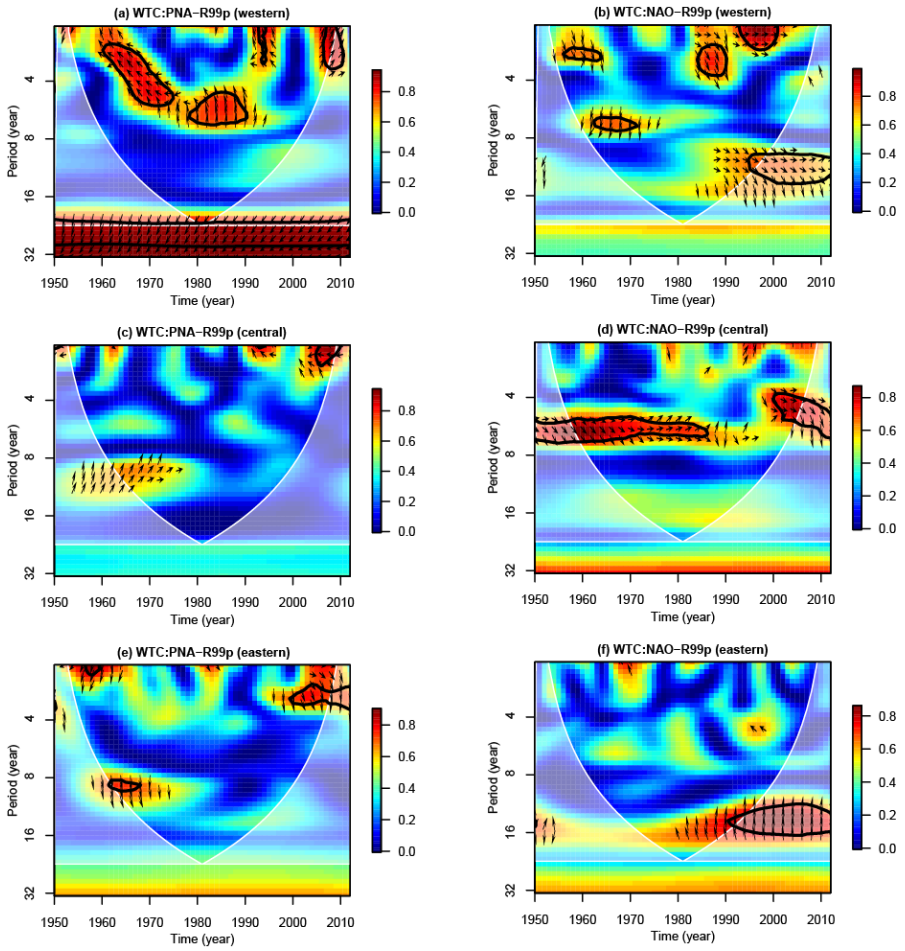

Figure 2.8 Same as Figure 2.7 but for the PNA and NAO.

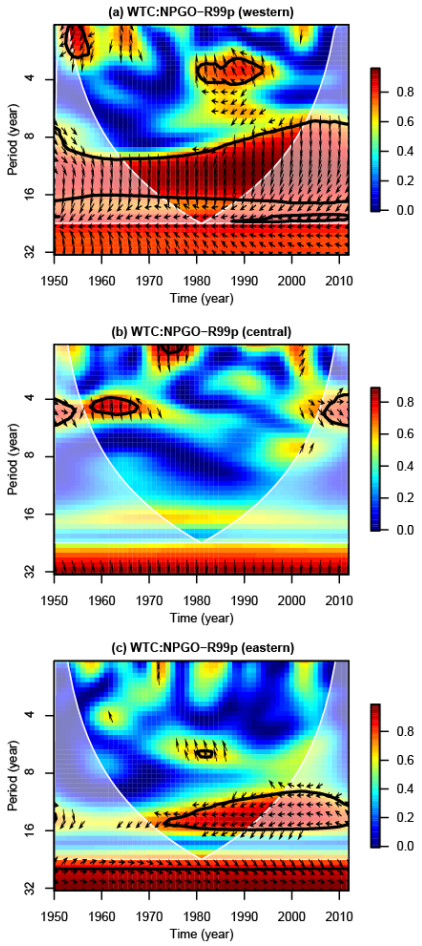

Figure 2.9 Same as Figure 2.7 but for the NPGO.

2.4.5.3 Relations of Atmospheric Circulations with Climate patterns and Anomalous Precipitation

Oceanic and atmospheric circulation patterns are potential drivers behind climate extremes worldwide through their impacts on sea surface temperatures, surface winds, and sea level pressure (Limsakul and Singhruck, 2016; Xi et al., 2018). Using storm back-trajectory analyses, Tan et al. (2018b) showed that extreme precipitation events in southwestern Canada are generally associated with the atmospheric river over the North Pacific, while moisture pathways for central and eastern Canada follow westerlies in mid-latitudes coming from the North Pacific Ocean or the northern polar jet stream over high-latitudes regions.

Using boosted regression tree analysis, Theobald et al. (2018) demonstrated that teleconnections do not act in isolation, and their complex interactions with synoptic atmospheric circulation can affect precipitation variability. Furthermore, Tan et al. (2018c) applied the self-organizing map (SOM) algorithm on vertically integrated water vapor transport (IVT) data to analyze large-scale meteorological patterns (LSMPs) associated with precipitation extremes for summer and fall in Canada. During summer, the occurrence of LSMPs associated with ENSO in western Canada is higher than that in eastern Canada (Tan et al., 2018c), as shown by more extensive statistically significant wavelet-coherence between MEI and R99p in Figure 2.7(a) than that in Figure 2.7(e). In addition, Tan et al. (2018) further show that LSMPs associated with more frequent occurrence of extreme precipitation over western Canada are more likely to occur during positive phases of ENSO, as shown by the coherence phase in Figure 2.7(a), implying that ENSO has considerable influence on certain LSMPs patterns identified by Tan et al. (2018c). Similarly, the occurrence of LSMPs associated with NAO in western Canada is larger than that in eastern Canada (Tan et al., 2018c), which again agrees with the more extensive wavelet-coherence of NAO-R99p in Figure 2.8(b) than that in Figure 2.8(f). Additionally, LSMPs patterns associated with less frequent summer extreme precipitation events over western Canada tend to occur during the negative phase of NAO, which has also been shown by the coherence phase in Figure 2.8(b), indicating that NAO also has a significant influence on certain LSMPs patterns they have identified.

Furthermore, it has been shown that regional positive (negative) precipitation anomalies are generally associated with mid-tropospheric convergence (divergence), located to the right (left) of the ridge axis and left (right) of the trough. Extremely large IVT over western Canada is related to the Aleutian low and Gulf cyclone, which forces moisture from North Pacific to western Canada,

however, it is not necessarily associated with positive precipitation anomalies or frequent extreme precipitation events, because intensive moisture fluxes sometimes just pass over a region without precipitating. In comparison, anomalously low IVT is associated with more frequent extreme precipitation events, partly caused by an extremely low ground surface temperature that facilitates the moisture flux to precipitate (Tan et al., 2018c).

2.4.6 Correlation between extreme precipitation and seasonal CAPE, specific humidity, and temperature

Table 2.4 shows that extreme precipitation tends to occur more frequently in summer and winter for eastern Canada, in summer for central Canada, and in summer and winter for western Canada. To investigate the possible impacts of CAPE, specific humidity, and temperature on extreme precipitation of Canada, Figure 2.10 shows the spatial distribution of trends in seasonal CAPE, specific humidity, and surface temperature respectively.

In summer, both CAPE and specific humidity show increasing trends in central and eastern Canada, but decreasing trends along the southern border and parts of northern Canada in 1950-2012. For seasonal surface temperature, negative trends were widespread in central Canada, while positive trends dominated northern and southern Canada. In winter, there had been more increasing trends in CAPE in central and southeastern Canada, and more increasing trends in specific humidity over central and western Canada. However, widespread increasing trends in the winter surface temperature were detected across Canada except for the easternmost part.

Table 2.4 Months from January (1) to December (12) are ranked in terms of the number of extreme precipitation events occurred in each month.

Province	Month		
West			
BC	1	11	12
YK	6	7	8
Central			
AB	6	7	8
MB	7	6	8
NU	8	9	7
SK	6	7	8
NT	7	8	6
East			
NB	1	11	2
NL	1	3	2
NS	1	12	2
ON	9	7	6
PE	2	8	12
QC	8	9	7

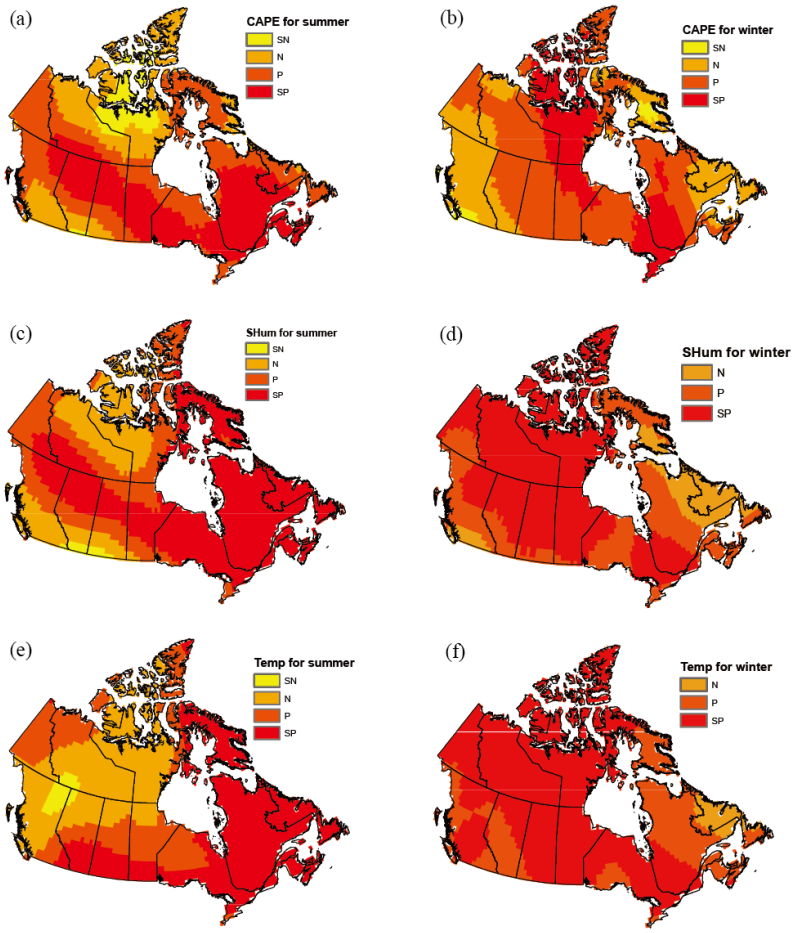

Figure 2.10 Spatial distribution of the seasonal CAPE, specific humidity, and surface temperature trend from 1985 to 2012. The abbreviations are P: positive trend, SP: significant positive trend, N: negative trend, SN: significant negative trend.

Using the Spearman rank correlation, the influence of CAPE, specific humidity, and surface temperature on extreme precipitation (Rx1day) is further investigated (Figure 2.11). Given CAPE values are much higher in summer than in other seasons, the correlation analysis is only conducted for the summer. Figures 2.11(a) and (b) show that summer CAPE and specific humidity values are positively correlated with extreme precipitation in southern Canada, respectively. The annual cycle of CAPE generally reaches its maximum during summer in northern hemisphere (Riemann-Campe et al., 2009) and summer precipitation is often of convective origin, for which latent heat

release is the primary source of energy driving the upward air motions (Guichard et al., 2004; Lenderink and Van Meijgaard, 2008). Apparently, increasing trends of extreme precipitation detected in this region are at least partly attributed to increasing CAPE and specific humidity in the summer. Our results agree with Lepore et al. (2015), who investigated the dependency of rainfall extremes on temperature and CAPE in the United States. They found that rainfall intensity quantiles are related to CAPE by a power-law relationship. In Turkey, Lolis and Türkeş (2016) also found that the occurrence of extreme precipitation events in summer is linked to low upper air temperatures and high static instability (through CAPE) associated with the summer heating of land and upper air disturbances. Similarly, Murugavel et al. (2012) also found that increasing CAPE over India compensates the weakening of monsoon circulation and it is responsible for the increase in the frequency of extreme events over the 1984-2008 period. From simulating the future regional climate of the Great Lakes using a regional climate model called Weather Research and Forecasting (WRF), Orgeville et al. (2014) projected the future moisture availability and the rainfall of the Great Lakes basin to increase because of climate change. Besides, extreme rainfall is projected to increase more than the mean annual rainfall because extreme rainfall is projected to originate from the mid-troposphere where warming is projected to be higher than surface warming.

For the CP, negative correlation between extreme precipitation and specific humidity (Figure 2.11(c)), and between extreme precipitation and temperature (Figure 2.11(e)) have been detected in winter. This means that winter extreme precipitation has decreased even though both specific humidity and surface temperature have increased under climate warming. Zhang et al. (2001) detected both positive and negative trends in summer heavy rainfall, but negative trends in winter heavy snowfall in central CP, respectively. Vincent and Mekis (2006) confirmed that annual total

snowfall in southern Canada has decreased significantly in the second half of the twentieth century, and annual maximum snow depth in Canada have also decreased (Kunkel et al., 2016; Vincent et al., 2015), which is likely related to climate warming impact. Wang and Zhang (2008) used statistically downscaled principal components of sea level pressure and specific humidity as covariates to a GEV to derive winter maximum daily precipitation over North America. From projected changes in covariates obtained from climate change simulations of the Canadian GCM (CGCM3.1) forced by the IPCC SRES-A2 scenarios, they projected that the maximum daily precipitation over the CP to decrease. This is because higher humidity in the CP are associated with smaller GEV location parameters, which means that higher humidity is associated with large-scale circulations unfavorable for precipitation in the CP, where circulations exert a stronger influence over humidity. Additionally, climate models projected a smaller decrease in the intensity of daily snowfall extreme than in the mean snowfall over many terrestrial regions of Northern Hemisphere due to global warming (O'Gorman, 2014). This could be related to the theory of rain-snow phase transition that snowfall extremes occur in a range near the optimal temperature that is insensitive to warming (Dai, 2008). These together may contribute to the negative correlation with specific humidity and the general decline of extreme precipitation in the central CP.

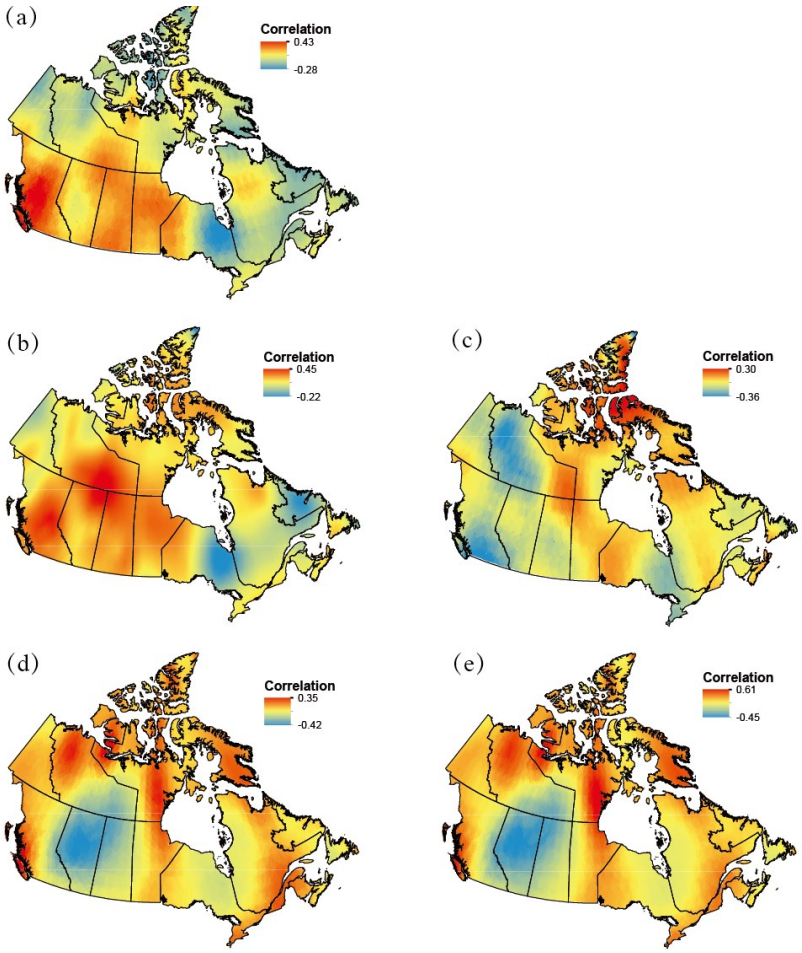

Figure 2.11 Spatial distribution of Spearman rank correlation between extreme precipitation and (a) summer CAPE, (b) summer specific humidity, (c) winter specific humidity, (d) summer temperature, and (e) winter temperature.

From simulations of the Canadian Regional Climate Model, Mladjic et al. (2011) projected that 1–7 day precipitation extremes of 20-, 50-, and 100-yr return levels will increase over most of Canada, especially for northern regions, which would have severe implications for managing water resources of Canada such as sewer systems, flood control, and water storage systems. However, precipitation extremes of some regions in southern Canada (mainly the central CP) are projected to decrease. Results of Mladjic et al. (2011) and Zhou et al. (2018) generally agree with our results based on historical precipitation data of Canada. In addition, Emori and Brown (2005) separated

the dynamic (atmospheric motion) change and atmospheric moisture content (thermodynamic) change of extreme precipitation changes projected in 6 climate model experiments. Their climate model results consistently show that over the sub-tropics, the thermodynamic change for extreme precipitation is an overall increase as a result of increased atmospheric moisture, while for mean precipitation the thermodynamic change is small or it decreases. Tandon et al. (2018) also noted that large-scale upward motion of air during extreme precipitation events could be related to changes in vertical stability in subtropical areas or changes in the seasonal mean circulation near the equator. Therefore, while changes to the summer extreme precipitation could be attributed to the thermodynamic impact, winter extreme precipitation changes are more complicated and are likely attributed to the combined thermodynamic and dynamic effects (Ban et al., 2018; Tandon et al., 2018; Zhou et al., 2018).

2.5 Summary and Conclusions

Due to the effects of climate warming, hydrologic extremes such as droughts and floods have occurred more frequently and in greater severity globally in recent decades, resulting in severe environmental and societal impacts (Beniston and Stephenson, 2004). This study analyzed monotonic trends of 10 extreme precipitation indices and possible relationships between R95p/R99p and several climate patterns over Canada. Statistically significant trends have been detected for all indices except for SDII and R20mm. Except for CDD, most indices analyzed exhibit positive trends, which demonstrate that increasing extreme precipitation events have occurred in Canada over 1950-2012, constituting a growing risk for urban settlements and infrastructure losses (Lovino et al., 2018). In addition, probability distribution functions of these indices plotted over three subsequent sub-periods further confirm this conclusion. Spatially, even

though these extreme precipitation indices exhibit a mixture of increasing and decreasing trends, positive trends dominate over negative trends across the southern and northern part of Canada, except for CDD. While in the central CP, more decreasing trends were detected.

From wavelet analysis and wavelet transform coherence plots, extreme precipitation of western Canada was strongly teleconnected to MEI, PDO, PNA, and NPGO, that of central Canada was highly associated with NAO and NPGO, and for eastern Canada by MEI, PNA, and NPGO. However, teleconnections do not act in isolation, and their complex interactions with synoptic atmospheric circulation can affect precipitation variability. For example, LSMPs related to more frequent extreme precipitation in western Canada tend to occur during the positive phase of PNA, ENSO, and PDO.

Detected increasing trends in extreme precipitation in southern Canada are related to the increasing CAPE and specific humidity in summer, while decreasing extreme precipitation over central CP is associated with the decreasing snowfall and the influence of circulation in winter. It is noted that while changes to the summer extreme precipitation could be explained by the thermodynamic impact, winter extreme precipitation changes are more complicated and are likely attributed to the combined thermodynamic and dynamic effects.

In addition to the influence of large-scale climate patterns, land reclamation, urbanization, and other human activities can also cause changes in climate extremes (Xi et al., 2018). For example, as terrestrial evapotranspiration is the primary moisture source to many extreme precipitation events in Canada (Tan et al., 2018b), urbanization and reclamation that change the land surface

could also have impacts on extreme precipitation events. Therefore, a comprehensive analysis of the influence of climatic and non-climatic factors on precipitation extremes will require further research.

Chapter 3. Changes to the 1979-2013 Summer Convective Available Potential Energy (CAPE) and Extreme Precipitation over North America

3.1 Introduction

Convective Available Potential Energy (CAPE) (Equation 1), an integral of the parcel buoyancy between the levels of free convection and neutral buoyancy vertically, is a popular index to measure meteorological conditions for the occurrence of intensive precipitation events (Seeley and Romps, 2015). Large CAPE (Joules/kg) has been widely used to represent conditions favorable for the occurrence of severe convective storms and tornado events (Brooks et al., 2007; Doswell and Evans, 2003; Rasmussen and Blanchard, 1998). Therefore, changing trends in CAPE data of a region could be used to identify changes in convective systems of that region (Murugavel et al., 2012; Riemann-Campe et al., 2009).

$$CAPE = \int_{LFC}^{LNB} R_d \left(T_{vp} - T_{ve} \right) dln(p)$$

$where$:

T_{vp} = virtual temperature of air parcel

T_{ve} = virtual temperature of environment of the air parcel (3-1)

LFC = Level of free convection

LNB = Level of neutral buoyancy

R_d = Gas constant of dry air

p = Pressure

Statistically significant trends in CAPE derived from radiosonde records since the late 20th century have been detected in different parts of the world, e.g., the 1979-2014 CAPE in West Africa (Meukaleuni et al., 2016), the 1984-2008 CAPE over the Indian sub-continent (Murugavel et al., 2012) the 1958-2001 CAPE over the Tropics(Riemann-Campe et al., 2009), and the CAPE data in the western Pacific and Caribbean (DeMott and Randall, 2004). Given the positive relationship

between CAPE, Sea Surface Temperature (SST) and specific humidity (Riemann-Campe et al., 2009; Seeley and Romps, 2015), we would expect an increase in CAPE values and extreme weather events due to the observed and projected warming trends for the 21st century by successive assessment reports of the Intergovernmental Panel on Climate Change (IPCC). The continuous increasing trend in the global mean temperature compared to observations since instrumental records has likely contributed to more frequent and severe hydrologic extremes occurring across the world in recent years (Groisman et al., 2004; Hartmann et al., 2013; Jiang et al., 2015).

The objective of this study is to identify change points and increasing or decreasing trends in CAPE values over United States (US) and southern Canada for the summer of 1979-2013, and how they relate to trends in single or multiple extreme precipitation events, average surface temperature and surface specific humidity over this period. Study area, data, and methodology are given in Section 3.2, results and discussions in Section 3.3 and conclusions in Section 3.4.

3.2 Study Area, data and methodology

As North America (NA) extends from about 10˚ north of the Equator to the North Pole, its climate ranges from equatorial and humid subtropical in Mexico and southeastern United States (US) to bitter cold, polar deserts in the Canadian Arctic. Further, its climate is also influenced by the Rocky Mountains of the west to vast expanses of the Great Plains in central US and Canada and coastal lowlands of southern and eastern US. Due to the low temperature, the CAPE values are much smaller in northern Canada compare to that in southern Canada. Therefore, this study is focused on the US and southern Canada, where orographic precipitation dominates the Pacific Northwest

between May and October, while convective and cyclonic (frontal) precipitations dominate the May-September season in the Great Plains, and the Atlantic and Gulf coast regions, respectively. As expected, southern USA has a warmer temperature than the Rockies and southern Canada (Gutowski et al., 2008; Karl and Koss, 1984).

3.3 Datasets

Monthly CAPE data in this study was taken from the North American Land Data Assimilation System-phase 2 (NLDAS-2), a collaborative project among American research institutes, including NCEP (National Center for Environmental Prediction), Environmental Modeling Center, Princeton University and others (Mitchell, 2004; Xia et al., 2012). NLDAS-2 data, assimilated from a large quantity of observed and climate model reanalysis data, and validated against observations, is available at 0.125˚ spatial resolution over central North America. The CAPE data of NLDAS-2 was interpolated from NCEP's North America Regional Reanalysis (NARR) data generated from, among others, lateral boundary conditions of NCEP-DOE R-2 reanalysis data (Kanamitsu et al., 2002), NCEP's operational version of Eta regional climate model (Mesinger et al., 2006) and some observed climate data assimilation systems. Monthly specific humidity data at various pressure levels are also derived from the NARR dataset, and observed daily precipitation and temperature data for stations across the US and southern Canada were collected from the Global Historical Climatology Network (GHCN)-Daily, which is a processing system for the official archive of US daily data. GHCN also incorporated quality-assured data from over 80,000 stations for 180 countries (Menne et al., 2012). Only GHCN stations with less than 1% of missing precipitation or temperature data for the summer of 1979-2013 were selected for trend analysis in

the US and southern Canada where monthly and seasonal precipitation and temperature data are computed from daily data of GHCN stations.

3.4 Research Methodology

The mean summer CAPE data for 1979-2013 show significant spatial and temporal variability across the US and southern Canada with the warm summer of June-August dominated by intensive convective storms and maximum CAPE values, particularly in the warmer southern US region (Figure 3.1). Therefore, in this study, changes in CAPE and extreme precipitation over North America were mainly analyzed for the June-August season. Homogeneity tests in CAPE data were conducted to identify any change points in the 1979-2013 study period using the Wilcoxon rank-sum test (Fu et al., 2014; Gibbons and Chakraborti, 2011), a widely used method to detect whether two samples come from the same population. The nonparametric Theil-Sen regression estimator (Sen, 1968; Theil, 1992; Wilcox, 1998) was used to estimate trends in CAPE, extreme precipitation, surface temperature and specific humidity while statistical significance of seasonal trends at $p<0.05$ were tested using the nonparametric Mann-Kendall test capable of handling seasonality, missing values, and non-normality in a time series (Gan et al., 2013; Hirsch et al., 1982; Kendall, 1948; Mann, 1945). Extreme precipitation indices of the Expert Team on Climate Change Detection and Indices (ETCCDI, http://etccdi.pacificclimate.org/) were used as a proxy to identify changes in extreme precipitation at GHCN stations. These are RX1day (RX5day) which is the maximum precipitation depth in one (five) day, and R20mm is the number of days where daily precipitation exceeded 20 mm (e.g., Gizaw and Gan, 2016). Trends for these indices of every summer of 1979-2013, for mean air temperature recorded at GHCN stations and surface specific humidity derived from NARR data over the US and southern Canada were computed.

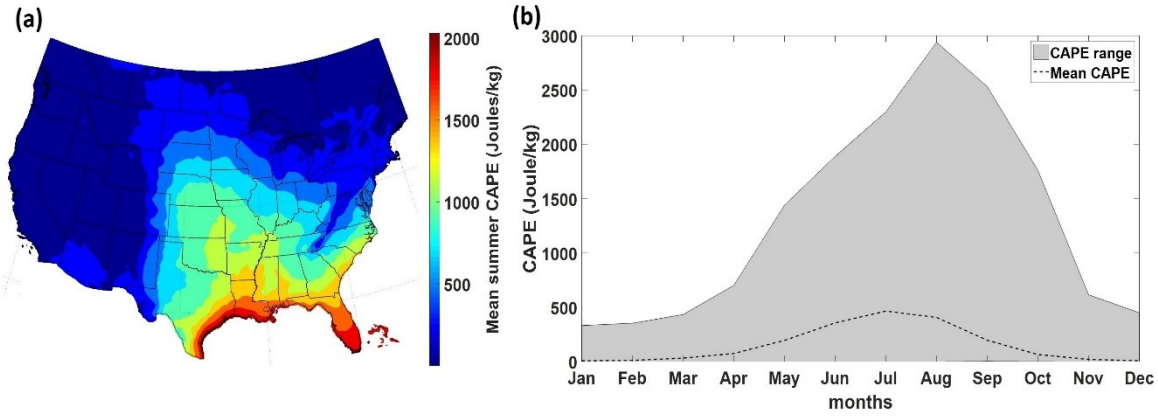

Figure 3.1 (a) Mean summer (June-August) CAPE for 1979-2013 period, (b) Mean annual CAPE values over the US and southern Canada, the gray area shows the range of CAPE data while the dotted line shows the mean annual profile of CAPE over the region.

3.5 Results and Discussion

3.5.1 Change point analysis in summer CAPE data and trend analysis in CAPE and extreme precipitation indices

Change point analysis on summer CAPE data using the Wilcoxon-rank-sum test shows statistically significant change points (years) in the Great Plains, Rocky Mountains and its foothills, most parts of the northeastern US, southern Québec and Ontario and the Great Lakes region, parts of the Atlantic and Gulf Coastal regions such as southern Florida, Texas and parts of western British Columbia (Figure 3.2). Overall, 80% of detected change points occurred between 1997 and 2003 with 70% occurring from 2000 to 2003, which could be partly caused by the change in radiosonde instruments over this period to measure climate variables needed for computing CAPE. By a detailed study on systematic errors of global radiosonde data from 1997 to 2006, Wang and Zhang (2008) showed that the introduction of protective shields in the late 2000 and 2001 for humidity sensors of Vaisala RS-80A and RS-80H radiosondes used in parts of the US have reduced biases of precipitable water in wet and dry days. Vincent and Milewska (2007) also examined potential biases in radiosonde data for Canada and identified a major decreasing step change in temperature

and relative humidity departures around 1995. After examining the history of radiosonde stations in the 1980s and 1990s, they concluded that detected changes in trends around 1995 were probably due to the correction of radiation that was implemented gradually in Vaisala RS-80 sensors from 1995 to late 1999. As these types of radiosondes were also used in parts of the US, we believe that detected change points in CAPE data are most likely caused by changes in the instrumentation of radiosondes. Since change points are mostly detected in the early 2000s, trend analysis was done separately over 1979-2001 and 2002-2013 for areas where statistically significant change points are detected, and over 1979-2013 for areas where no statistically significant change point was detected.

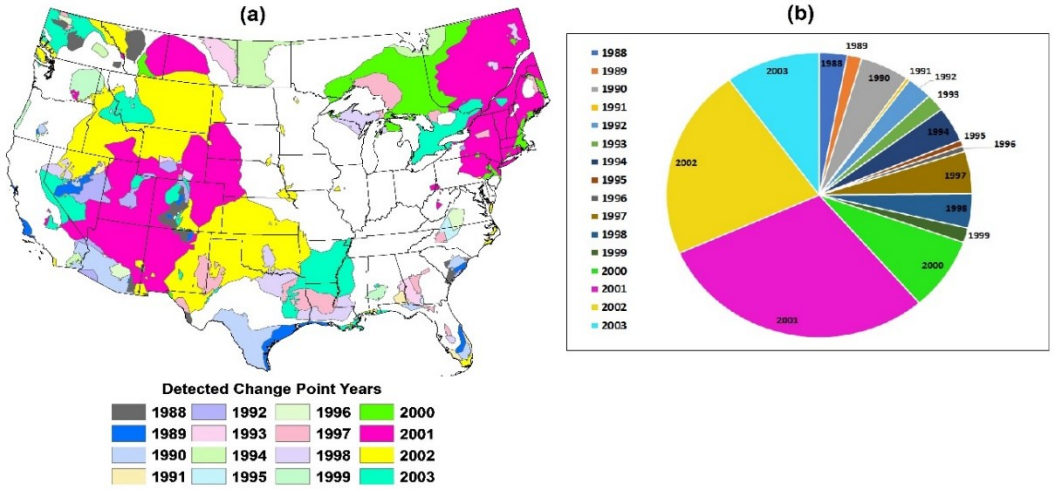

Figure 3.2 Detected change point years in summer CAPE data over the US and southern Canada for the 1979-2013 period, (a) areas in the US and southern Canada where statistically significant change points in CAPE data were detected, (b) the proportion of detected change points.

For CAPE data with detected change points, increasing trends in CAPE values for the 1979-2001 period were as high as 20 Joules/kg/year (Figure 3.3) in areas which include most of the Great Plains extending from northern Texas northward to parts of the Canadian Prairies (CP), low laying areas in the Atlantic and Gulf coast such as southern Texas and Florida. Detectable increasing trends for the 2002-2013 period include the northeastern Atlantic coast, the Great Lakes region,

particularly southern Ontario and Québec, and parts of southern British Columbia near the Pacific coast. However, increasing trends detected for parts of Texas, Oklahoma, and Louisiana in 1979-2001 were largely reversed in 2002-2013. The US mid-west experienced both mild increasing and decreasing trends, whereas areas west of the Rockies mainly experienced minor or no trends. Statistically significant trend magnitudes were mainly detected for some areas in the Atlantic and Gulf coast, and in the Great Plains (Figure 3.3).

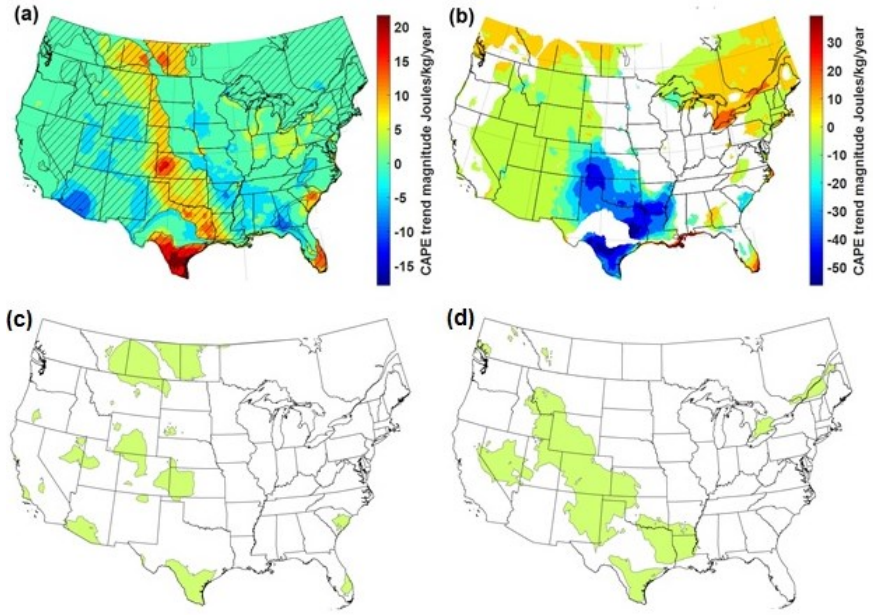

Figure 3.3 Detected trends in CAPE data (a) trend magnitudes from 1979-2001 (hatched areas indicate regions where change points were detected) and 1979-2013 regions where no change points were detected, (b) trend magnitudes in CAPE data for 2002-2013 for regions where change points were detected. (c) and (d) show regions (shaded in light green) where the detected trend magnitudes are statistically significant for (a) and (b), respectively.

The spatial distribution of increasing or decreasing trends of extreme precipitation indices, namely, RX1day, RX5day, and R20mm, detected for GHCN stations (Figures 3.4 to 3.6) are similar to the spatial distribution of trends detected in CAPE data (compare Figure 3.4 and Figure 3.3). For instance, increasing trends dominate the eastern Atlantic coast of the US for all extreme precipitation indices analyzed. This corresponds to the mild to moderate increasing trends in CAPE

data detected in this region for 1979-2001 and 2002-2013. Increasing trends in RX1day and RX5day were also detected for 1979-2001 for GHCN stations in southern Florida and parts of northern Texas in the Atlantic and Gulf coastal regions and for most stations in the Great Plains extending from northern Texas to the CP. Similar trends in CAPE data were also detected for 1979-2001. Furthermore, Figures 3.4 to 3.6 also show that more GHCN stations in southern Texas had decreasing trends for the 2002-2013 period, which agrees with the results obtained for CAPE data. Trends in the US mid-west and the Great Lakes were mixed, with most GHCN stations showing both mild increasing and decreasing trends for both the pre and the post-2001 periods. For the mountainous region of western US where summer CAPE values are small (Figure 3.1), either minor or no trends were detected in extreme precipitation indices over 1979-2013.

Detected trends in R20mm show similar spatial variability to trends in RX1day and RX5day. However, no trend was detected in R20mm for most GHCN stations in the US and southern Canada. For GHCN stations located in regions where no statistically significant change points in CAPE data were detected, average trends in RX1day and RX5day were about 0.2 mm/decade and 0.5 mm/decade over 1979-2013, respectively. For GHCN stations located in regions with statistically significant change points in CAPE data, trends in RX1day and RX5day were 0.2 mm/decade and 1.2 mm/ decade over 1979-2001, and 1.2 mm/decade and 1.7 mm/decade over 2002-2013, respectively. Even though detected trends in extreme precipitation indices vary spatially, on the whole, extreme precipitation indices show an overall increasing trend, albeit less than 10% of the trends are statistically significant. Furthermore, trends in RX1day and RX5day are higher for the post change-point, the 2002-2013 period which likely means that recent

consistent warming trends detected (IPCC, 2013) favor the occurrence of more extreme precipitation events over the study area.

In summary, increasing trends of both CAPE and extreme precipitation indices have been detected, particularly in eastern US and parts of the Atlantic and Gulf coast (southern Florida), and mixed increasing and decreasing trends in areas such as the Great Plains.

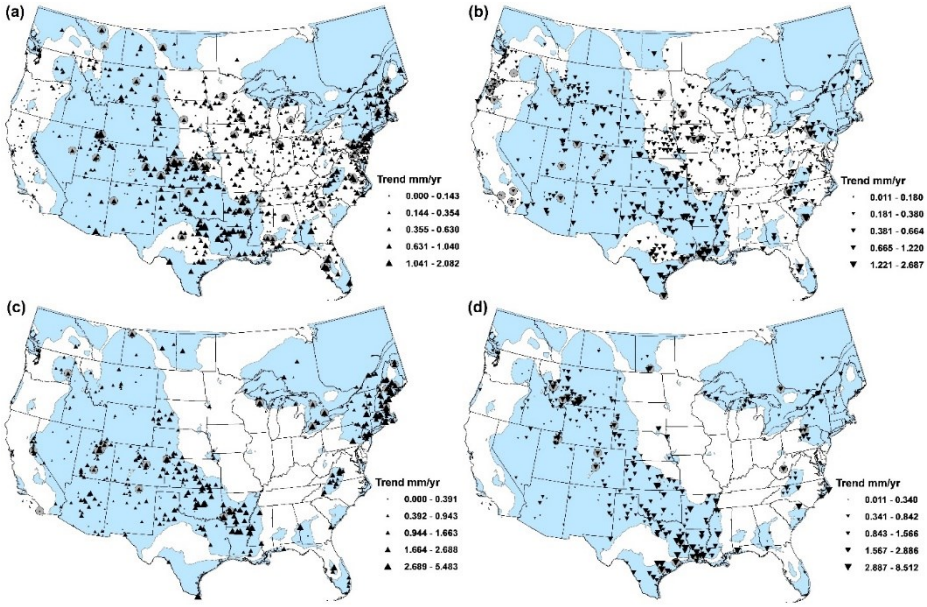

Figure 3.4 Trend magnitudes at GHCN stations for RX1day, (a) and (b) respectively show increasing and decreasing trends for RX1day from 1979-2001 for areas with detected change points in CAPE data (shaded in light blue) and 1979-2013 for areas with no detected change points in CAPE data. (c) and (d) respectively show increasing and decreasing trends for periods after detected change points in CAPE data (2002-2013)

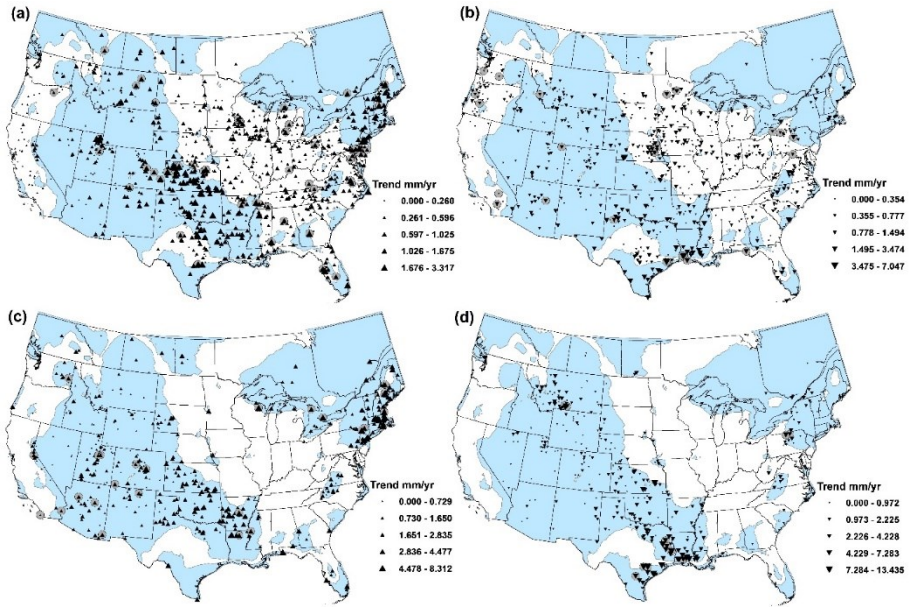

Figure 3.5 As in Figure 3.4 but for RX5day.

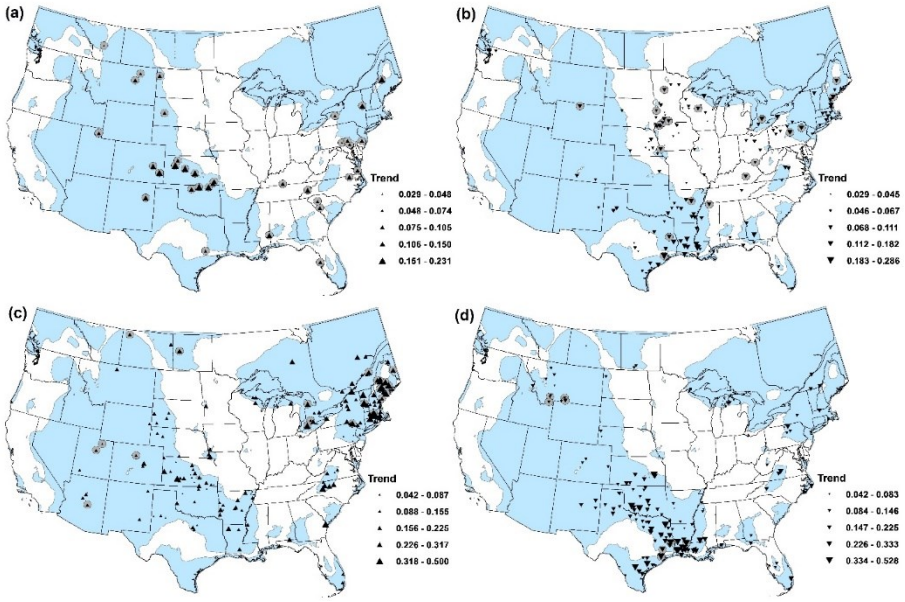

Figure 3.6 As in Figure 3.4 but for R20mm.

3.5.2 Trends in summer temperature and surface specific humidity, correlation of CAPE with climate indices and comparison with other climate variables

Because the rate of depletion of moisture from the atmosphere by precipitation far exceeds its rate of replenishment, the higher water-holding capacity of a warmer atmosphere will likely favor a general increase in the occurrence of extreme precipitation events, particularly convective precipitation (Trenberth, 1999). Corresponding to detected increasing trends in CAPE and extreme precipitation indices over the summer of 1979-2013, average trends in the average 2m air temperature were about 0.14 ˚C/decade over 1979-2013, and most summer temperature trends detected were positive (Figure 3.7). For those GHCN stations where statistically significant change points in CAPE data were detected, average trends in 2m mean air temperature were about 0.1˚C/decade in 1979-2001 but 0.3˚C/decade in 2002-2013. About 15% of the detected increasing trends at the GHCN stations were statistically significant at $p<0.05$. Decreasing trends were also detected for several stations around the US Great Plains and the Pacific coast of California, but only 3% of the detected decreasing trends were statistically significant (Figure 3.7). Similarly, the distribution of change points (years) and detected trends of specific humidity were spatially comparable with that of CAPE data, for more than 55% of detected change points in specific humidity also occurred between 2000 and 2003 (Figure 3.8).

In general, the rainfall falling rate far exceeds the evaporation rate. Since the water holding capacity of the atmosphere increases by about 7% for every degree Celsius increase in temperature, known as the Clausius-Clapeyron (C-C) rate, this means that a warmer atmosphere could favor more intense extreme precipitation events (Trenberth, 1999). With the C-C rate as the basis, different studies have found varying rates of increase in extreme rainfall with respect to increase

in temperature for different parts of the world (Berg et al., 2013; Lenderink and Van Meijgaard, 2008; Utsumi et al., 2011). Similarly, detected increasing trends in temperature and specific humidity for eastern US and southern Canada (Figures 3.7 and 3.8) complement increasing trends in CAPE and extreme precipitation indices in these regions. Therefore, increase in air temperature and specific humidity could be responsible for much of the increasing trends in extreme precipitation indices and CAPE over the convective storm dominated regions of eastern US and parts of southern Canada since CAPE is strongly dependent on surface specific humidity (Riemann-Campe et al., 2009).

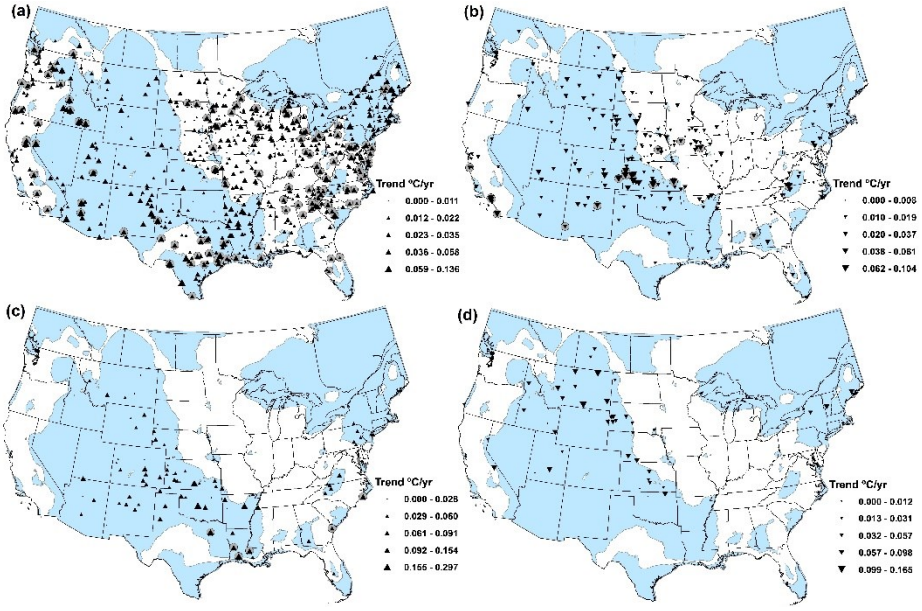

Figure 3.7 As in Figure 3.4 but for 2m average air temperature.

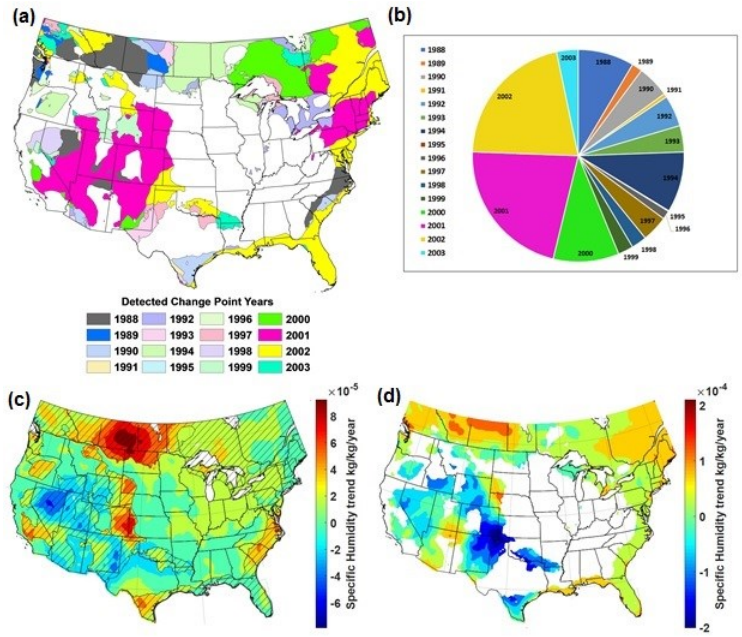

Figure 3.8 Detected change point years and trends in summer specific humidity over the US and southern Canada for the 1979-2013 period, (a) and (b) same as in Figure 3.4 (a) and (b) but for specific humidity, (c) and (d) same as in Figure 3.5 (a) and (b) but for specific humidity.

The Spearman rank correlation between the gridded CAPE dataset interpolated to selected GHCN stations and extreme precipitation indices (RX1day, RX5day, and R20mm) are positive for over 75% of the stations (Figure 3.9). However, about 90% of the positive correlations detected range between 0.10 and 0.50, which means that only about 10% of the stations show Spearman correlation between 0.50 and 1.0 with the CAPE data. Altogether about 45% of stations show Spearman correlations that are 0.30 and higher, which are statistically significant. In general, positive Spearman correlations dominate most regions, irrespective of whether increasing or decreasing trends are detected in both CAPE and extreme precipitation indices (Figures 3.9 to 3.11). With the exception of mountainous areas dominated by orographic precipitation, statistically significant Spearman correlations (≥0.3) are also detected between CAPE and average temperature of the selected GHCN stations (Figure 3.12).

Finally, the above trend and change point detection results obtained from the CAPE data of NLDAS-2 and climate data of GHCN are qualitatively compared with results obtained from the NCEP reanalysis dataset, and GPCP precipitation data. For the latter, simple differences between 2002-2013 and 1979-2001 June-Aug the mean of surface precipitable water, air temperature, sea surface temperature, specific humidity of the USA and southern Canada are presented in Figure 3.13. Figure 3.13 shows that over 1979-2013, surface precipitable water had increased by about 1-2 kg/m2 at Atlantic/Gulf Coastal Plains or southeastern states of US and at its eastern coastal region while Canadian Prairies, Rocky Mountains, Great Plains, and Great Basin had decreased by up to about 0.5 kg/m2, especially at the Great Plain areas. Similar spatial patterns of changes are observed in the specific humidity (g/kg) with some minor differences, that specific humidity had increased up to 1g/kg in Gulf Coast areas but had decreased almost proportionally in the Rockies and Great Plain areas. However, comparing air temperature with precipitable water and specific humidity, spatial pattern of changes observed between the two periods are partially opposite to each other, in that air temperature had increased less in the Gulf Coastal areas than in the Rocky and Great Plain areas while specific humidity and precipitable water had changed in an opposite manner. Interestingly, the sea surface temperature (SST) of the east coast had increased up to 0.5 ˚C but had decreased by a similar amount along the west coast of the US and southern Canada. Apparently, changes in SST had contributed to the observed regional changes in precipitable water and specific humidity and also could have contributed to higher CAPE values (Seeley and Romps, 2015). According to GPCP, precipitation had increased up to 0.5 mm/day along the east coast and Atlantic/Gulf coast areas, parts of the Canadian Prairies but had broadly decreased in the western US, the Great Plains, the Rockies and Great Basin to the west coast areas.

To some extent, detected changes on surface precipitable water and specific humidity from a simple difference between 2002-2013 and 1979-2001 data complement the trend analysis of CAPE data, in that areas where surface precipitable water and specific humidity had increased/decreased somewhat agree with areas where large statistically significant increasing/decreasing trends were detected for CAPE, even though as expected, there are some differences between their spatial distributions.

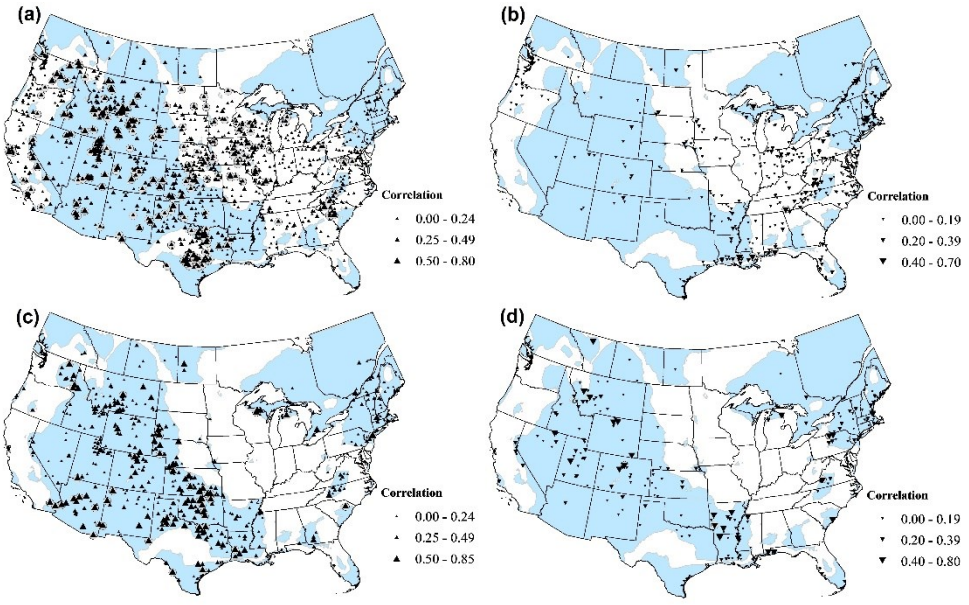

Figure 3.9 Spearman rank correlation between gridded CAPE data interpolated to selected GHCN stations and the RX1day index, where (a) and (b) respectively show positive and negative Spearman correlation between CAPE and RX1day over 1979-2001 for areas with detected change points in CAPE data (shaded in light blue), but over 1979-2013 for areas with no detected change points in CAPE data; (c) and (d) respectively show corresponding positive and negative Spearman correlations for periods after change points are detected in the CAPE data (2002-2013).

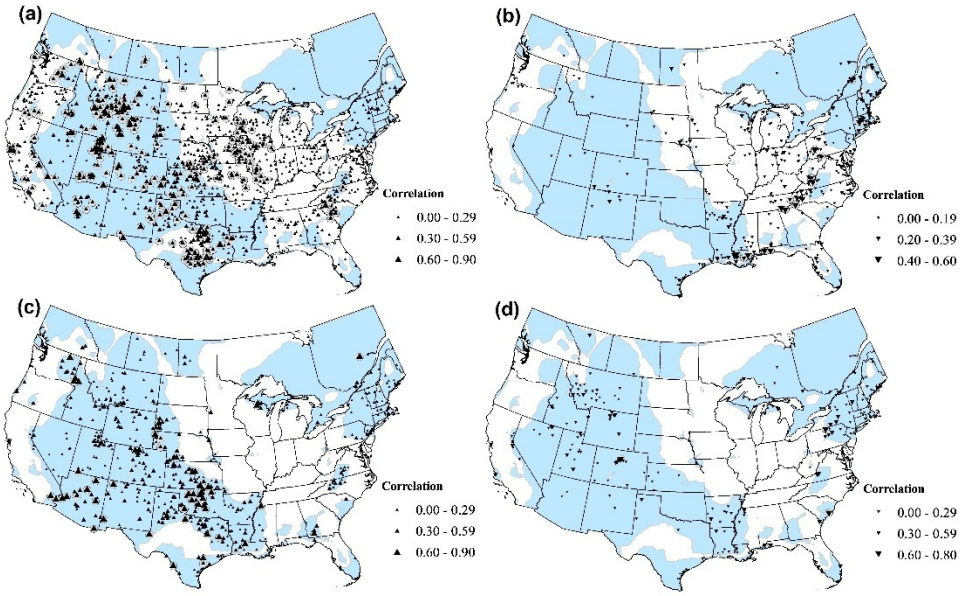

Figure 3.10 As in Figure 3.9 but for RX5day.

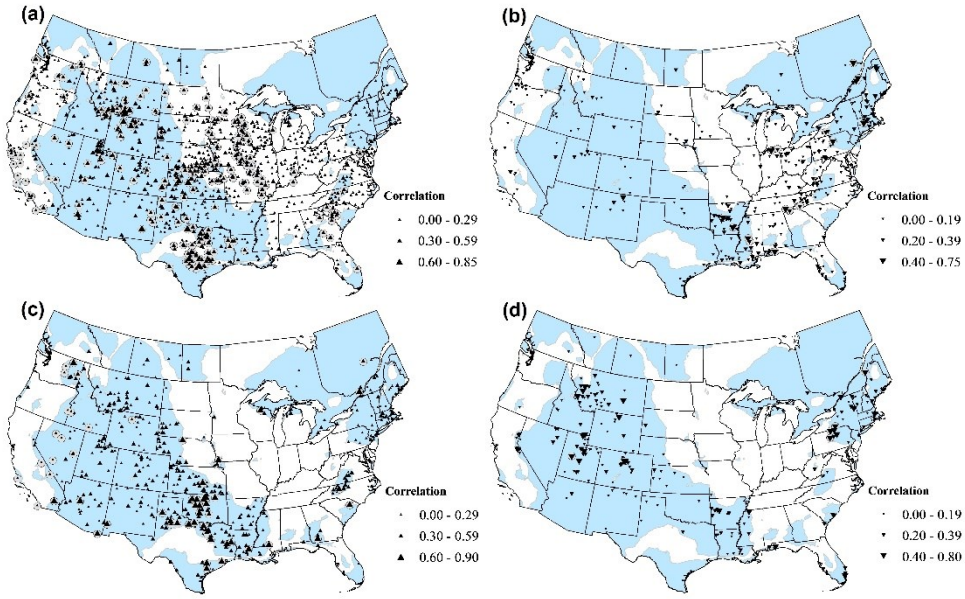

Figure 3.11 As in Figure 3.9 but for R20mm.

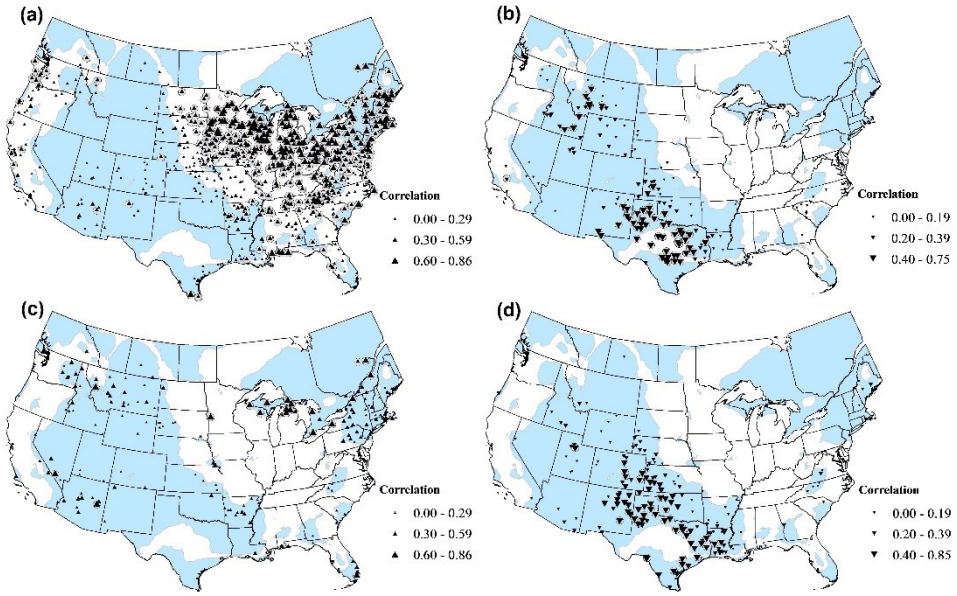

Figure 3.12 As in Figure 3.9 but for 2m average temperature

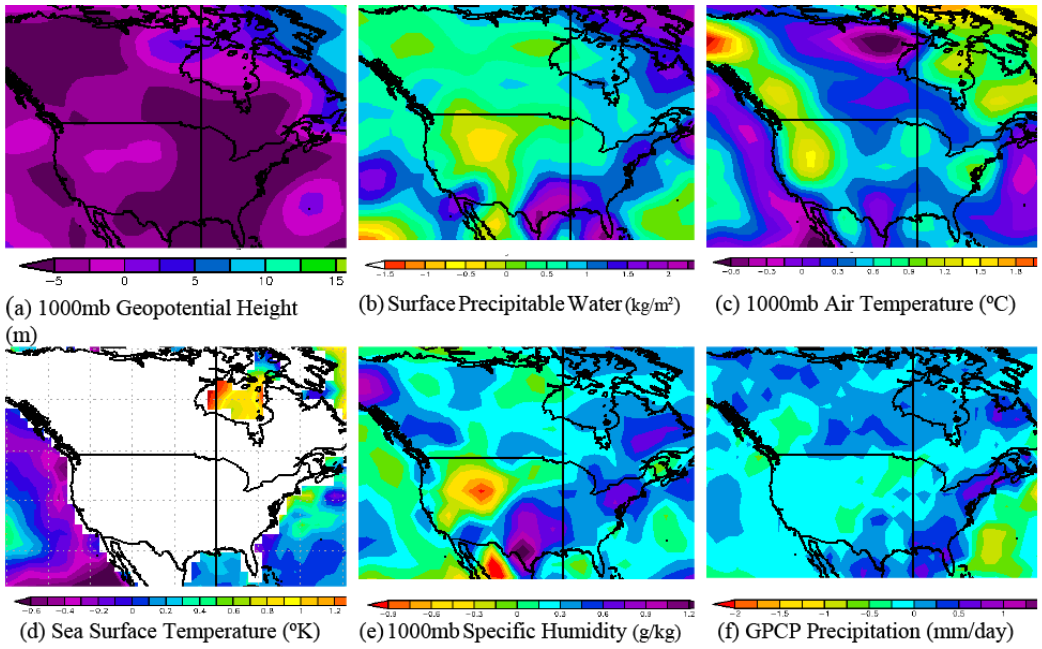

Figure 3.13 Differences between 2002-2013 and 1979-2001 June-August averages of the mean of (a) Geopotential height (m), (b) surface precipitable water (kg/m2), (c) 1000mb air temperature (°C), (d) sea surface temperature (°C), (e) 1000mb Specific Humidity (g/kg) from the NCEP reanalysis dataset, and (f) precipitation (mm/day) from the GPCP dataset.

3.6 Summary and Conclusions

Analysis of the 1979-2013 North American summer CAPE data shows that there have been statistically significant change points (years) detected in CAPE data over the 2000-2003 period for most areas in the Great Plains, Rockies, Great Lakes, northeastern Atlantic coast of US, and southern parts of Ontario and Québec. A trend analysis in CAPE and extreme precipitation indices was conducted for the 1979-2013 period in areas where no statistically significant change point was detected in CAPE data, but in two periods, 1979-2001 and 2002-2013, if statistically significant change points in CAPE were detected. Increasing trends in CAPE were detected in areas along the Atlantic and Gulf coastal plains, eastern and northern Atlantic coast of the US, the Great Lakes, parts of southern Ontario, Québec, southern Alberta, Saskatchewan, and Manitoba. Similarly, increasing trends were also detected in single or multiple event extreme precipitation indices (RX1day, RX5day, and R20mm) over much of northeastern Atlantic coast of the US and southern Canada, parts of the Atlantic and Gulf coastal plains, the Canadian Prairies and the Great Plains. Further, the Spearman rank correlation between CAPE and extreme precipitation indices are predominantly positive, of which about 45% is statistically significant, which demonstrates the relationship between CAPE and extreme precipitation of southern Canada and the USA.

In contrast, most parts of the US mid-west and areas west of the Rockies experienced modest increasing or decreasing trends in both CAPE and extreme precipitation indices. Increasing trends in 2m average air temperature were mainly detected for GHCN stations analyzed in the study, with a mean trend ranging from 0.1 to 0.3 ˚C/decade for US and southern Canada. Furthermore, increasing trends in the summer surface specific humidity closely resembled the detected trends in CAPE data. The observed increase in surface 2m air temperatures and in surface specific humidity

could therefore be the major cause for increasing trends observed in extreme precipitation indices and CAPE over the summer of 1979-2013 in much of eastern US and some parts of southern Canada (Berg et al., 2013; Lenderink and Van Meijgaard, 2008; Utsumi et al., 2011). To some extent, detected changes on surface precipitable water and specific humidity from the NCEP reanalysis and GPCP datasets complement the trend analysis of CAPE data, because areas where surface precipitable water and specific humidity had increased/decreased somewhat agree with areas where large statistically significant increasing CAPE trends were also detected. Ficklin et al. (2015) detected increasing trends in temperature over much of the USA but decreasing trends in precipitation and specific humidity over large areas in southwestern US for 1979-2013 and also increasing trends in droughts in south-western US and parts of Texas which also complements our results on detected decreasing trends in extreme precipitation, particularly in northern and eastern Texas for the 2002-2013 period. Our results suggest that if the detected increasing trends in temperature and specific humidity for some regions in the US and south Canada persist through the 21st century, areas in the US Atlantic corridor and some parts of southern Canada could experience more frequent and intense extreme precipitation events.

Lastly, various studies have shown that large-scale climate anomalies have also contributed to detected trends and change points in extreme precipitation of parts of North America (e.g., Tan et al., 2017, 2016). Islam and Gan (2015) showed that climate change could cause an overall decrease in the streamflow of southern Alberta, Canada, but under the combined impact of climate change and El Niño Southern Oscillation, a higher (less) decrease in the streamflow of the southern Alberta of Canada by 2050s was simulated if the climate anomaly considered was El Niño (La Niña).

Therefore, it will be interesting to investigate the possible combined impact of climate warming and large-scale climate anomalies such as ENSO on the future CAPE of North America.

Chapter 4. Spatiotemporal Changes of Drought Characteristics and Dynamic Influences of Climate Patterns in Canada

4.1 Introduction

In recent decades, there have been growing concerns regarding droughts given increased incidences in the frequency and intensity of droughts have been observed worldwide, giving rise to billions of dollars in economic losses. Moreover, the severity of drought will likely increase by the end of the 21st century for many regions (Dai, 2013; Wilhite, 2000). For example, the severe drought across northern China in 1997 resulted in 226 days of zero flow in the lower reach of the Yellow River (Cong et al., 2009), and another drought in 2000 damaged more than 40 million hectares of crops (Yu et al., 2014). From the trend analysis, Joshi *et al.* (2016) found that drought occurrences increased significantly in the northeast and central India over the second half of the 20th century. In Mexico, Escalante-Sandoval and Nuñez-Garcia (2017) suggested that climate change under RCP 4.5 and 8.5 scenarios would significantly increase the duration and intensity of droughts. Meanwhile, an analysis of the spatial and temporal characteristics of droughts in the continental United States (US) also revealed that drought duration, severity, and intensity have increased in the western and eastern US over the past century (Ge et al., 2016). On the whole, the global percentage of dry areas has increased by 1.74% per decade from 1950 to 2008 (Dai, 2011a).

Drought is a creeping recurrent natural hazard but unfortunately, there is no easily identifiable onsets and terminations. It is an extreme climatic phenomenon that can last for weeks, months, or even years, and the number of people affected by drought and the spatial extent of drought are typically larger than that of other natural hazards such as floods and hurricanes (Ge et al., 2016). As mentioned in the fifth assessment report (AR5) of the Intergovernmental Panel on Climate

Change (IPCC), drought is defined as "a period of abnormally dry weather long enough to cause a serious hydrological imbalance", but it is a relative term that requires the specification of the appropriate precipitation-related activity (IPCC, 2014).

Wilhite and Glantz (1985) classified droughts into four categories: a) meteorological drought, b) hydrologic drought, c) agricultural drought, and d) socio-economic drought. This study will focus on meteorological drought, which is defined as a deficiency of precipitation across a region during a certain time period (Zhang, 2012), as it is a precursor of hydrological, agricultural, and socio-economic droughts. To quantify a drought, drought indices have been widely applied because they can provide a comprehensive delineation of drought, making drought characteristics such as duration, severity, and intensity measurable (Jiang et al., 2014b). More importantly, these indices allow for direct comparison between regions of different climatic conditions. The commonly used meteorological drought indices include the Palmer Drought Severity Index (PDSI) (Palmer, 1965), the Crop Moisture Index (CMI) (Palmer, 1968), the Standardized Precipitation Index (SPI) (Mckee *et al.*, 1993, 1995), the self-calibrating PDSI (sc_PDSI) (Wells et al., 2004), the Reconnaissance Drought Index (RDI) (Tsakiris et al., 2007), the Standardized Precipitation Evapotranspiration Index (SPEI) (Vicente-Serrano et al., 2010), and the Water Surplus Variability Index (WSVI) (Gocic and Trajkovic, 2015).

Specifically, in Canada, droughts have been identified as one of the most damaging natural disasters that have enormous impacts on agriculture, industry, municipal services, and human health, among other sectors. For example, the 2001–2002 drought in the Canadian Prairies (CP) swept almost the entire southern part of the country, and it was one of the top ten worst droughts

observed over the instrumental period (Bonsal and Regier, 2007). In Alberta, crop producers lost $413 million and $1.33 billion in 2001 and 2002, respectively, while the estimated reduction in crop production in Saskatchewan accounted for losses of $925 million and $1.49 billion in 2001 and 2002, respectively (Wheaton et al., 2008). Furthermore, the drought that occurred in the spring and summer of 2015 is noteworthy in terms of its severity, extent, and impacts. Large areas in southern British Columbia were assigned the highest drought rating, and the Alberta government designated the province as an Agricultural Disaster Area (Szeto et al., 2016). Moreover, the extreme dry and warm conditions led to one of the most active and persistent wildfire seasons for western Canada, and some rivers ran at their lowest historic flow levels in 100 years (CMOS, 2016).

These aforementioned overwhelming drought conditions have been major concerns to both the Canadian government and the general public in recent decades. As a result, many studies have evaluated the dryness or wetness variations over Canada using different drought indices. For example, Quiring and Papakryiakou (2003) compared four agricultural drought indices, whose results revealed that the Z-index (derived from the Palmer model) was better for measuring agricultural drought and predicting crop yield during growing seasons from 1920 to 1999. Gobena and Gan (2013) who assessed the trend in summer moisture availability in western Canada using the sc_PDSI detected a significant increasing dryness and wetness in the CP and west of the continental divide, respectively, from 1950 to 2003. Using PDSI and SPI, Bonsal *et al.* (2012) assessed the variability of summer drought duration and intensity in the CP, and they pointed out the necessity of considering the impact of climate warming to evaluate future droughts. Various studies have been conducted regarding droughts in the CP, but so far only limited research has

been conducted to examine the drought characteristics across Canada. Even though Asong *et al.* (2018) investigated the coherence between Canadian drought and large-scale climate oscillations using wavelet analysis, the dynamic and time-varying relationships between large-scale climate signals and Canadian drought characters have yet to be examined.

Therefore, the objectives of this study are to (1) assess the spatial and temporal variability of drought duration, frequency, area, and severity in Canada from 1950 to 2016; (2) identify subregions characterized by distinct drought behaviors; and (3) investigate the dynamic effects of large-scale climate drivers on droughts in Canada. The paper is organized as follows. The data and methods are described in Section 4.2, while Sections 4.3 and 4.4 provide the results and discussion, respectively. Summary and conclusions are presented in Section 4.5.

4.2 Data and Methods

4.2.1 Data

In this study, we used the SPEI for drought identification and evaluation. The monthly precipitation and potential evapotranspiration data from 1950–2016 with a spatial resolution of $0.5° \times 0.5°$ in latitude and longitude were obtained from the Climatic Research Unit Version 4.03 (CRU TS4.03) (http://www.cru.uea.ac.uk/data/). The CRU TS dataset has been adopted by IPCC as it has undergone strict time uniformity tests in data reconstruction, has a high spatial resolution, and a long time series (Q. Wang et al., 2014). Potential evapotranspiration (PET) is taken from the CRU TS dataset, in which PET was estimated using the FAO-56 Penman-Monteith method (Harris et al., 2014) considered to be an accurate and robust PET equation (Guo et al., 2018b).

The CRU dataset has been widely applied in drought analysis. For example, Guenang and Mkankam Kamga (2014) found that the SPI calculated using the CRU exhibits similar results with those calculated from station data in Cameroon from 1951 to 2005. Based on the CRU dataset, Guo *et al.* (2018) examined droughts in Central Asia and found a tendency towards more dryness after 2003 over the period 1966-2015. Hu *et al.* (2018) found that the CRU dataset performed better in capturing drought events in central Asia than the Global Precipitation Climatology Centre (GPCC) and Willmott and Matsuura (WM) precipitation datasets. In addition, Gobena and Gan (2013) used gridded vapor pressure, cloud cover, and wind speed data from the CRU dataset to calculate PET in western Canada. The CRU data has been used to validate model simulated precipitation and drought characteristics over the CP (PaiMazumder et al., 2013). Swain and Hayhoe (2015) used the CRU data to compute historical SPI index to assess how spring and summer drought will change over North America. Moreover, Rapaić et al. (2015) evaluated the performance of eight gridded datasets (CANGRD, CRU-TS3.1, CRUTEM4.1, GISTEMP, GPCC, GPCP, HadCRUT3, and UDEL) and eight reanalyses (20CR, CFSR, ERA-40, ERA-Interim, JRA25, MERRA, NARR, and NCEP2) for the Canadian Arctic, and they found that CRUTS3.1 agreed most closely with CANGRD in all seasons.

To study the influence of various climate patterns on drought conditions, we have selected certain large-scale climate oscillations that have contributed to the precipitation and temperature variability over Canada (Coulibaly, 2006; Tan et al., 2016; Yang et al., 2019). For example, monthly indices of El Niño–Southern Oscillation (ENSO), Pacific Decadal Oscillation (PDO) (https://www.esrl.noaa.gov/psd/gcos_wgsp/Timeseries/), Pacific-North American Oscillation (PNA), Atlantic Multi-decadal Oscillation (AMO), Arctic Oscillation (AO)

(https://www.esrl.noaa.gov/psd/data/climateindices/list/), and solar activity represented by sunspots (http://sidc.oma.be/index.php3) were selected.

4.2.2 The Runs Theory

Diverse drought conditions are characterized in terms of frequency, duration, severity, and intensity. To provide an analytical solution to drought events, Yevjevich (1967) proposed the runs theory for identifying drought parameters. A run is defined as a portion of the time series of a variable, in which all values are either less or greater than the selected truncated value; accordingly, it is referred to as either a negative or a positive run. Drought frequency (DF) is the number of drought events occurred in the period considered; drought duration (DD), expressed in months, is the duration in which a drought parameter is continuously less than the critical level; and drought severity (DS) is the cumulative deficit of a drought parameter below the critical level. More details on drought parameters can be referred to Mishra and Singh (2010).

4.2.3 The Standardized Precipitation Evapotranspiration Index (SPEI)

PDSI is a milestone in the development of drought indices as it integrates prior precipitation, moisture supply, runoff, and evaporation demand at the surface level. Nevertheless, it suffers from having a fixed temporal scale and an autoregressive characteristic, whereby index values have a long-term memory of previous conditions (Vicente-Serrano et al., 2010), even with the improved sc_PDSI (Zhao *et al.*, 2017). The SPI, transformed from a precipitation time series using a probabilistic method, can be estimated at different time scales which allow drought events to be compared across time and space (Y. Wang et al., 2017). However, SPI is criticized for only using

precipitation data without including other important climate variables such as temperature, water balance, and wind speed.

To address the shortcoming of SPI, SPEI is devised to combine the multi-temporal nature of SPI and the sensitivity of PDSI in providing a more comprehensive approach to investigate the effect of global warming on drought conditions. In this study, SPEI is based on monthly climatic water balance, the difference between precipitation and potential evapotranspiration. (Vicente-Serrano et al., 2010). Since SPEI could indicate water deficits caused not only by precipitation shortages but also by excessive evapotranspiration, it is a robust index for drought monitoring and analysis in the context of climate change at global and regional scales. Details about SPEI have been extensively described (Beguería et al., 2014; Vicente-Serrano et al., 2010). On a global scale, Wang *et al.* (2014) studied the changing characteristics of severe droughts based on the SPEI and revealed an overall increasing trend in the global extent of drought areas from 1902 to 2008.

A 3-month SPEI index for a given month is based on the current month and preceding two months, e. g., the 3-month SPEI in February represents the December-January-February precipitation and PET. Thus, the 3-month SPEI values for February, May, August, and November were used in the seasonal analysis for winter, spring, summer, and autumn, respectively, whereas the 12-month SPEI values for December were used in the annual analysis (He et al., 2015). Table 4.1 shows the classification of drought based on SPEI values.

Table 4.1 Classification of SPEI drought category.

Drought category	Index value
Mild drought	-1.0 to -0.5
Moderate drought	-1.5 to -1.0
Severe drought	-2.0 to -1.5
Extreme drought	⩽-2.0

4.2.4 Trend Detection

The rank-based non-parametric Mann-Kendall (MK) trend test (Kendall, 1948; Mann, 1945) was applied to detect trends in the SPEI time series. As the autocorrelation can affect the probability of detecting trends, we have used the modified MK trend test which subtracts a trend estimator from the original time series to eliminate the effect of autocorrelation (Hamed and Rao, 1998). The modified MK test was then applied to the SPEI time series, and trends with p-values less than 0.05 were considered statistically significant. Trend magnitudes were evaluated using the non-parametric Sen's slope estimator (Gan, 1998; Sen, 1968) and abrupt change points were detected using the Pettitt test (Pettitt, 1979).

4.2.5 Drought Regionalization

Due to the possible impacts of complicated topographical properties and diverse climate types within Canada, the study area was divided into different homogeneous sub-regions. In this study, k-means clustering was conducted on seasonal SPEI to partition regions into mutually exclusive sub-regions, and the optimal number of clusters was determined using the R package "NbClust" (Charrad et al., 2014). The package provides 30 validity indices (e.g., Gap Statistic, Silhouette index, etc.) to determine the number of clusters in a dataset based on different distance measures

and aggregation methods. For each index, NbClust proposes the best number of clusters and we can then compare all indices to choose the number of clusters.

Typically, k-means clustering can produce distinct clusters with the aim of (1) minimizing variability within clusters and (2) maximizing variability among clusters (Santos et al., 2010). Gong and Richman (1995) stated that nonhierarchical methods, such as the k-means algorithm, outperformed hierarchical methods (Ward's method and average linkage method) when dealing with precipitation data. Given the large number of grids (over 6000) in the dataset, k-means clustering provides a more decent partition result. To investigate the spatial and temporal variability of droughts in Portugal, Santos *et al.* (2010) applied k-means clustering to the SPI series and found three clusters. Meanwhile, Zhang et al. (2001) used the k-means clustering to assess the spatial and temporal characteristics of heavy precipitation events over Canada. In order to study the pooled frequency analysis of droughts in the CP, Sadri and Burn (2014) also applied the k-means clustering to form sub-regions. More recently, Liu *et al.* (2018) partitioned a study area by k-means clustering to study the long-term change of PET in China from 1961 to 2013.

4.2.6 Bayesian Dynamic Linear Model

To assess the time-varying influences of large-scale climate drivers on drought, the Bayesian Dynamic Linear (BDL) model from the R package "dlm" was used (Petris, 2010). Unlike the traditional linear regression which has static regression coefficients, BDL is able to model the dynamic and time-varying relationships between climate drivers and drought, and therefore it has higher accuracy than the traditional linear regression (Nguyen and Galelli, 2018). BDL has been widely applied to identify the time-varying characteristics of time series in hydrology and climate

research. For example, Ciupak *et al.* (2015) used BDL in modeling the annual hydrographs and 1-, 2-, and 3-day lead time streamflow forecasting in Poland. Gao *et al.* (2017) applied BDL to assess the dynamic influence of ENSO, IOD, PDO, NAO, and AMO on extreme regional precipitation in China from 1960 to 2014. However, only limited studies have employed the BDL model in drought analysis.

The BDL model can be described as follows (T. Gao et al., 2017; Petris et al., 2013):

$$\begin{cases} y_t = \alpha_t + x_t\beta_t + \nu_t, & \nu_t \sim N(0, V_t) \\ \alpha_t = \alpha_{t-1} + \omega_{\alpha,t}, & \omega_{\alpha,t} \sim N(0, W_{\alpha,t}) \\ \beta_t = \beta_{t-1} + \omega_{\beta,t}, & \omega_{\beta,t} \sim N(0, W_{\beta,t}) \end{cases} \quad (4\text{-}1)$$

where y_t is the response variable (a drought index), x_t is the covariate (a climate pattern), and α_t and β_t are the dynamic intercept and slope coefficients, respectively, at time t.

4.3 Results

4.3.1 Homogenous Regions

Given Canada has many climatic regimes and the huge orographic effects of the Canadian Rockies, Canada has experienced a wide range of spatial variability in precipitation and temperature (Tan et al., 2018b). Results show that grids belonging to the same group are generally located in a continuous region, implying that the temporal distribution of the SPEI is spatially coherent. From Figure 4.1, four subregions were identified in Canada, namely, subregion 1 (S1) in the south and southeast, sub-region 2 (S2) in Arctic Canada, sub-region 3 (S3) in the west coast, and sub-region 4 (S4) in north-central. Figure 4.2 shows the mean annual SPEI series for the four sub-regions of

Canada. Among them, both S1 and S4 have a significant increasing trend from 1950 to 2016, indicating that annually droughts in the south and north-central Canada has become less severe.

Using k-means clustering, Zhang et al. (2001) studied heavy precipitation events over Canada (excluding the high Arctic) during 1900-98 and found four clusters for heavy rainfall during spring and two clusters for heavy rainfall and snowfall in other seasons. It is noted that their cluster delineating southern Canada extends from southern British Columbia, through southern Canadian prairie, to southeastern Canada, which generally agrees with cluster S1 in our study. Moreover, Whitfield et al. (2002) examined the variability in the seasonality of temperature and precipitation in Canada and determined that the variations in climate are occurring at a broader scale than the local climate regime: most of the temperature and precipitation clusters span one or more ecozones despite their different climatic conditions. This could be related to large-scale atmospheric circulation changes affecting regions much larger than single climatological or ecological zones.

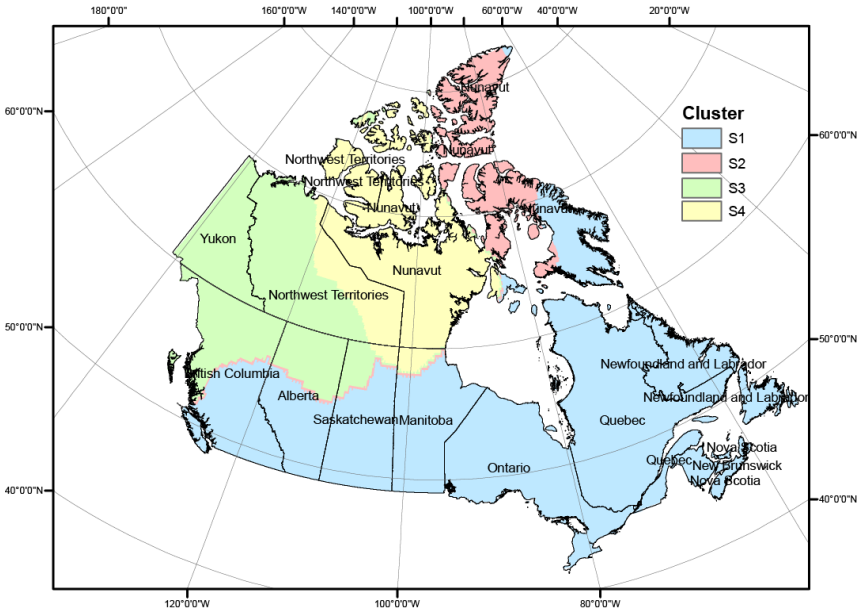

Figure 4.1 Study area and spatial distribution of four subregions.

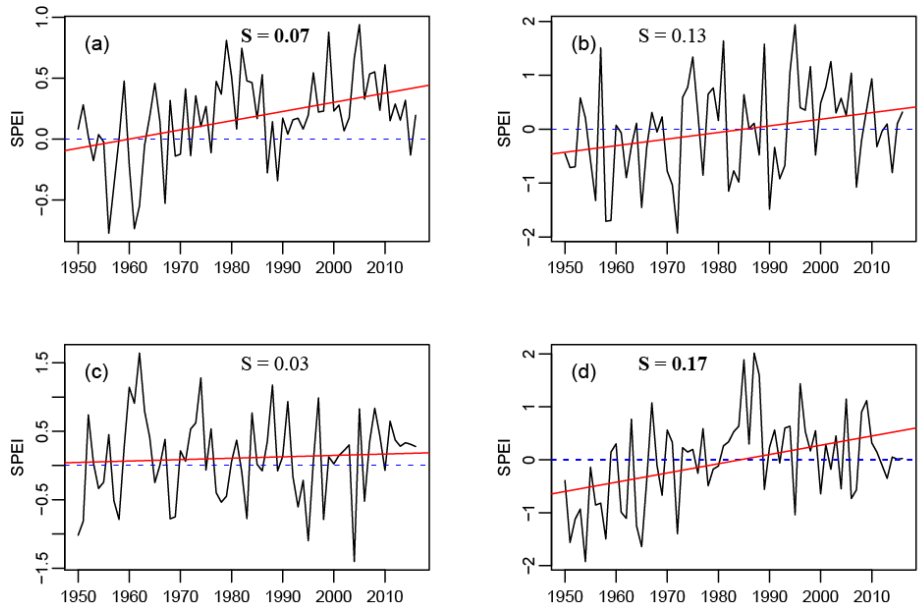

Figure 4.2 Annual SPEI series for four subregions: S1 (a), S2 (b), S3 (c), and S4 (d). The red line is the linear trend and S is the trend using Sen's slope (significant values are in bold).

4.3.2 Seasonal Drought Trends

To further study the temporal evolution of drought, the MMK test was employed to estimate the SPEI trend in each season. Figure 4.3 presents the spatial distribution of the MMK trend statistic of the seasonal SPEI. In general, droughts show remarkable spatial variations in different seasons; however, positive trends dominate over major parts of Canada while most negative trends in spring, summer, and autumn are not statistically significant, which is consistent with the results in Figure 4.2. In spring, scattered significant increasing trends are predominantly found in S1 and S4. In summer, S3 exhibits more significant increasing trends compared with that in Figure 4.3(a). Furthermore, southern Alberta and Saskatchewan (S1) have exhibited more negative trends in summer compared with that in spring. Moreover, the majority of decreasing trends are located in the southeast, although they are not significant. In autumn, the spatial distribution is similar to that for spring, except that there are more negative trends in Alberta, east S2, and east S3, whereas for

winter (Figure 4.3d), a prevalent decreasing trend appears mostly in southwest Canada, which means that among the four seasons, winter has an apparent drying tendency.

From 1950 to 1998, Zhang *et al.* (2000) found that precipitation in Canada has increased by 5% to 35%, but with significant negative trends found in the southwest during winter (Mekis and Vincent, 2011). In addition, warming in the south and west (Bonsal et al., 2017) and cooling in the northeast is evident in winter and spring. Together, these trends could have contributed to the tendency of drying detected in southwest Canada in winter and wetter spring detected in northern Canada. Using the singular value decomposition (SVD), Shabbar and Skinner (2004) reported that the first SVD pattern of the summer PDSI in Canada exhibited both interannual and decadal variability with a general wetting trend from 1940 to 2002. Meyn *et al.* (2010) analyzed trends in wildfire and summer drought in British Columbia from 1920 to 2000 and revealed that the summer sc_PDSI exhibited a positive trend, which significantly contributed to the decrease in wildfire frequency and area burned. Similarly, Gobena and Gan (2013) reported that summer moisture availability in southern British Columbia has shown a significant increasing trend from 1950 to 2003, which corresponds with the increasing trend in Figure 4.3(b). In addition to the previous research, our results further emphasize that the drought risk in winter has worsened.

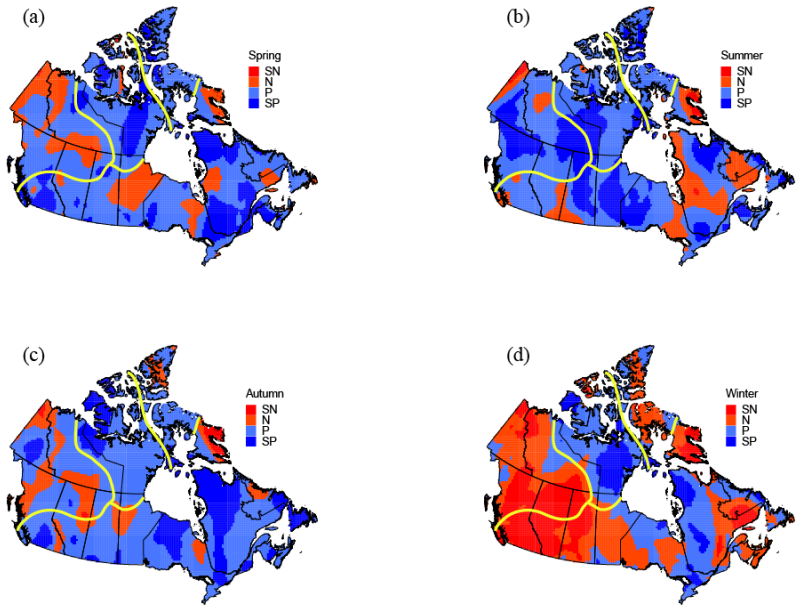

Figure 4.3 Spatial distributions of the MMK trend statistic of the seasonal SPEI at 95% significance level. The abbreviations are P: positive trend, SP: significant positive trend, N: negative trend, and SN: significant negative trend. The yellow curves denote the cluster boundaries.

4.3.3 Changes in Drought Frequency (DF)

Changes in the drought frequency (SPEI<-1) over Canada were investigated for 5-year (lustrum) periods (1950–1954, 1955–1959, etc.) in 1950–2016, as shown in Figure 4.4. Overall, there were more drought events during the first two lustrums (1950–1959) than the last two lustrums periods (1996–2015) for all regions. Additionally, S1 and S4 experienced significant decreasing trends of -0.15 and -0.32 per decade, respectively. Spinoni *et al.* (2014) reported that North America has experienced a significant decrease in drought frequency over 1951–2010, which they estimated using SPI, and is verified in this study using SPEI (Figure 4.4).

Among all sub-regions, droughts in S1 are less frequent (4.7/lustrum), compared with S2 (6.0/lustrum), S3 (5.1/lustrum) and S4 (6.2/lustrum). On the other hand, as pointed out by Bonsal *et al.* (2011a), the low frequency has generally led to a lower adaptive capability, thus making the

region more vulnerable to the impacts of drought (Hryciw et al., 2013). For example, the CP and interior valleys of British Columbia are susceptible to drought primarily due to their location in the leeward side of major mountain ranges, with low precipitation of high spatial and temporal variability. Although the drought frequency in northern Canada is higher (S2 and S4), it is less of concern largely because of its low population density and a lack of agricultural activity. Even though significant warming has been reported over Canada (Zhang et al., 2000), it has not resulted in an increase in the drought frequency, which tends to exhibit decadal variability consistent with that of precipitation (Bonsal et al., 2011).

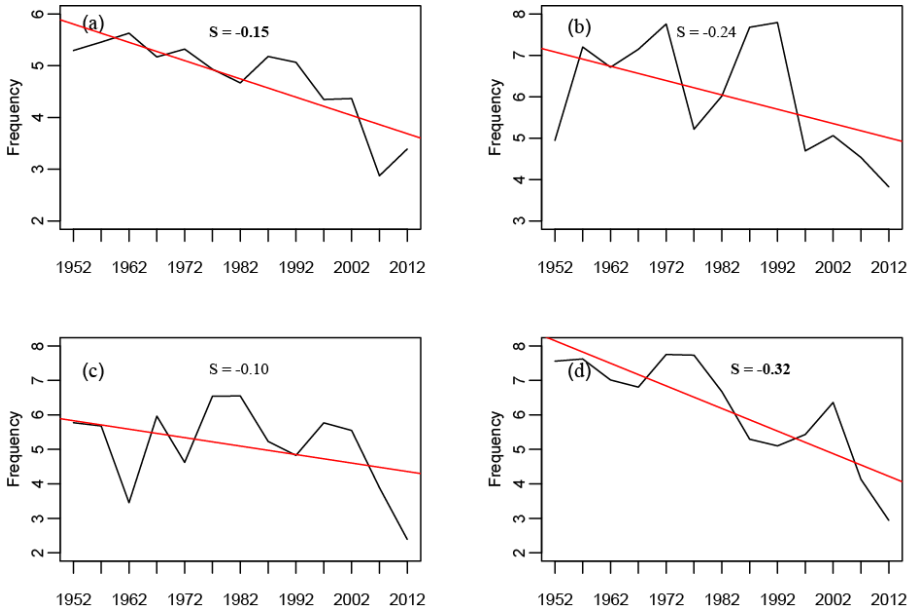

Figure 4.4 Temporal variation of quinquennial drought frequency for S1 (a), S2 (b), S3 (c), and S4 (d). 1952 denotes 1950–1954 and 1962 denotes 1960–1964, etc. The red line is the linear trend and S is the trend using Sen's slope (significant values are in bold).

4.3.4 Changes in Drought Duration

4.3.4.1 Longest drought duration (LDD)

In this study, the longest drought duration (LDD) is defined as the longest consecutive months with SPEI<-1 over 1950–2016. From the spatial distribution of LDD shown in Figure 4.5(a), it is

evident that the LDD in most parts of Canada is less than 12 months. In addition, it seems that the LDD in Canada has a dipolar pattern: northern Canada tends to have a longer LDD (12–24 months), whereas the CP and southeast region have a shorter LDD (3–6 months). The decadal spatial distribution of the occurring time of LDD in Figure 4.5(b), illustrates that S2 and S4 (northeast Canada) have been stricken by their LDDs primarily in the 1950s and 1960s. However, the CP and east S1 have been affected in more recent decades (after the 1990s), suggesting that south and east Canada have experienced more long-lasting droughts in the past few decades.

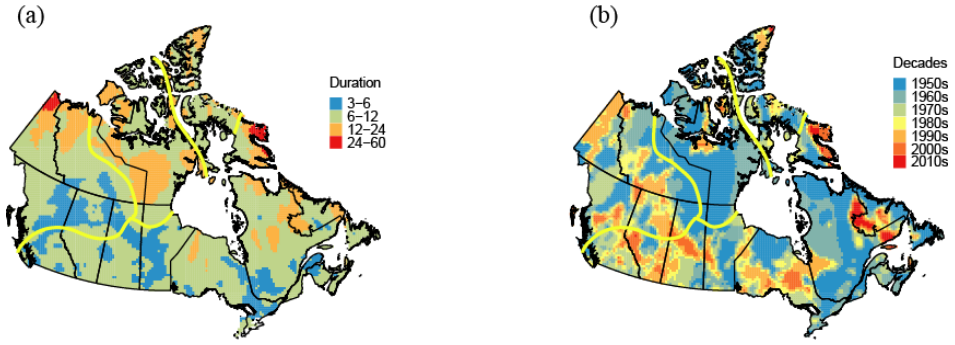

Figure 4.5 Spatial distribution of (a) the longest drought duration and (b) the longest drought duration occurring time.

4.3.4.2 Total drought duration (TDD)

Figure 4.6(a-d) depicts the temporal variations of the annual TDD for the four sub-regions. Except for S3 (Figure 4.6c), all sub-regions (S1, S2, and S4) have exhibited significant decreasing trends at -0.20 month/decade, -0.42 month/decade, and -0.69 month/decade, respectively. Moreover, S1, S2, and S4 all experienced short-duration droughts circa the 1980s; in contrast, S3 encountered droughts of short durations in the 2000s. A change point analysis (Table 4.2) shows that Canada's west coast underwent an abrupt change in the 2000s, whereas the remainder of the country was subjected to an earlier abrupt change in TDD in 1980s.

4.3.4.3 Severe and extreme drought duration (SEDD)

Figure 4.6(e-f) depicts the temporal evolution of the annual SEDD ($\mathrm{SPEI} < -1.5$) for four sub-regions. Unlike the TDD, the annual SEDDs exhibit a significant decreasing tendency for all sub-regions at -0.11 month/decade, -0.32 month/decade, -0.14 month/decade, and -0.48 month/decade, respectively. In addition, the annual SEDDs have experienced change points similar to the annual TDD (Table 4.2). Consistent with Figure 4.6(d), S4 has the largest decreasing SEDD trend among all sub-regions. In addition, given the decreasing trends estimated using Sen's slope for S2 (-0.42 month/decade and -0.32 month/decade), S4 (-0.69 month/decade and -0.48 month/decade), and S3 (-0.19/decade and -0.14/decade) in Figure 4.6, it is evident that severe and extreme events have contributed significantly to the general decline of TDD in northern Canada.

Among all sub-regions, the mean TDDs in S1 are less persistent (2.1 month/year), compared with S2 (3.2 month/year), S3 (2.2 month/year) and S4 (3.1 month/year). However, the CP suffered one of the most severe and prolonged droughts in Canadian history from 1999 to 2005 (Greene et al., 2011), which was well captured by the SPEI in Figure 4.5(b). Furthermore, the region that experienced the LDD in the CP was predominantly located in Alberta and Saskatchewan (S1), which is also consistent with Greene *et al.* (2011). From Figure 4.5(a), the droughts in southern Ontario and Quebec are typically short in duration, and they tend to occur in more recent decades.

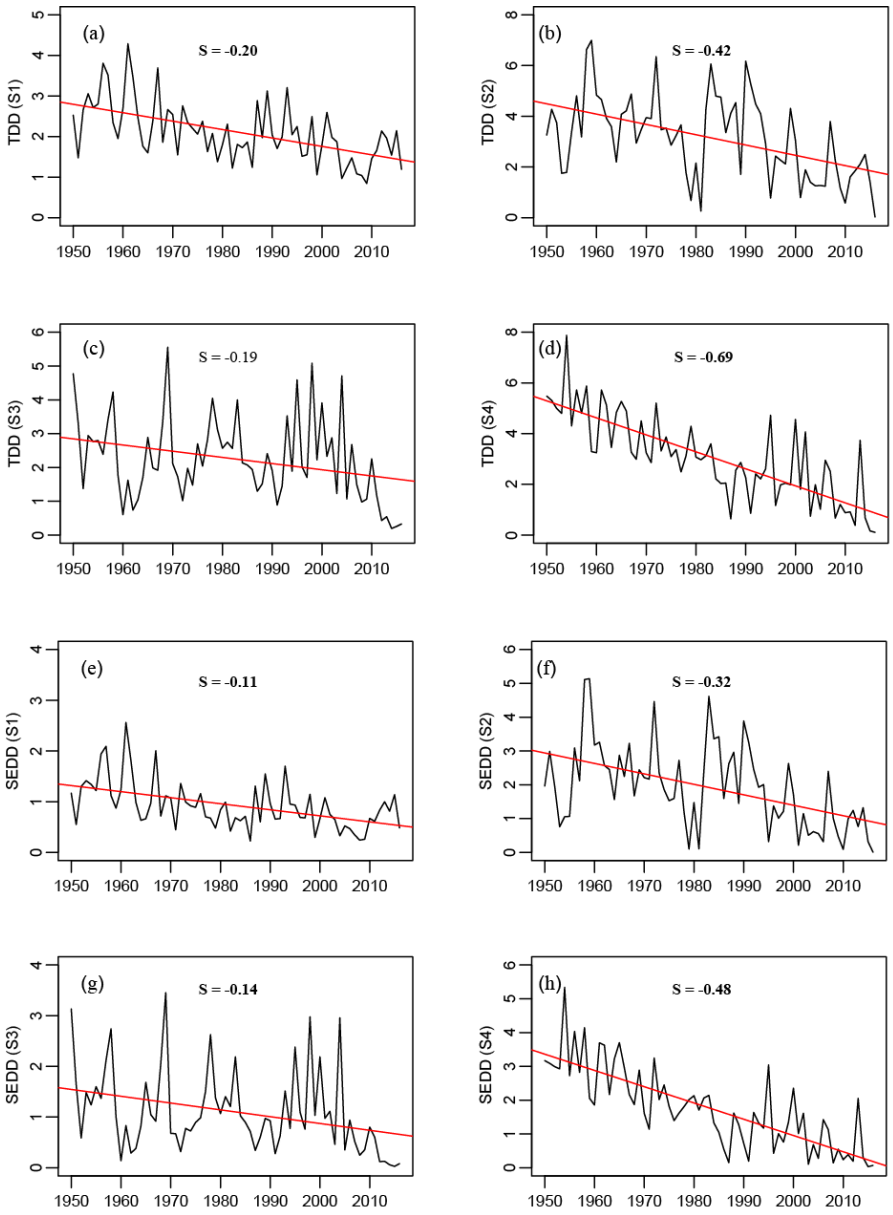

Figure 4.6 Temporal variation of annual total drought duration (TDD) (a, b, c, d) and severe-extreme drought duration (SEDD) (e, f, g, h) for S1, S2, S3, and S4. The red line is the linear trend and S is the trend per decade using Sen's slope (significant values are in bold).

4.3.5 Changes in Drought Area

4.3.5.1 Total drought area (TDA)

The annual temporal variability of the TDA during 1950–2016 over different sub-regions is presented in Figure 4.7(a-d). The TDA is the percentage of grids with $\mathrm{SPEI} < -1$ over the total

grids. The most significant decreasing trend is found in S4, with a rate of -6%/decade (Figure 4.7d). Over the study period, TDAs are more widespread in S2 and S4 (24% and 23%, respectively), whereas TDA in S1 is the lowest (15%). On an annual time scale, widespread droughts have occurred in the 1950s for all sub-regions. Additionally, striking droughts occurred in 1961 and 1962 for S1 (>40%), in 1965, 1972, and 1990 for S2 (>70%), in 1983, 1995, and 2004 for S3 (>50%), and in 1964 and 1965 for S4 (>70%). As shown in Figure 4.7(a), there seems to be an increasing trend in TDA after 2005 for S1; however, the magnitude is much smaller than that during the period 1950–1970. In other words, spatially less extensive droughts had occurred in Canada after 2000s. Abrupt change points of TDA also occurred in the 1970s (Table 4.2), which are similar to that of drought frequency.

4.3.5.2 Severe and extreme drought area (SEDA)

Figure 4.7(e-f) exhibits the time series of the annual SEDA (SPEI<-1.5) for the four sub-regions. Similar to Figure 4.7a and d, the most significant decreasing trends for SEDA were found in S1 (-1%/decade) and S4 (3%/decade). Moreover, SEDAs are widespread in S2 and S4 (14% and 13%, respectively) and that for S1 is the lowest (6%). Again, similar to TDA, abrupt change points appeared in the 1970s (Table 4.2). From the decreasing trends estimated by TDA and SEDA for S2 (-0.03/decade and -0.009/decade) and S3 (-0.02/decade and -0.007/decade) shown in Figure 4.7, it seems that moderate drought events occurring in recent decades have resulted in an overall decline of drought area in S2 and S3.

An overall decline in the drought areas in Canada is also detected by Van Der Schrier *et al.* (2013). As demonstrated by Szeto *et al.* (2016), the extreme drought event in British Columbia and Alberta

(western S1) in 2015 was exceptional because of its severity and extent, which was well captured by the ridge during the 2010s in Figure 4.7(a) and (e). Bonsal et al. (2012) also noted that drought conditions in the twentieth century were relatively mild when compared to the pre-instrumental period on the CP, reinforcing our findings of a general decline in the drought areas of S1 (Table 4.3).

Table 4.2 Change points of annual drought duration, drought area, and drought severity.

Subregion	Drought duration		Drought area		Drought severity	
	Total drought	Severe and extreme drought	Total drought	Severe and extreme drought	Total drought	Severe and extreme drought
S1	**1976**	**1976**	**1974**	**1972**	**1976**	**1976**
S2	**1993**	**1994**	**1972**	**1972**	**1994**	**1994**
S3	**2004**	**2004**	1983	1985	**2004**	**2004**
S4	**1983**	**1983**	**1978**	**1978**	**1983**	**1983**
Whole	**1978**	**1978**	**1972**	**1972**	**1978**	**1978**

Change points that are statistically significant are in bold.

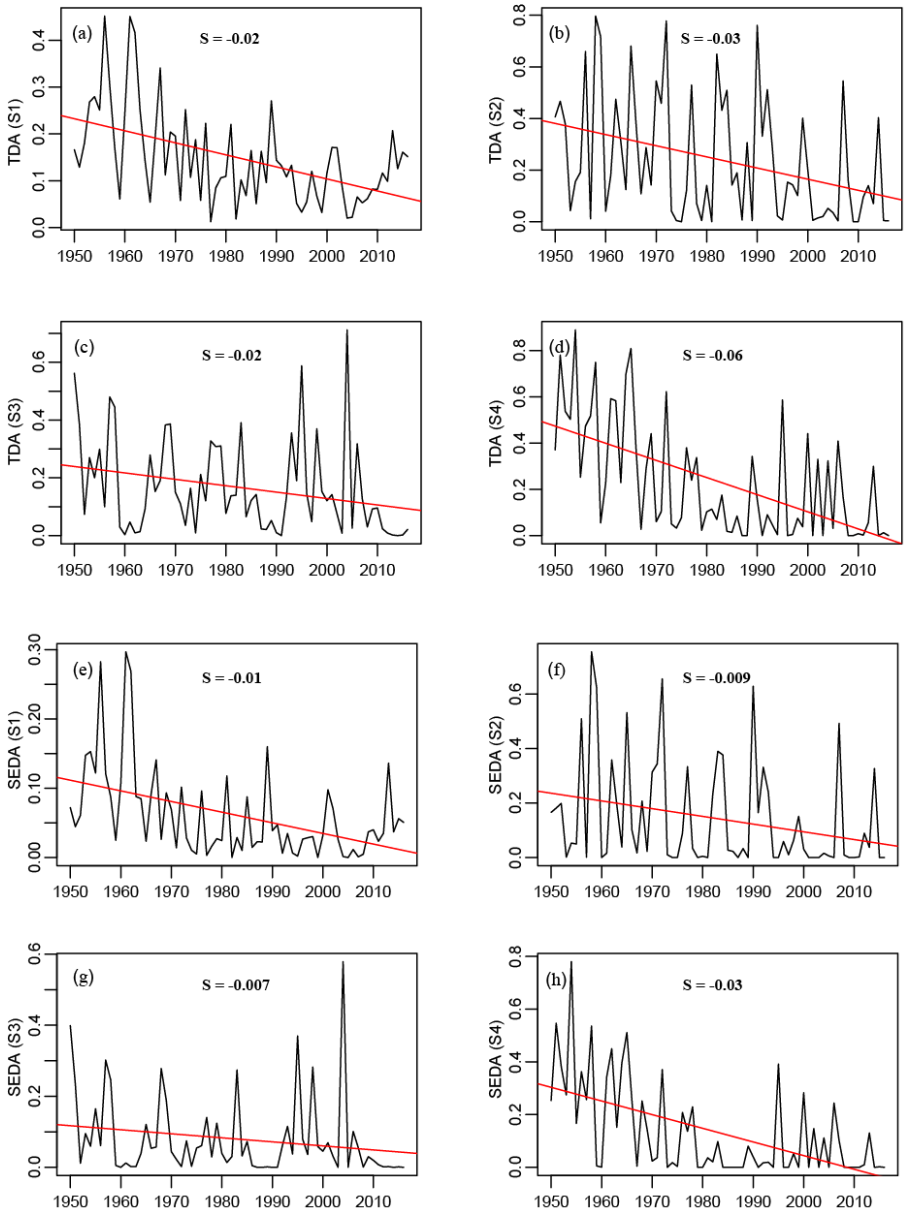

Figure 4.7 Temporal evolution of annual total drought area (TDA) (a, b, c, d) and severe-extreme drought area (SEDA) (e, f, g, h) for S1, S2, S3, and S4. The red line is the linear trend and S is the trend per decade using Sen's slope (significant values are in bold).

4.3.6 Changes in Drought Severity

4.3.6.1 Total drought severity (TDS)

TDS is defined as the absolute value of SPEI (<-1) multiplied with the duration. As shown in Figure 4.8(a-d), the annual TDS in all sub-regions has declined at -0.33/decade, -0.81/decade, -

0.35/decade, and -1.25/decade, respectively (Table 4.3), which means that the severity of drought events have generally mitigated from 1950 to 2016, especially for S4. All sub-regions suffered droughts of high-severity in the 1950s and 1995–2005 was a difficult period for S3. For S1, 1999–2005 is also marked by high severity, which has been reported by Hanesiak *et al.* (2011) and Hryciw *et al.* (2013).

4.3.6.2 Severe and extreme drought severity (SEDS)

Figure 4.8(e-f) presents the evolution of the annual SEDS (SPEI<-1.5) for four sub-regions. Coincidentally, all sub-regions have the same change points as that of TDS (Table 4.3). Similarly, all sub-regions experienced a negative trend in SEDS especially for S4 (-0.96/decade), and droughts of high-severity in the 1950s. From Figure 4.8(e), even though trends of SEDS became positive after 2005 for S1, the magnitude was small compared to that for the negative trend in 1950–1970, indicating that the 1950s was a decade impacted by severe and prolonged droughts. Given consistent negative trends estimated by the Sen's slope for S1 (-0.33/decade and -0.21/decade), S2 (-0.81/decade and -0.69/decade), S3 (-0.35/decade and -0.27/decade), and S4 (-1.25/decade and -0.96/decade) in Figure 4.8, the general decline in severe and extreme droughts have contributed significantly to the general decline of TDS across Canada over 1950-2016.

The above results agree with that of past drought studies. For example, using sc_PDSI and intermediate future climate scenarios simulated by 14 global climate models (GCMs) of CMIP5, Dai (2013) projected a large increase in wetness over high latitudes in North America. Moreover, under climate warming, summer and fall precipitation are projected to increase at high northern latitudes (Swain and Hayhoe, 2015), which would lead to wetter conditions in Canada. Choi and

Kim (2018) assessed how warming could affect spring and early summer droughts in North America and found that regions with drought relief are predominantly located in Canada and Alaska, partly due to more spring snowmelt. Based on projections from 21 GCMs of CMIP5, Swain and Hayhoe (2015) projected a pronounced increase in wet conditions across Canada in spring of the 2020s to 2080s, and the magnitude of projected changes in wetness may scale with global temperature. Even though regions such as Yukon (S3) is projected to become wetter with higher spring SPI, given the distribution of SPI is highly skewed, it could also experience prolonged dry conditions.

Table 4.3 The Sen's slope of drought duration, drought area, and drought severity

Subregion	Drought duration		Drought area		Drought severity	
	Total drought	Severe and extreme drought	Total drought	Severe and extreme drought	Total drought	Severe and extreme drought
S1	**-0.20**	**-0.11**	**-0.02**	**-0.01**	**-0.33**	**-0.21**
S2	**-0.42**	**-0.32**	**-0.03**	**-0.009**	**-0.81**	**-0.69**
S3	-0.19	**-0.14**	**-0.02**	**-0.007**	**-0.35**	**-0.27**
S4	**-0.69**	**-0.48**	**-0.06**	**-0.03**	**-1.25**	**-0.96**
Whole	**-0.32**	**-0.21**	**-0.04**	**-0.02**	**-0.56**	**-0.43**

Trends that are statistically significant are in bold and the unit is per decade.

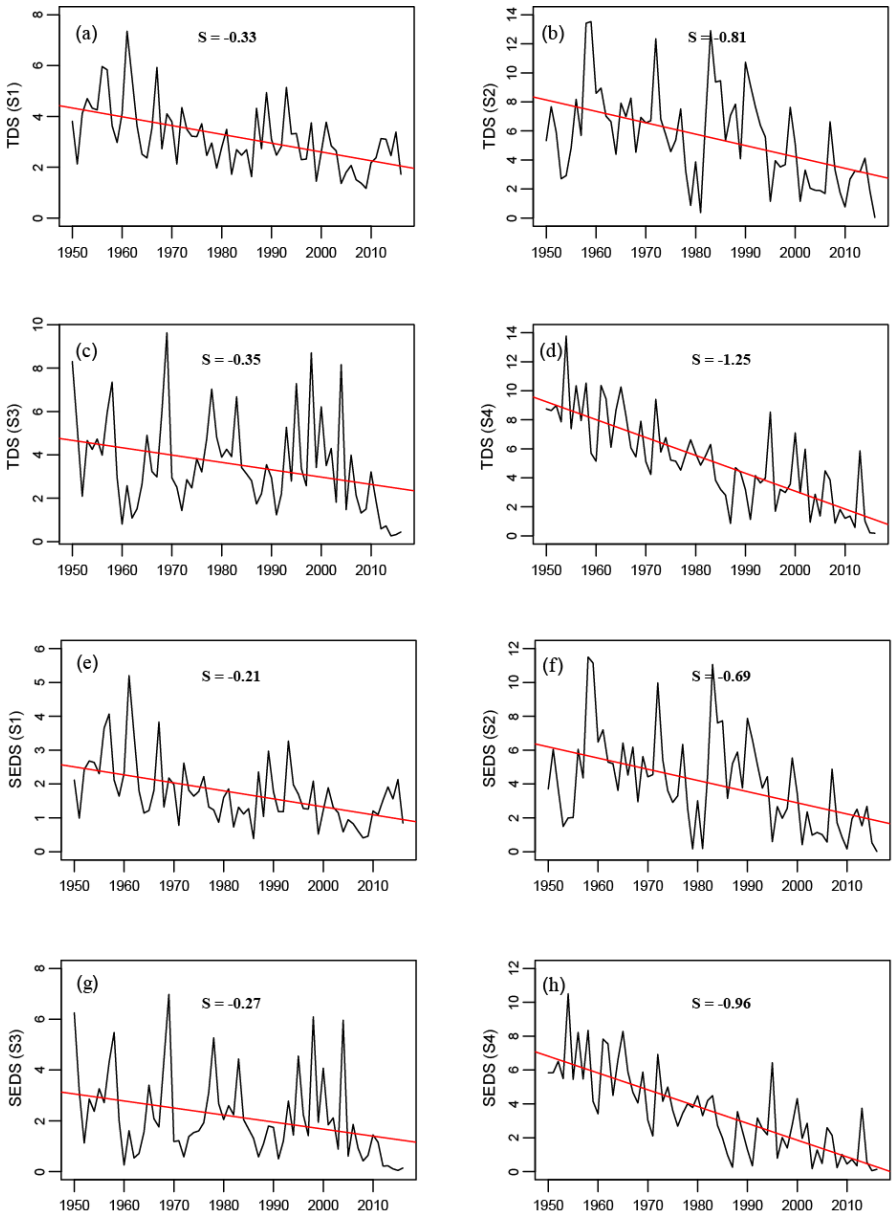

Figure 4.8 Temporal variability of annual total drought severity (TDS) (a, b, c, d) and severe-extreme drought severity (SEDS) (e, f, g, h) for S1, S2, S3, and S4. The red line is the linear trend and S is the trend per decade using Sen's slope (significant values are in bold).

4.3.7 Composite Analysis

Figure 4.9 depicts the composite mean and anomaly of precipitation and surface temperature across Canada between 1950–1979 and 1987–2016. From Figure 4.9(e), Canada has mainly experienced increasing precipitation (Vincent et al., 2015) except for some regions in the south,

which has contributed to the tendency to lower severity and frequency of droughts in Canada. The annual rainfall in Canada has increased by about 12.5% while the annual snowfall by about 4% from 1950 to 2009; however, the increase in snowfall was not consistent across the country. For example, western provinces (British Columbia, Alberta, and Saskatchewan) exhibited significant decreasing trends (Figure 4.9e) (Mekis and Vincent, 2011). In addition, higher surface temperatures were observed across Canada, especially in the north (Figure 4.9f) (Vincent et al., 2018). Therefore, these findings suggest that Canada has gradually become wetter and warmer since the 1950s.

Based on GCM outputs of CMIP5, Cook *et al.* (2014) assessed the relative contribution from changes in precipitation versus evapotranspiration to the magnitude and extent of drying induced by global warming. They show that overall more precipitation may cause the entire Northern Hemisphere to become wetter, especially in high latitudes where precipitation increase is projected to be the highest, but changes in mid-latitudes would be near neutral or marginally wetter. In contrast, an increase in PET could result in drying across all latitudes. In view of projected changes in PET and precipitation, the net result is a robust wetting occurring in NH's high latitudes (Dai, 2013). Naumann *et al.* (2018) investigated global drought conditions under different projected global warming levels. They revealed that the drought magnitude would halve with a 1.5°C warming primarily in the Russian Federation, southern Alaska, and Canada. Further, droughts are projected to be shorter in length for most land areas north of 55°N latitude, which further reinforces our findings. Therefore, the increase in precipitation is expected to substantially outweigh the impact of increased PET (resulting from increased temperature) to future droughts in Canada.

According to the Clausius–Clapeyron relationship, the atmospheric water holding capacity will increase by about 7% per K rise in temperature, and so warming will give rise to increased evaporation, atmospheric moisture, moist static energy and therefore storms are expected to be more intensive (O'Gorman and Schneider, 2009). With the Clausius–Clapeyron relationship as the basis, the 7% per K rise in water holding capacity is generally true, but different rates of increase in extreme rainfall with respect to increase in temperature have been detected (Berg et al., 2013; Lenderink and Van Meijgaard, 2008; Tan et al., 2018d), which is expected since precipitation is highly variable spatially. Contrasting drivers of precipitation change at the regional and global scales, globally there is high confidence that global mean precipitation increases ~2%/K of global mean warming (Held and Soden, 2006). Therefore likely attributed to the regional impact of global warming, the occurrences of severe and extreme droughts across the four sub-regions of Canada have generally declined over 1950-2016.

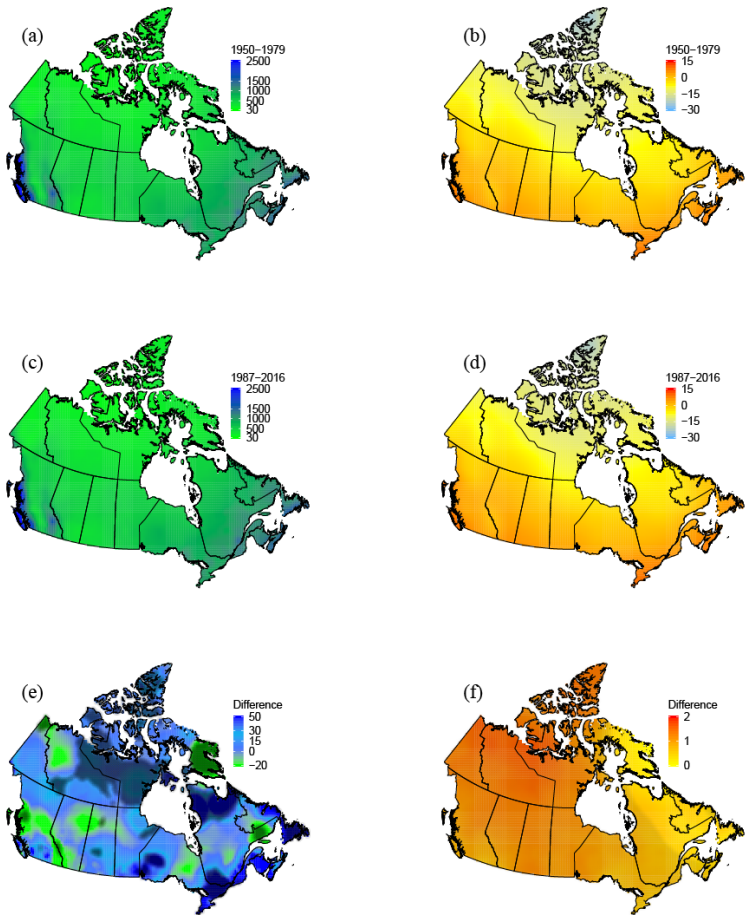

Figure 4.9 Composite mean of (a, c) precipitation, (b, d) temperature, and (e, f) their anomalies during 1950–1979 and 1987–2016. Regions with dots are at 95% significance level.

4.3.8 Dynamic Influence of Climate Drivers

Figure 4.10 presents the estimated dynamic regression slope coefficients of six climate drivers on four regional SPEI series. Figure 4.10(a) illustrates that the correlation between NINO3 and SPEI at S1 experienced a phase change from positive before 1970 to negative until 2015. However, NINO3 was negatively correlated with SPEI before 1985 (Figure 4.10s) in S4, and there was a trough circa 1970 and a ridge during the 1990s. For S3, the slope exhibited a decadal variability and gradually changed from positive to negative (Figure 4.10m). Additionally, the slope coefficients of NINO3 tend to approach 0 after 2005, implying that the effects of the ENSO weakened for all sub-regions of Canada in recent decades.

As the world's most significant inter-annual climate pattern, ENSO plays a substantial role in the variability of climate worldwide. In Canada, El Niño is typically associated with warmer and drier winters, whereas La Niña has the opposite effect. For example, the ENSO exerts a strong influence on the winter precipitation of southwest Canada and El Niño (La Niña) may lead to a 14% decrease (20% increase) in the mean winter precipitation (Gan et al., 2007). El Niño events are typically accompanied by a summer moisture deficit in most of western Canada, whereas La Niña events produce an abundance of summer moisture in extreme western Canada and in the southeastern part of the CP (Shabbar and Skinner, 2004). Our analysis further reveals the time-varying influences of ENSO on droughts in Canada. Given the large negative slope coefficient of S1 in 2001-2002 (Figure 4.10a), the strong influence of El Niño in S1 leading to a significant decline in SPEI is expected in 2001-2002, which corresponds to the severe 2001–2002 drought in the CP (Bonsal and Regier, 2007). Furthermore, the extreme drought in western Canada is also amplified by the intense El Niño episode of 2015–16 (Szeto et al., 2016).

For PDO, the slope coefficient of S1 changed from positive to negative in the 1970s (Figure 4.10b). Figure 4.10(t) depicts that PDO was negatively correlated with SPEI but its impact decreased from 1950 to 2016 in S4. Two troughs are found in both S1 and S3 circa 2000, respectively (Figure 4.10n), suggesting that PDO's effect became stronger at that time. For S2, the negative correlation was relatively stable after 2000 (Figure 4.10h). Bonsal *et al.* (1993) reported that positive PDO tends to give rise to extended dry spells during the growing season throughout the CP. Similarly, Gan *et al.* (2007) found that a positive (negative) phase of the PDO is associated with an 8% decrease (9% increase) in the mean winter precipitation in southwestern Canada (Sheffield et al.,

2013). Our results reveal that PDO is typically negatively correlated with the SPEI, which further confirms that a positive PDO contributes to drier conditions.

PNA exerted a predominant and persistent negative influence on the SPEI in S1 over 1950-2106 (Figure 4.10c), but a more positive influence in S4 (Figure 4.10u). For S2 and S3, the effects of the PNA have been typically weak: the correlation for S2 experienced a phase change circa 1980 (Figure 4.10i); and the impact of the PNA for S3 was minimal after the 1970s (Figure 4.10o), implying a reduction in the strength and a possible phase change in the future. The initiation of the positive PNA and associated positive geopotential height anomalies over western Canada results in large-scale subsidence over the region, leading to warmer and drier conditions (Bonsal and Shabbar, 2008). Given slope coefficients in S3 are predominantly negative (Figure 4.10o), while PNA was mostly in positive phases since the mid-1970s, SPEI is expected to decrease, resulting in drier climate in western Canada. The result is consistent with that of Gan *et al.* (2007) who show that a strong positive (negative) PNA would lead to a 12% decrease (9% increase) in mean precipitation in southwestern Canada.

Distinct effects of AMO are displayed in S1 and S3. For S1, the slope coefficients decreased from positive to negative circa 1980 (Figure 4.10d), but an opposite relationship is observed for S3 in 1985 (Figure 4.10p). The influence of AMO in S2 weakened over the years, although it remains positive. However, the slope for S3 changed circa 1985 (Figure 4.10p) from negative to positive. From Figure 4.10(d), the AMO warm phase in the late 1990s contributed to a negative slope that resulted in dryer conditions in S1, while the cool phase from 1960 to 1970 led to a positive slope and wetter conditions in S3, which agrees with the findings of Shabbar and Skinner (2004). In

addition, the AMO warm phase with a negative slope coefficient from 2015 to 2016 (Figure 4.10d) could stimulate drier conditions in S1, which may have further aggravated the 2015–16 extreme drought in western Canada.

The effects of AO changed from negative to positive for both S2 and S4 in 1995 and 1975, respectively. A trough appeared in S1 in 1970 (Figure 4.10e), which could mean a stronger effect of AO over S1 at that time, but after 1985 that effect decreased to a minimum until 2005. After that the slope coefficients tend to decrease, implying a reinforcing effect of AO over S1. For S3, the correlation fluctuates over 1950-2016, with a negative slope detected after 2010 (Figure 4.10q). The AO is a dominant climate driver affecting the winter temperature in eastern Canada, such that winters tend to be colder when AO is positive and vice versa (Bonsal et al., 2001). As shown in Figure 4.10(k), a phase change occurred circa 1995, showing a positive influence of AO over S2 since then.

The effects of sunspots on SPEI appear to be generally stable and predominantly negative after 1990 for S2, S3, and S4; while for S1, the influence changed from positive to negative in the 1980s, with an enhanced negative slope after the 1990s (Figure 4.10f). Noteworthy is that the slope coefficients tend to increase after the 2000s for S1, S3, and S4, indicating that the effects of sunspots have strengthened in recent decades. The solar cycles, which are driven by the sun's magnetic turbulence at an 11-year cycle, have the potential to influence climate systems on Earth (Larsen, 2005; Meehl et al., 2002). For example, using wavelet and copula analysis, Zhu *et al.* (2018) and Fang *et al.* (2018) showed that sunspot activities are closely associated with dry conditions in China. In Southern Canada, Fu *et al.* (2012) examined the combined influence of

solar activity and El Niño episodes on streamflow, and Prokoph *et al.* (2012) also found that years with major floods were most likely to occur during years with a low sunspot number. In contrast, the 1999–2005 Canadian drought occurred during a period with a high sunspot number. Sunspots are primarily negatively associated with the SPEI after the 1980s in S1 (Figure 4.10f), which further confirms that increasing sunspots could lead to a decrease in SPEI, indicating that dry events are more likely to occur during periods with high sunspot numbers.

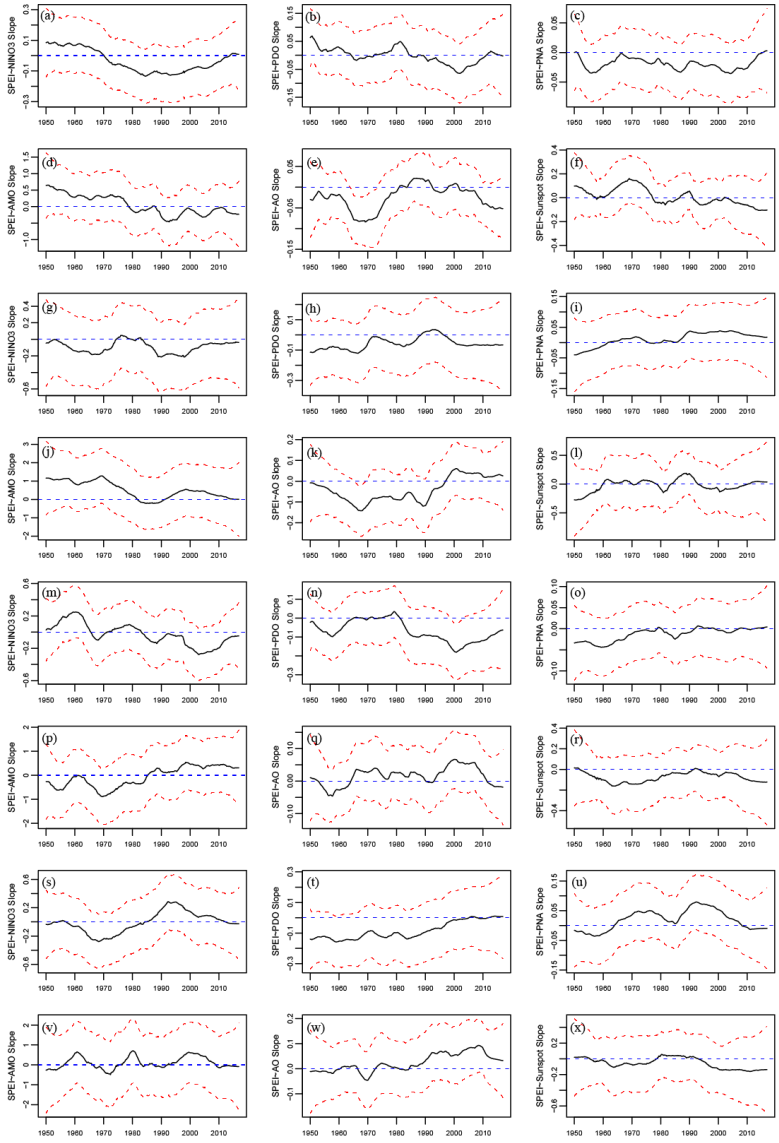

Figure 4.10 Variations in the relationship between regional SPEI and large-scale climate oscillations for S1 (a-f), S2 (g-l), S3 (m-r), and S4 (s-x). The solid black line denotes the estimated time-varying slopes, along with the 25th and 75th percentile credible interval lines (red dotted lines) from the Bayesian dynamic linear model.

4.4 Discussion

The global ocean covers over 70% of the Earth's surface and serves as a tremendous reservoir of water, energy, carbon, and other substances. It is a pivotal constituent of the climate system and interacts directly with the atmosphere (Bush and Lemmen, 2019). Various studies linking drought variability to major circulations of the Northern Hemisphere have identified a dynamic relationship over the past 300 years; however because the mechanisms linking regional climate variability with ocean-atmospheric circulation patterns are not firmly established, it remains challenging to provide a precise explanation of the cause of the atmospheric circulation shift and its dynamic influences on droughts, posing excessive challenges for predicting the onset, duration, and severity of droughts in Canada (Bonsai et al., 2005; Bonsal et al., 2017; Girardin et al., 2004a; Hanesiak et al., 2011; Tan et al., 2018c). The above results reveal the haphazard and dynamic nature of climate patterns' influence over the dryness of Canada divided into four sub-regions represented by the SPEI in 1950-2016. This is expected because climate patterns have been changing between positive and negative phases and at varying strength and frequencies, ranging from inter-annual to inter-decadal scales (Gan et al., 2007).

Figure 4.10 presents multiple phase changes for the dynamic regression slope coefficients in the 1970s, which could be attributed to the extraordinary climatic shift of the 1970s characterized by a significant shift from cooler to warmer tropical Pacific sea surface temperatures (SSTs) (Meehl et al., 2009). A number of studies have reported global-scale abrupt changes in atmospheric circulations and climate detected in the 1970s (Jacques-Coper and Garreaud, 2015; O'Kane et al., 2014). For example, the second SVD pattern of the summer PDSI in Canada displayed a decreasing

trend from 1940 to the mid-1970s, but thereafter increased abruptly (Shabbar and Skinner, 2004). As reported by Miller *et al.* (1994), the atmosphere-ocean climate system over the North Pacific Ocean abruptly changed its normal state, whereby SSTs cooled in the central Pacific and warmed off the coast of western North America. Meehl *et al.* (2009) found that the observed 1970s' climate shift may have been the result of changes in external forcing superimposed on an inherent fluctuation of the Pacific climate system, which include: (a) a reduction in the northward oceanic heat flux associated with the North Atlantic thermohaline circulation, and (b) a rapid increase in anthropogenic aerosol emissions, particularly over Europe and North America (Baines and Folland, 2007).

Droughts in southern Canada are associated with positive 500-hPa geopotential height anomalies centered over the Gulf of Alaska and Baffin Bay (Girardin et al., 2004b). Bonsal *et al.* (2001) suggested that El Niño episodes with a positive PDO are associated with strong positive winter temperature anomalies over most of Canada, which are the result of a deeper than normal Aleutian low, an amplification and eastward displacement of the western Canadian ridge, and negative 500-hPa height anomalies over the southeastern US. Girardin *et al.* (2004b) found that drought over the Abitibi Plains ecoregion (eastern Canada) displayed a shift in 1850: drought was correlated with PDO before 1850, but after which it was more correlated with the NAO, suggesting the diminishing effects of Pacific forcing (Wu et al., 2018). Moreover, the shift that occurred circa 1850 reflects a northward displacement of the polar jet stream induced by a warmer sea surface temperature along the North Pacific coast, which inhibits the outflow of cold and dry Arctic air over most of Canada and allows the incursion of air masses from the Atlantic subtropical regions. Using redundancy analysis, Girardin *et al.* (2004b) also described the changing relationship

between atmospheric circulation indices and droughts in Canada. They demonstrated that the first principal component (PC1) was negatively correlated with the PDO and positively with the NAO and Southern Oscillation (SO) from 1706 to 1998. However, for PC2, its relationship with the PDO changed from positive to negative during 1880–1979, and the effect of the SO weakened during 1850–1949.

Dai (2011b) shows that meteorological droughts often result from persistent anomalous large-scale atmospheric circulation patterns induced by anomalous tropical SST or other remote climatic conditions, and that is why many statistical methods have employed large-scale atmospheric circulations as natural precursors to predict droughts (Hao et al., 2018). However, the 1999–2005 CP drought was related to a northward extension of a persistent drought in America, instead of droughts usually attributed to distinct meridional flows over the North Pacific and North America (Bonsai et al., 2005). Furthermore, a lack of consistent positive PNA and PDO patterns during the recent most severe drought in 2001-02 differs from past droughts that tend to be associated with large-scale teleconnections (Hanesiak et al., 2011). Therefore, from a large-scale teleconnection perspective, this 1999-2005 drought is different from past droughts of the CP, which again confirms our findings on the non-steady and dynamic relationships between large-scale climate oscillations and droughts in Canada.

Similarly, Rajagopalan *et al.* (2000) who examined the teleconnection of past summer U.S. droughts to ENSO, recommended the application of the BDL model to better capture non-stationarities in the relationship between droughts and ENSO over the twentieth century. Meanwhile, from CMIP5 climate models' simulations, Coats *et al.* (2013) investigated the

teleconnection between tropical Pacific SSTs and 200 mb geopotential height in North America. They concluded that the non-stationarity of this teleconnection was associated with changes in tropical Pacific SSTs, which again highlights the role of ocean dynamics in the non-stationary nature of teleconnections observed in North America.

Except for large-scale climate oscillations, Greene *et al.* (2011) who studied cloud characteristics during the 1999–2005 drought in the CP, found that months with below-average precipitation tend to have negative cloud amount anomalies, and the occurrence of thick and medium clouds decreased with drought severity. Our results further demonstrate the dynamic influences of large-scale climate oscillations on droughts in Canada and reveal considerable changes in the relationship. It seems that the effects of the ENSO across Canada have generally weakened in the past few decades, especially after the 2000s. For S1, all large-scale climate drivers exerted more negative influences on drought variability after the 1980s, while ENSO, AMO, and sunspots underwent a phase change in 1970, 1980, and 1990, respectively. For S2, except for PDO, other climate indices are more positively correlated with SPEI after the 1990s. For S3, PDO, PNA, and sunspots are negatively correlated with drought variability. For S4, more positive relationships can be found with PNA and AO after the 1970s, and the effect of PDO weakened over 1950–2016.

4.5 Summary and Conclusions

Given understanding the spatiotemporal characteristics of drought is crucial for drought risk mitigation, this article aims to provide a comprehensive assessment of drought conditions across Canada. The CRU dataset was used to calculate SPEI for four sub-regions of Canada for 1950–2016. Spatial and temporal variations of drought duration, frequency, percent area, and severity

were investigated. The dynamic influences of large-scale climate drivers on the drought variability of Canada in terms of SPEI were also identified. The primary conclusions can be summarized as follows:

(1) The 1950s was one of the recent decades most influenced by severe and prolonged drought events. Seasonally, wetting trends dominate over major parts of Canada in spring, summer, and autumn; however, a prevalent winter drying trend has been detected in southwest Canada.

(2) For the drought frequency (DF), S1 and S4 have experienced significant declining trends. Although DF is higher in northern Canada, it is less of concern mainly because of its low population density and a lack of agricultural activity. A significant increase in temperature has been reported over Canada, but this has not resulted in an increase in the drought frequency.

(3) The longest drought duration (LDD) in Canada exhibits a dipolar pattern: the northern part of Canada has a longer drought duration, whereas the southern part has a shorter duration. In terms of TDD, the most significant decreasing trends were found in S4. Spatially, dry areas were widespread in S2 and S4. Temporally, widespread droughts occurred across Canada in the 1950s, and there was an increasing trend after 2005 for S1. For the severe & extreme drought duration (SEDD), all sub-regions exhibited a significant decreasing trend, which contributed significantly to the general decline of the total drought duration (TDD) in northern Canada.

(4) The annual total drought severity (TDS) and severe and extreme drought severity (SEDS) have also exhibited negative trends, especially for S4, implying that droughts have generally declined from 1950 to 2016. All sub-regions suffered extremely severe droughts in the 1950s. The general decline in severe and extreme droughts across Canada has resulted in the general decline of annual TDS across Canada.

(5) Our results further demonstrate the dynamic influence of large-scale climate drivers on droughts in Canada but with considerable changes in the relationship over 1950-2016, which is partly associated with the climate shift detected in the 1970s. The effects of ENSO weakened across Canada in the past few decades, especially after the 2000s; and ENSO, AMO, and sunspots experienced a phase change in 1970, 1980, and 1990, respectively. For S1, climate patterns generally exerted more negative than positive influence on the drought variability expressed in terms of dynamic regression slope coefficients after the 1980s. For S2, except for PDO, other climate indices were more positively correlated with the SPEI after the 1990s. For S3, PDO, PNA, and sunspots were negatively correlated with the drought variability, when both ENSO and AMO experienced a phase change circa 1985. For S4, more positive relationships were identified for PNA and AO after the 1970s, and the effect of PDO has weakened during 1950–2016. Overall, likely attributed to the regional impact of global warming, the occurrences of severe and extreme droughts across the four sub-regions of Canada has generally declined over the last seven decades since 1950.

Chapter 5. Changing Characteristics of Dry and Wet Spells in Canada

5.1 Introduction

Climate extremes variability including the sequencing and persistence of daily precipitation has become a fundamental issue throughout the scientific community due to its significant threats to agriculture, hydrology, energy, and terrestrial functions (Casanueva et al., 2014; Roque-Malo and Kumar, 2017). According to the Synthesis Report of the Intergovernmental Panel on Climate Change (IPCC) Fifth Assessment Report, in many mid-latitude dry regions, mean precipitation will likely decline, while in many mid-latitude wet regions mean precipitation is going to rise under the RCP8.5 scenario. Meanwhile, extreme precipitation events over most mid-latitude areas are highly likely to become more intense and more frequent as global mean surface temperature rises. As a result, global losses from climate-related extremes such as heatwaves, droughts, floods, cyclones, and wildfires have increased considerably in recent decades (Pachauri et al., 2014).

Many research projects have characterized the non-stationarity of heavy precipitation and its intensification (Bracken et al., 2015; Gizaw and Gan, 2016a; R. Jiang et al., 2016; Tan and Gan, 2017). This amplification is closely related to atmospheric warming as noted by Allan and Soden (2008), there is a direct linkage between a warmer climate and an increase in extreme precipitation events in both satellite observations and climate model simulations (Dominguez et al., 2012). For example, using six extreme indices, Gizaw and Gan (2016a) assessed the impact of climate change on future extreme precipitation and suggested a projected increase in the volume of precipitation expected in very wet and extremely wet days in southern Alberta, Canada, which could potentially increase the risk of future flooding. Except for heavy precipitation, there are studies investigating the spatial and temporal patterns of drought, which is defined as a period of abnormally dry

weather long enough to cause a serious hydrological imbalance (Pachauri et al., 2014). As one of the most disastrous types of natural disasters, drought has caused billions of dollars of damage worldwide each year (Faustin Katchele et al., 2017). Gobena and Gan (2013) investigated climate change impacts on summer moisture availability in Canada from 1941 to 2003 using the Palmer Drought Severity Index, and they reported that moisture availability in the Canadian Prairies (CP) has displayed a significant negative trend, whereas southern British Columbia has shown a significant positive trend.

Most previous studies are based on monthly precipitation; however, relying only on the monthly precipitation amount or frequency can sometimes result in misleading conclusions (Cindrić et al., 2010). For example, if an extreme precipitation event is recorded during a period that is followed by a long dry spell, one may conclude that the analyzed period was wet. The analysis for evaluating the effects of rainfall patterns on the grassland in Kansas, USA reveals that a 50% increase in dry spell duration without a change in total rainfall quantity could lead to a 10% reduction in net primary productivity (Fay et al., 2003). Therefore, how dry and wet spells change over time becomes very important as their changing pattern can provide more useful insights into specific precipitation regime, which would be beneficial to agricultural, irrigation, and field operation systems (Cindrić et al., 2010).

Accordingly, numerous studies have investigated the fluctuations of dryness and wetness around the world (Ionita et al., 2015; Kutiel and Türkeş, 2017; R. Wang et al., 2017). A study by Beniston *et al.* (2007) examined changes in the Mediterranean's annual maximum length of wet spell predicted by three regional climate models (RCMs), and the results indicate a considerable drying

trend. By comparing two 3-member ensembles of simulations with a regional climate model, May (2008) showed that both the frequency and the length of dry spells were substantially increased over most of the European continent, while an opposite trend was found in the frequency and the length of wet spells. In Croatia, Cindrić *et al.* (2010) studied the climatological features of the mean and maximum dry spell durations, and they found prevailing increasing trends during winter and spring but a negative trend in autumn. The dry spells in India have increased significantly over the north and central regions (Panda and Kumar, 2014) and the predictability of both dry and wet spells have undergone a rapid increase (Neena and Goswami, 2010). In north-central China, the increase in dry spell duration has been found to be positively correlated with a northward shift in planetary waves (Zhang et al., 2015). Using high-resolution gridded data from 1901 to 2013, Vinnarasi and Dhanya (2016) analyzed characteristics of extreme dry and wet spells over the Indian summer monsoon, and they found apparent signs of wet regions turning drier and dry regions turning wetter. Gan *et al.* (2016) also demonstrated that warm spell duration and dry spell number are projected to increase in Africa in the context of global warming, and this could affect local water resources management and capacity building.

With regard to Canada, Bonsal and Lawford (1999) analyzed the teleconnections between ENSO and summer dry spells on the CP from 1948 to 1991, and they found that the average number of dry spells associated with El Niño (La Niña) events is significantly higher (lower) than for non-El Niño (non-La Niña) periods. Using daily precipitation data generated by the Canadian Regional Climate Model (CRCM), Sushama *et al.* (2010) suggest that both mean number of dry days and return levels of maximum dry spell durations are projected to increase for the southern part of Canada.

In spite of this, few previous studies have systematically and simultaneously examined dry and wet spell characteristics and performed a comprehensive evaluation with sufficiently long daily precipitation in Canada. Although Roque-Malo and Kumar (2017) have studied the non-extreme precipitation variability across North America and found that wet and dry periods have undergone significant changes, they selected only a small number of stations in Canada, thus making the results for Canada less comprehensive. As addressed by Li and Babovic (2018), dry and wet spell characteristics can indicate the temporal persistence and day-to-day variability of precipitation time series, which can be used to assess the performance of a weather generator and the long-term predictability of climate models. In this study, we look at both extreme and non-extreme dry and wet spell characteristics using daily precipitation data.

Furthermore, a detailed view of the changing characteristics of dry and wet spells will be beneficial to effective water resources management and flood/drought risk mitigation in Canada. To this end, the purposes of this research are to (1) characterize changes in extreme and non-extreme dry and wet spells, (2) build return period maps for dry and wet spells by selecting the optimum probability distribution, and (3) describe how dryness and wetness variability are affected by large-scale atmospheric circulations. The paper is organized as follows: with a brief introduction in Section 5.1, Section 5.2 presents an overview of the data and methodology, followed by results and discussion in Section 5.3. The main conclusions are outlined in Section 5.4.

5.2 Data and methods

5.2.1 Precipitation data

In this study, the Climate Prediction Center (CPC) Global Unified Precipitation data (Xie et al., 2010) were used over the 1979-2018 period. The CPC data are based on gauge records with uniform quality control (Hou et al., 2014), and are available at 0.5×0.5 degree. Comprehensive quality control procedures were applied to the original station data to remove suspicious and extremely large values through comparisons with climatological statistics at target stations, concurrent radar and satellite observations, and numerical model forecasts (Chen et al., 2008). Then, station reports were interpolated through the optimal interpolation to produce analyzed fields of daily precipitation with consideration of orographic effects (Xie et al., 2007).

The CPC data have been extensively used in climate research and have often served as reference data for many trend analysis and validation studies. For instance, Dominguez *et al.* (2012) simulated a statistically significant increase in the intensity of winter precipitation extremes over the western United States, and they used CPC precipitation as the observation dataset to compare to the model simulations. Additionally, in order to identify the uncertainties and errors associated with reanalyzed precipitation products, precipitation estimates from six reanalyzes were compared against the CPC data over the contiguous United States from 1980 to 2013 (Cui et al., 2017). Therefore, we used the CPC daily precipitation data to extract dry and wet spells.

5.2.2 Climate indices

We selected certain large-scale climate patterns that have been related to the dryness and wetness variability observed over Canada (Bonsal et al., 2011; Tan and Gan, 2017; Zhang et al., 2010),

such as PNA and ENSO. For example, the dominant dry variability in the CP and northern central region are found to be associated principally with the PNA and MEI compared to other large-scale climate indices (Asong et al., 2018). St. George (2007) concluded that the state of the winter PNA is an essential control on streamflow in the Winnipeg River basin (eastern Canada) at both interannual and decadal time-scales. In addition, Yang *et al.* (2019) found that the extreme precipitation occurring in Canada is closely teleconnected to MEI and PNA using wavelet coherence analysis.

The PNA is one of the most prominent modes of low-frequency variability in the Northern Hemisphere extratropics; it denotes a quadripole pattern of 500 millibar height anomalies, with anomalies of similar (opposite) signs located over the Aleutian Islands and southeastern United States (Hawaii and central Canada). The multivariate ENSO index version 2 (MEI) was used to represent ENSO, with negative (positive) values indicating the cold (warm) ENSO phase, i.e., La Niña (El Niño). The MEI is the leading empirical orthogonal function (EOF) of five variables (sea level pressure, sea surface temperature, zonal wind, meridional wind, and outgoing long-wave radiation) over the tropical Pacific basin, providing a more comprehensive description of ENSO events than conventional ENSO indices (Wolter and Timlin, 1998).

Monthly time series of PNA was downloaded from Climate Prediction Centre (https://www.cpc.ncep.noaa.gov/products/precip/CWlink/pna/pna.shtml), and MEI indices were obtained from the National Oceanic and Atmospheric Administration https://www.esrl.noaa.gov/psd/enso/mei/.

5.2.3 Extraction of wet and dry spells

Dry spells, defined as extended periods of dry days, can serve as an indicator of drought conditions and are often used in the management of water resource systems (Sushama et al., 2010). Following the Expert Team on Climate Change Detection and Indices (ETCCDI, http://etccdi.pacificclimate.org/), a dry spell is defined as consecutive days with daily precipitation < 1mm, while a wet spell is defined as consecutive days with daily precipitation equal to or exceeding this threshold. This definition has also been adopted by Philippon *et al.* (2015), Jiang *et al.* (2016a), and Raymond *et al.* (2018). To investigate changes in wet and dry spells in Switzerland, Fischer *et al.* (2015) defined that a day was considered to be wet if daily precipitation was equal to or above 1mm. All of these studies provide the feasibility to use 1mm as the threshold to identify a dry or wet spell. The number of these spells per year then yields the dry and wet spell frequency.

Singh and Ranade (2010) and Li *et al.* (2016) have developed several dry and wet spells indices to better describe the general and extreme features of dry and wet spells. Here we adopt six indices and their details are listed in Table 5.1. We mainly focus on dry spells with a duration ≥ 7 days because dry spells with longer duration are associated with stronger impacts for the society and environment. By contrast, a wet spell duration is usually shorter than a dry spell, and we focus on wet spells with a duration ≥ 3 days. The first four indices are general features of dry and wet spells, such as the number of spells and their duration, while the last two indices are defined to explore the extreme characteristics.

Table 5.1 Dry and wet spell indices used in this study.

Indices	Definition	Units
DSN	Number of dry spell per year	
WSN	Number of wet spell per year	
DSD	The duration of DS per year	day
WSD	Total duration of WS per year	day
MDSD	Annual maximum dry spell duration	day
MWSD	Annual maximum wet spell duration	day

5.2.4 Trend analysis

The non-parametric Mann-Kendall (MK) test at 5% significance level was employed to detect the existence of statistically significant monotonic long-term trends. As the MK test makes no assumptions regarding data distribution and can handle gaps in data records, it is recommended for analyzing time series with skewed distributions and it has been frequently applied in quantifying and testing the significance of trends in climate data (Frazier and Giambelluca, 2016; Gizaw and Gan, 2016b; Jiang et al., 2015; Tan and Gan, 2015). More details regarding this method can be obtained from Mann (1945), Kendall (1948), and Hamed and Rao (1998). The trend magnitude was analyzed using the non-parametric Sen's slope estimator (Sen, 1968).

5.2.5 Return level analysis

Extreme events can be identified by the block maxima (BM) method (Ahmed et al., 2016; Coles, 2001; Khaliq et al., 2006). The BM approach in climate and hydrology research is commonly a block size of one year (annual maximum series, AMS) (Santos et al., 2011), and it models extreme events using a generalized extreme value (GEV) distribution, which combines the Gumbel, Fréchet, and Weibull distributions (Bohlinger and Sorteberg, 2018; Santos et al., 2011; Tan and Gan, 2017). Using the BM approach, Lana *et al.* (2006) examined the statistical patterns of extreme dry spells

in Catalonia and obtained estimation for dry spells with return periods of 2, 5, 10, and 25 years from 1950 to 2000. The BM method is used here and parameters of the GEV distribution are obtained by means of maximum likelihood estimation (MLE) (Gilleland and Katz, 2016). For the present study, the spatial distribution of the return level corresponding to the 5- and 25-year return periods was estimated.

The GEV distribution function is given as (Coles, 2001; Gilleland and Katz, 2016):

$$G(\mathrm{x}) = \exp\left[-\left\{ 1 + \xi\left(\frac{x-u}{\sigma} \right) \right\}^{-1/\xi} \right] \quad (5\text{-}1)$$

Where scale parameter $\sigma > 0$, location parameter $\mu > -\infty$, and shape parameter $\xi < \infty$. Equation 1 contains three types of distribution functions depending on the sign of the shape parameter. The Fréchet distribution results from $\xi > 0$ and the Weibull distribution is from $\xi < 0$. The Gumbel type is obtained by taking the limit as $\xi \to 0$ giving

$$G(\mathrm{x}) = \exp\left[-\exp\left\{ -\left(\frac{x-\mu}{\sigma} \right) \right\} \right], \quad -\infty < x < \infty \quad (5\text{-}2)$$

The parameters of all distributions were estimated by the maximum likelihood estimation (MLE). In order to select the best marginal distribution, the Akaike information criterion (AIC) (Akaike, 1974) was used to compare the results from different distributions as suggested by Kim *et al.* (2017): a smaller AIC indicates better goodness of fit. The nonparametric Kolmogorov-Smirnov (KS) test was also used to further assess the suitability of the distributions (Ayantobo et al., 2018; Mascaro, 2018).

Milly *et al.* (2008) asserted that stationarity has been compromised as a default assumption in water resources risk assessment and planning because anthropogenic climate change is altering the means and extremes of precipitation, evapotranspiration, and streamflow. In this case, it is necessary to adopt non-stationary GEV distributions with varying climatic covariates as a diagnostic tool (Tramblay and Hertig, 2018). In this study, we employ large-scale climate indices as a covariate, imposing a linear trend on the location and scale parameters to detect the influence of large-scale climate patterns on dry and wet spells.

$$\begin{aligned} \mu(x_t) &= \mu_0 + \mu_1 x_t \\ \sigma(x_t) &= \sigma_0 + \sigma_1 x_t \end{aligned} \quad (5\text{-}3)$$

The models are then compared by means of the likelihood ratio test to decide whether the inclusion of non-stationarity has improved the model (Gilleland and Katz, 2016; Wilcox et al., 2018).

5.2.6 Bayesian quantile regression

Many previous studies have paid much attention to the mean trend of climate extremes estimated by linear regression models; however, climate change and large-scale climate oscillations may result in changes in the upper tail of the probability distribution of climate variables that are associated with extreme events (Tan et al., 2018a). In this study, we focus on investigating slopes of regression in different quantiles of the conditional distributions of dry and wet spell indices, particularly those in the upper quantiles. For a predictor variable, quantile regression calculates the conditional quantiles of a response variable and differs from conventional linear regression that only considers the conditional mean of the response variable (Koenker and Bassett, 1978; Koenker and Hallock, 2001; Wasko and Sharma, 2014). Details about simple quantile regression can be further referred to Koenker and Hallock (2001) and McMillen (2013).

The classic linear quantile regression minimizes the functional

$$\hat{\beta}_\tau = \text{argmin} \sum_{i=1}^{n} \rho_\tau \left(y_i - x_i^T \beta \right)^2 \quad (5\text{-}4)$$

where $\rho_\tau(x) = x(\tau - I(x < 0))$ is a loss function, $I(\bullet$ is an indicator function, and $\hat{\beta}_\tau$ is the τth regression quantile. Meanwhile, the minimization of Equation (4) is equivalent to the maximization of a regression likelihood function formed by asymmetric Laplace densities, which is given by Yu and Zhang (2005):

$$f(x \mid \mu, \sigma, \tau) = \frac{\tau(1-\tau)}{\sigma} \exp\left[-\rho_\tau \left(\frac{x-\mu}{\sigma} \right) \right] \quad (5\text{-}5)$$

From this inference, Bayesian inference can provide the entire posterior distribution of the parameter of interest including parameter uncertainty (Yu and Moyeed, 2001). Therefore, we use the Bayesian quantile regression method developed in the R package "bayesQR" (Benoit and Van den Poel, 2017) to explore the influence of large-scale climate patterns on dry and wet spells in Canada.

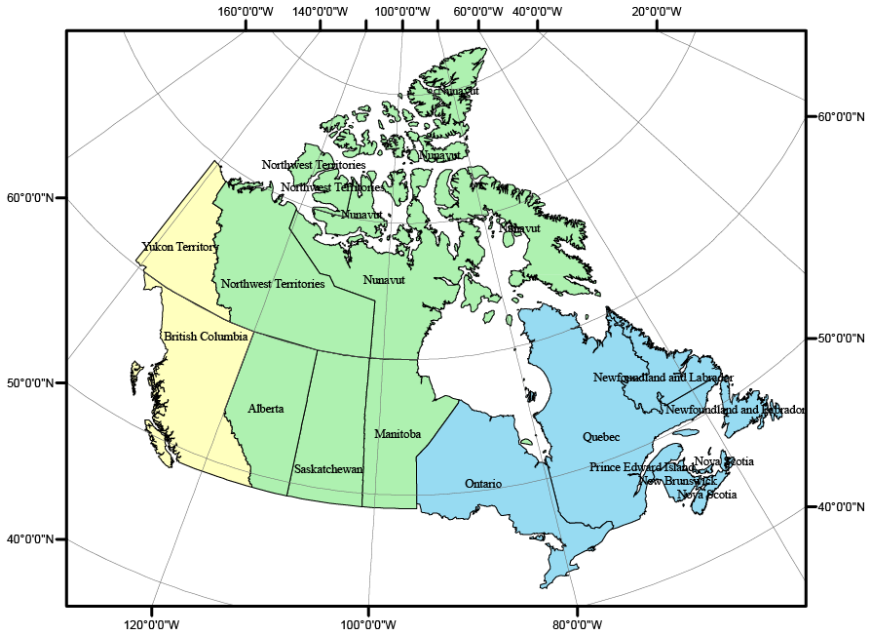

Figure 5.1 The provinces and territories of Canada. Abbreviations: Alberta (AB), Saskatchewan (SK), Manitoba (MB), Newfoundland and Labrador (NL), Prince Edward Island (PE), Nova Scotia (NS), Northwest Territories (NT), Nunavut (NU), Ontario (ON), New Brunswick (NB), Yukon Territory (YT), British Columbia (BC), Quebec (QC).

5.3 Results

5.3.1 Dry spell characters

Figure 5.2 shows the spatial pattern of dry spell characteristics. As shown in Figure 5.2(a), central Canada has the highest number of dry spells (DSN). In contrast, western BC has the lowest DSN, which is expected because of its abundant precipitation. Meanwhile, there is a mixing trend of DSN: positive trends dominate over northern Ontario and western Quebec, while most negative trends are confined in the northwest and southwest (Figure 5.2b). It is worth mentioning that DSN displays an increasing trend in the southern CP, which indicates the adverse impacts of the changing climate on agriculture. Figure 5.2(c) presents the spatial distribution of dry spell duration (DSD). Similarly, long-lasting dry spells are mainly located in central Canada, while western BC and eastern Canada have experienced more short-duration dry spells. As shown in Figure 5.2(d),

there is a significant upward trend for DSD in the southern CP, while more downward trends can be found in northern Canada. It was evident from Figure 5.2(e) that annual maximum dry spell duration (MDSD) in central Canada generally has medium to long duration, and MDSD in the CP has mostly shown an increasing tendency. Together, these trends suggest that dry spells have become less severe in major parts of Canada except in the southern CP from 1979 to 2018.

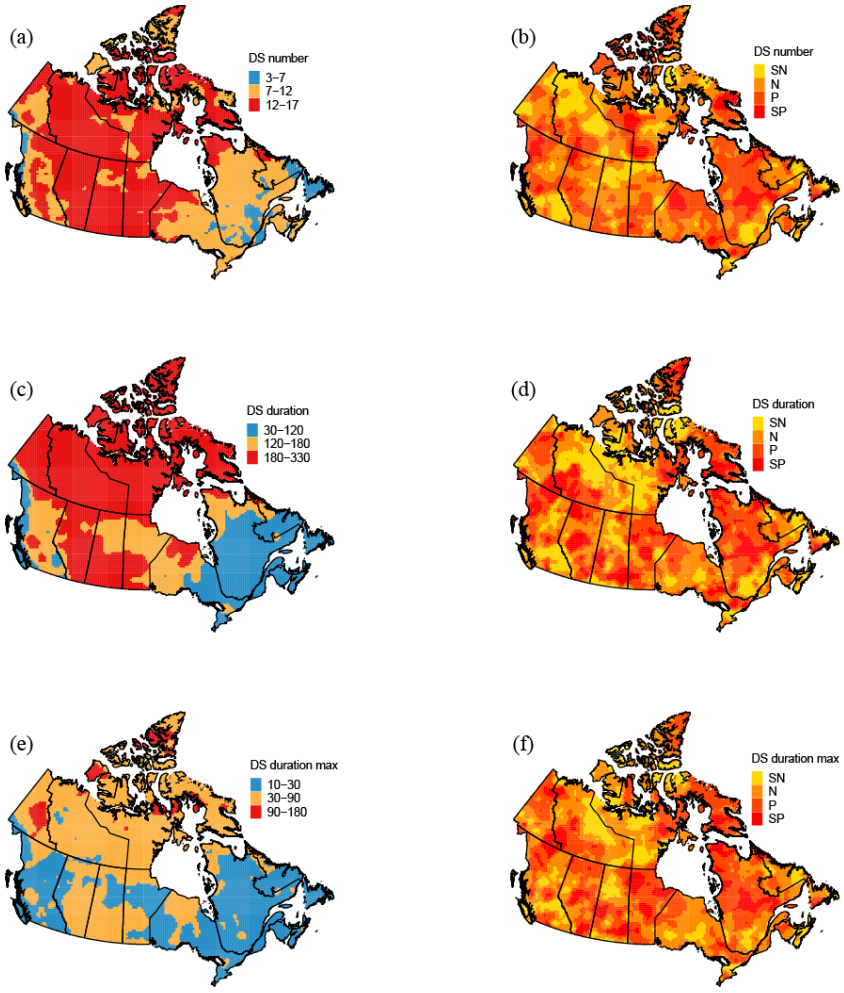

Figure 5.2 Spatial patterns of dry spell (a) number, (c) duration, (e) annual maximum duration, and their corresponding trends (b, d, f). The abbreviations are P: positive trend, SP: significant positive trend, N: negative trend, and SN: significant negative trend.

To further analyze the temporal variation in dry spells, DSN and DSD were separated into two 20-year subperiods: 1979–1998 and 1999–2018 (Figure 5.3). From the Kolmogorov–Smirnov test, it

is noted that the distribution of DSN in western Canada in subperiod 1 is statistically different from that in subperiod 2, indicating a shift in dry spell occurrence. In addition, DSD of central and eastern Canada from subperiod 1 is statistically different from that in subperiod 2. Generally, DSN and DSD in western and eastern Canada tend to shift to the left from subperiod 1 to 2, which suggests that, probabilistically, dry spells have occurred less frequently and in shorter duration in these regions. In contrast, dry spells in central Canada have occurred more frequently and with a shorter duration.

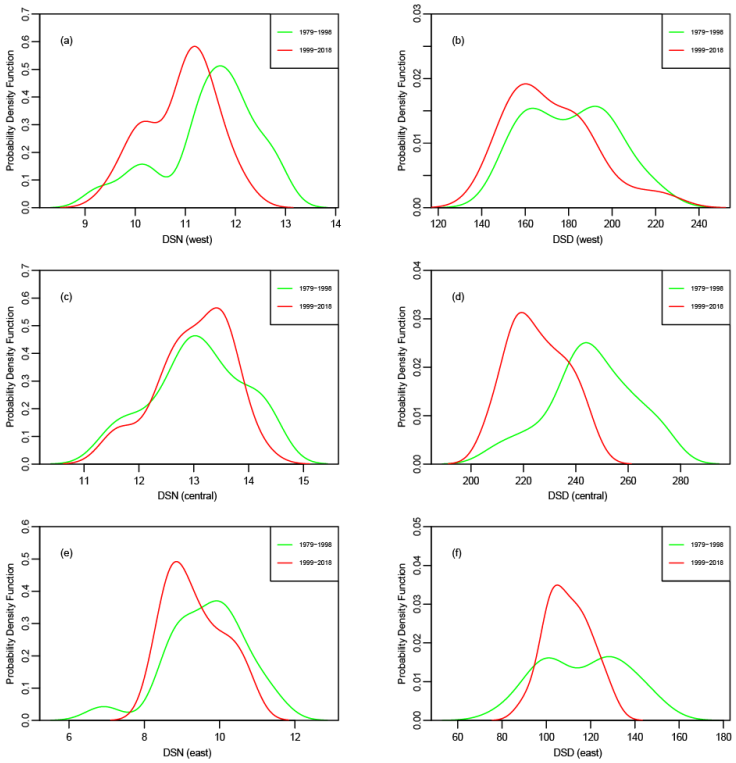

Figure 5.3 Annual probability density functions for DSN and DSD for two subperiods: 1979–1998 and 1999–2018.

Bonsal *et al.* (2011) pointed out that the CP and interior valleys of BC are vulnerable to dry conditions mostly due to their locations in the leeward of major mountain ranges resulting in low precipitation with high variability. Although a high frequency of dry spell event is observed over most of the Arctic regions, the DSD has declined, which is also reported by Polade *et al.* (2014).

From an ensemble of 9 global general circulation models (GCMs), Tebaldi *et al.* (2006) suggest an increase of extreme precipitation and a shortening of dry spells in the mid- and high latitudes of the northern hemisphere. In contrast, the lower latitudes would undergo a tendency towards more extreme precipitation and longer dry spells. Furthermore, using the Canadian Regional Climate Models (CRCM) integrations, Sushama *et al.* (2010) also project an increase in DSD for the southern Prairies (Figure 5.2d).

5.3.2 Wet spell characters

The spatial distribution of wet spell characteristics for the 1979-2018 period is shown in Figure 5.4. Wet spells in western BC and eastern Canada have occurred more frequently (14-32/year) compared with how often they occur in central Canada (1-7/year) (Figure 5.4a), and there is a widespread increasing trend for the wet spell number (WSN) across central Canada. For the wet spell duration (WSD) in Figure 5.4(c), central Canada has a duration of 3-30 days, which is significantly shorter than that in west BC (90-210 days). Figure 5.4(d) indicates an overall wetting trend in central Canada except for in the southern CP, a result which corresponds with the drying trend found in Figure 5.2(d). As shown in Figure 5.4(e), annual maximum wet spell duration (MWSD) with 2-14 days is extensive across Canada, while longer wet spells are restricted to west BC. In addition, the shortening of MWSD is found in west BC, southern CP, and eastern Canada, which again implies the deteriorating drying condition in the southern CP.

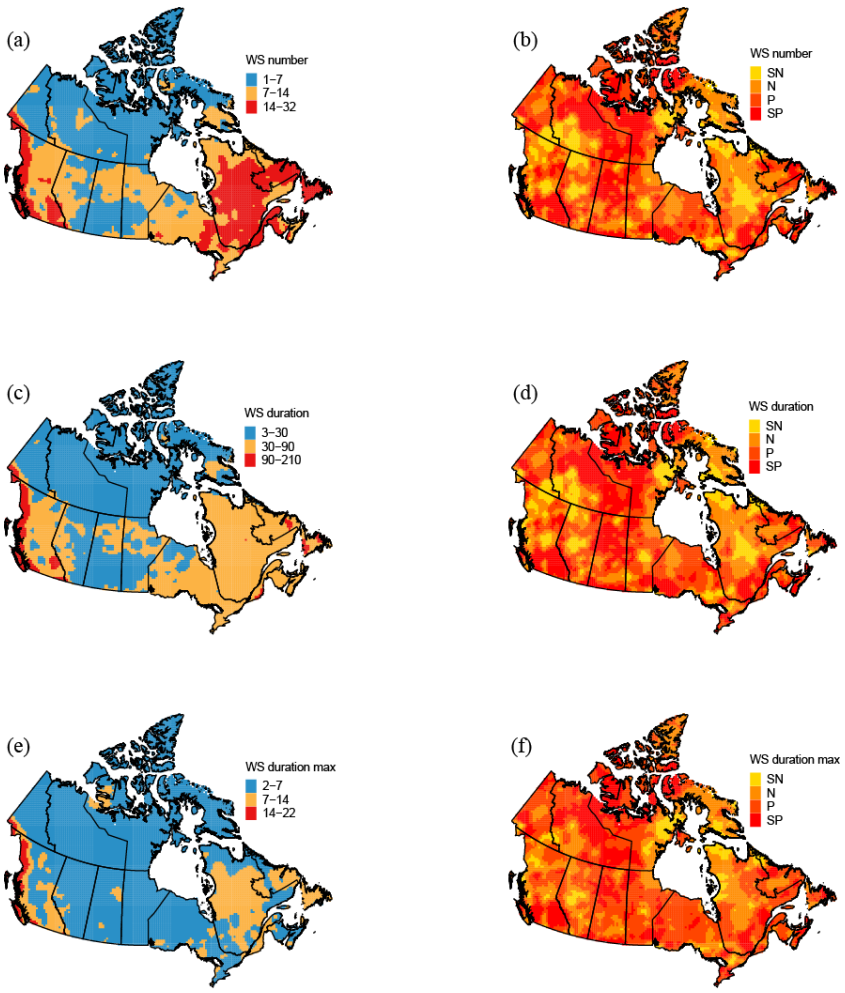

Figure 5.4 Same as Figure 5.2 but for the wet spell.

Figure 5.5 presents the probability distribution functions for WSN and WSD during 1979–1998 and 1999–2018. It is worth mentioning that the distributions of both DSN and DSD in subperiod 1 are statistically different from those in subperiod 2 across Canada, suggesting a transition in wet spell characteristics. On the whole, both WSN and WSD are inclined to shift to the right, which demonstrates that there have been more wet spells with longer duration in terms of probability across Canada.

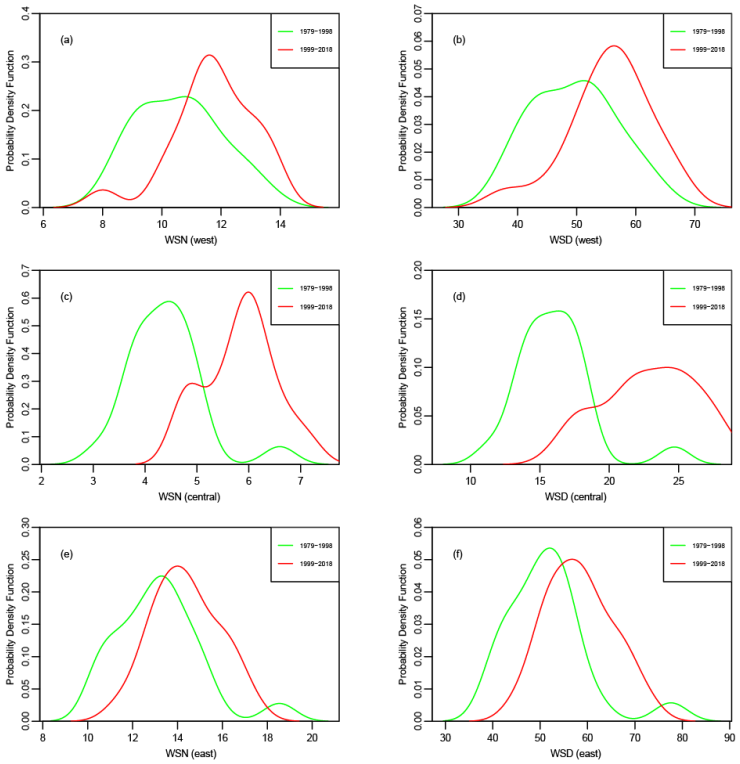

Figure 5.5 Annual probability density functions for WSN and WSD for two subperiods: 1979–1998 and 1999–2018.

Changes in the frequency and duration of dry and wet spells could have more profound impacts on our environment and society than changes in total precipitation (Ye, 2018). From daily precipitation data, Roque-Malo and Kumar (2017) investigated the wet period changes in Canada, and they found that southeast Canada showed strong increasing trends in WSD during from 1960 to 2010, a conclusion which is reinforced by our findings in Figure 2(d). Meanwhile, in mid-latitude Canada, the latter half of the 20th century was noticeably wetter than in previous decades (Dai et al., 1998), and this trend could have contributed to the overall increase of WSN. However, for the southern CP, there have been longer periods between rainfall events (more consecutive dry days) even though precipitation has generally increased, which could be a potential threat to agriculture.

5.3.3 Nonstationary return level of dry and wet spells

5.3.3.1 Dry spell

The annual maximum dry and wet spells modeled by the GEV using PNA and MEI as covariates are shown in Figure 5.6. From Figure 5.6(a), it can be seen that the PNA has greater influences on MDSD than the MEI, especially in the central CP and eastern Ontario. However, in northern and southwest Canada, the MEI has shown stronger impacts. As shown in Table 5.2, the percentage of grids showing stationarity and non-stationarity is 39.4% and 60.6%, respectively. As noted by Milly *et al.* (2008), stationarity should no longer serve as a default hypothesis in water resources management because of the considerable anthropogenic impacts on precipitation, evapotranspiration, and runoff. Among all the grids, 37.2% have shown non-stationarity with the PNA, and 23.4% are more affected by the MEI, indicating a stronger influence of the PNA on dry spells. Meanwhile, the location parameter has shown greater effects than the scale parameter in both indices (16.8% and 10.6%).

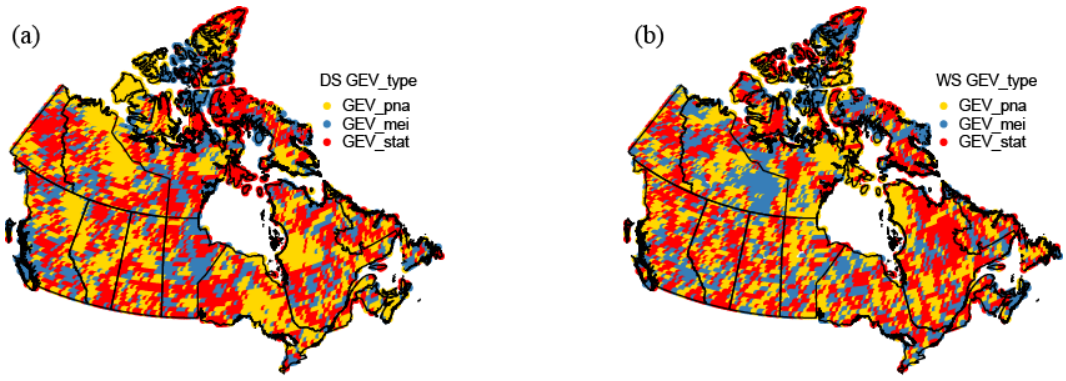

Figure 5.6 Spatial distribution of (a) dry spell type and (b) wet spell type.

Table 5.2 Percentage of dry spell grids with stationarity and non-stationarity.

Stationarity	Non-stationarity					
	PNA_loc	PNA_scale	PNA_both	MEI_loc	MEI_scale	MEI_both
39.4%	16.8%	11.2%	9.2%	10.6%	8.2%	4.6%

Figure 5.7(a) depicts the spatial distribution of the 5-year MDSD under negative PNA and ENSO phases. The first feature to be underlined is the high duration (>60 days) over northern and northwest Canada. By comparison, dry spells with shorter duration are located over southwest and eastern regions. In the CP, the majority of dry spells are characterized by a 30-60 day duration; however, some areas in the south are expected to undergo long-lasting dry spells. The 5-year MDSD under positive PNA and ENSO phases is shown in Figure 5.7(b). Analogously, persistent dry spells are detected in northern and northwest Canada, but the extent is broader than is shown in Figure 5.7(a), suggesting that positive phases of PNA and ENSO could have stronger impacts on MDSD. Although the dry spell return level in northern Canada is higher than in other regions, it is less of a concern mainly due to the low population and lack of agricultural activities (Bonsal et al., 2011). Figure 5.7(c) presents the 25-year return level of MDSD under negative PNA and ENSO phases. It is noted that the spatial pattern is similar to that of the 5-year return level. Moreover, MDSD has generally increased compared with Figure 5.7(a) due to the larger return period. As a whole, regions with higher dry spell duration under positive phases (Figure 5.7d) have enlarged compared to those in the negative phases.

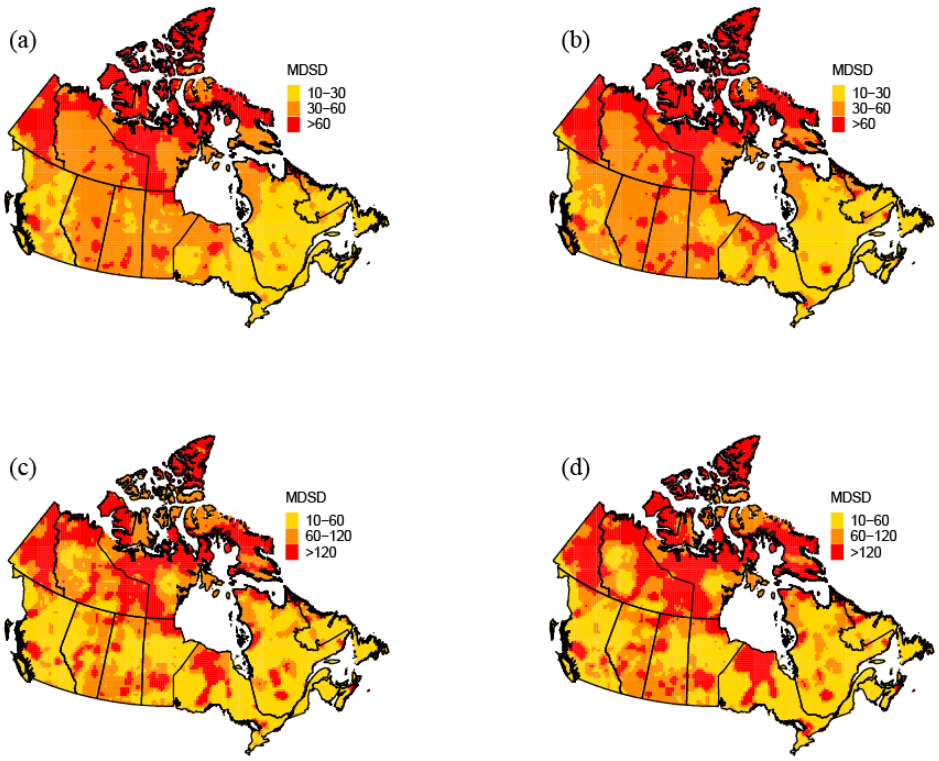

Figure 5.7 Spatial patterns of (a, b) 5-year and (c, d) 25-year MDSD under (a, c) negative and (b, d) positive MEI and PNA phases.

5.3.3.2 Wet spell

Similar to what is shown in Figure 5.6(a), the MEI also has strong influence on wet spells in northern Canada. In eastern Canada, stationary wet spells are more widespread. In addition, MWSD types have revealed major differences compared to dry spells. For example, the MEI has more influence on wet spells than dry spells in eastern Northwest Territories (NT) and western Ontario (Figure 5.6b). The percentages of wet spell grids showing stationarity and non-stationarity are listed in Table 5.3. Once again, the stationarity has been compromised as 63% of the grids are found to be non-stationary, of which 33.5% have exhibited non-stationarity with the PNA, while 29.5% are more related to the MEI, implying a greater effect of the PNA on wet spells. It is worth mentioning that the location parameter has the highest impact for both types (15.0% and 12.5%), which is consistent with the dry spell.

Table 5.3 Percentage of wet spell grids with stationarity and non-stationarity.

Stationarity	Non-stationarity					
	PNA_loc	PNA_scale	PNA_both	MEI_loc	MEI_scale	MEI_both
37.0%	15.0%	12.7%	5.8%	12.5%	12.0%	5.0%

Figure 5.8(a) shows the spatial pattern of the 5-year MWSD under negative PNA and ENSO phases. Generally, a 7-10 day duration is extensive across the country, especially in central Canada, while sustained wet spells are mainly confined to parts of western BC, southern CP, and eastern Canada. In contrast, the 5-year MWSD under positive PNA and ENSO phases has revealed less sustained wet spells (Figure 5.8b), indicating more powerful effects of negative phases of PNA and ENSO on MWSD. As can be seen in Figure 5.8(c), the 25-year MWSD under negative phases has exhibited more persistent wet spells (>16 days) over western BC and southeast Canada compared with Figure 5.8(d). Overall, this may suggest the importance of negative phases on lengthening the wet spells.

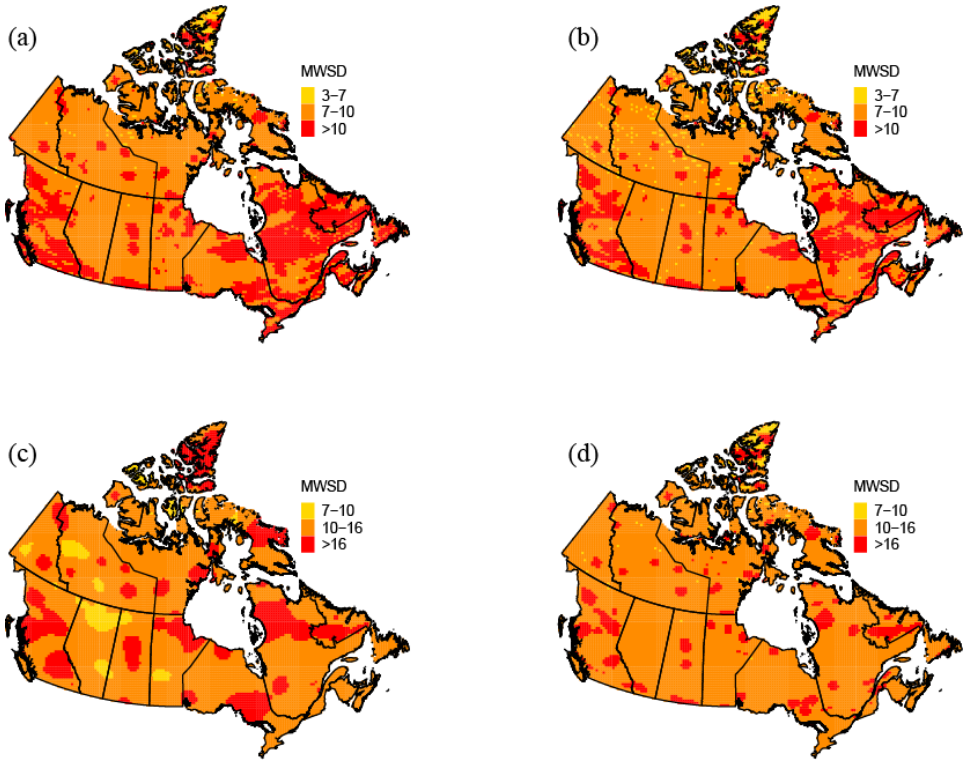

Figure 5.8 Same as Figure 5.5 but for the MWSD.

5.3.4 Effects of large-scale circulation patterns

The potential teleconnections between dry/wet spell duration and the ENSO (PNA) are investigated by computing the posterior mean of the slope using Bayesian quantile regression. Generally, the quantile relationships between the ENSO/PNA and DSD/WSD show significant differences in different regions (Figure 5.9 and 5.10). For western Canada, the effects of MEI on dry spells are stronger for high quantiles than low quantiles. Additionally, the correlation with ENSO changes from negative to positive at the 0.2 quantile, where higher DSD quantiles increase with MEI values. This means that for western Canada, high (low) DSD quantiles in El Niño years (with larger MEI values) tend to be higher (lower) than those in La Niña years (Figure 5.9a), and it is associated with the moisture deficit caused by El Niño events (Shabbar and Skinner, 2004). The effect of PNA on DSD in western Canada is relatively stable except for the 0.9 quantile,

implying that PNA has exerted more influence on extreme dry spells (Figure 5.9b). For central Canada, there is a consistently positive slope for all quantiles (Figure 5.9c), suggesting that increasing MEI values tend to prolong the DSD. In contrast, there is a mixing effect of PNA on DSD (negative in low quantiles and positive in high quantiles) in central Canada. The magnitudes of the slopes for MEI and PNA stay positive and fluctuate significantly at different quantile levels in eastern Canada (Figure 5.9e and f), with the most significant magnitude detected around the medium for both indices.

Figure 5.10 presents the correlation between WSD and large-scale climate patterns. For western Canada, the response of WSD to ENSO is negative, and it occurs more at low quantiles than at high quantiles, which indicates that WSD with increasing MEI values tends to be lower, especially during El Niño years (Figure 5.10a). As the PNA increases, WSD at 0.2-0.8 quantiles is expected to increase; however, WSD at the 0.9 quantile is anticipated to decrease (Figure 5.10b). For central Canada, both MEI and PNA have a negative (positive) slope at low (high) quantiles, indicating the opposite behavior in low and high WSD, which further demonstrates the limitation of conventional linear regression. In addition, the effects of PNA on WSD are much weaker at low quantiles than at high quantiles due to the lower regression coefficients at 0.2-0.6 quantiles. As MEI increases (towards El Niño-like conditions), WSD at all quantile levels tends to decrease in eastern Canada (Figure 5.10e) especially for extreme wet spells, while for the PNA, a similar pattern is found except for the positive slope at the 0.2 quantile.

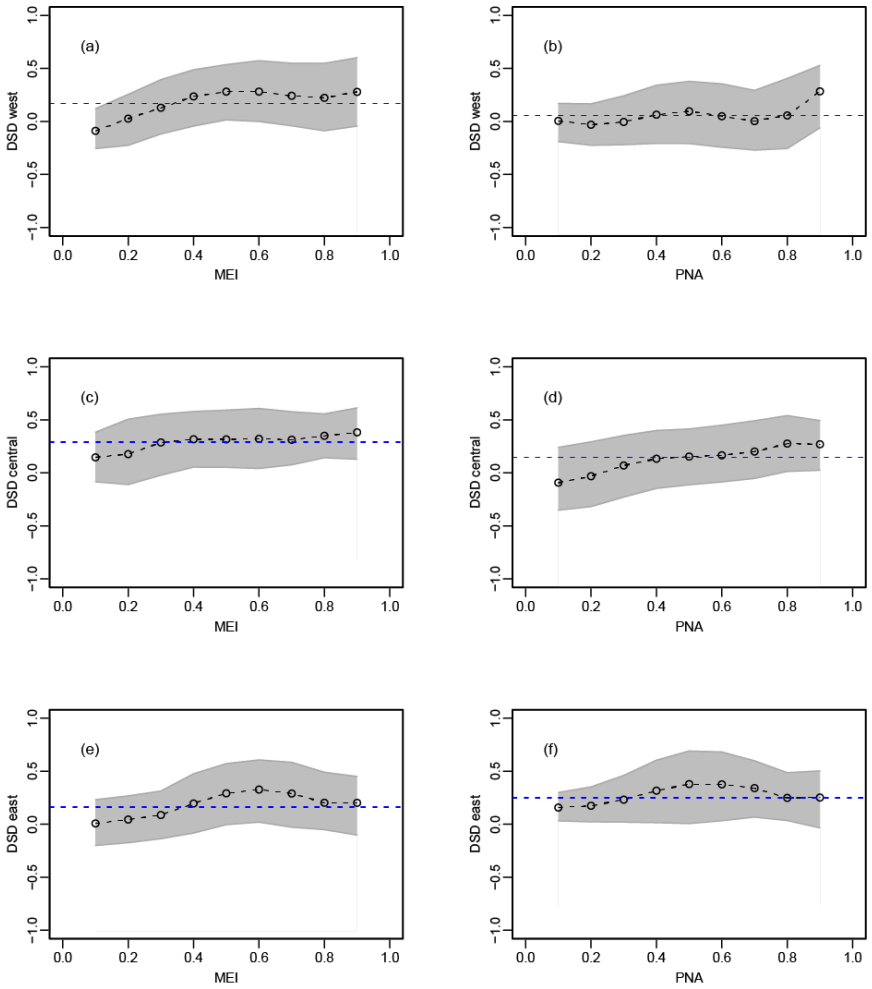

Figure 5.9 Regression coefficients between DSD and climate indices varying with quantile levels from the Bayesian quantile regression in (a, b) western, (c, d) central, and (e, f) eastern Canada. The grey bands show the 95% confidence intervals and the blue dashed line represents the classical linear regression.

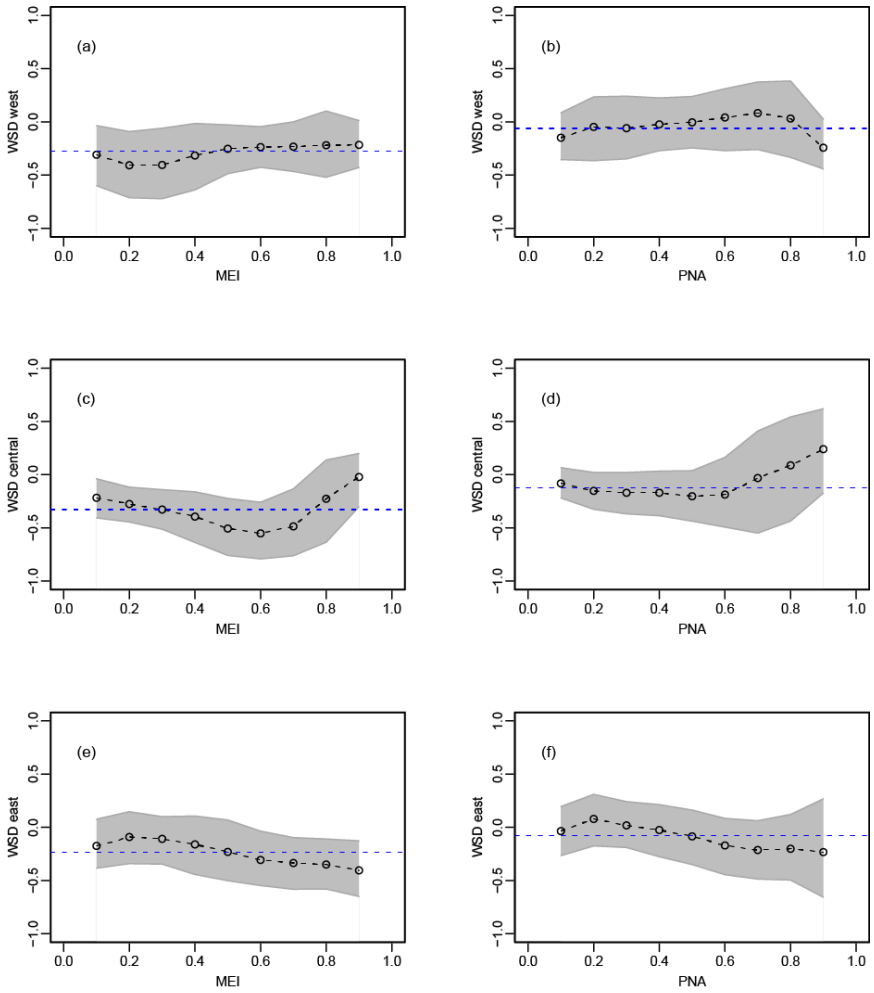

Figure 5.10 Same as Figure 5.9 but for the WSD.

5.3.5 Discussion

According to the Intergovernmental Panel on Climate Change (IPCC) special report on extreme events and disasters, the observed Earth warming would alter climate extremes through changes in their frequency, severity, and spatial distribution, as well as through increases in vulnerability due to climate impacts (Field et al., 2012).

Figure 5.2 and 5.7 show that dry spells have demonstrated significant changes across Canada, particularly for the southern CP, agreeing with previous findings that both mean number of dry

days and return levels of maximum DSD are projected to increase for this drought-prone region as the annual evaporation typically exceeds precipitation (Sushama et al., 2010). Using the Canadian Regional Climate Model (CRCM), Plummer *et al.* (2006) projected a tendency towards a small increase (on the order of 10%) in precipitation over most regions and seasons in Canada; however, the southern CP is expected to experience a slight decline in precipitation. Our findings suggest a decline in DSN and DSD for higher latitudes, and it could be attributed to the warmer temperature observed across Canada, especially in the north (Vincent et al., 2018). The decreasing DSD is linked with the stronger moisture-holding capacity of the warmer air, leading to more moisture convergence and precipitation. As a result, long dry spells are broken down into several short dry spells (Sushama et al., 2010). For the southern CP, the increase in DSN during the studied period is mainly associated with declining precipitation. Although Northern Ontario and Quebec show an increase in DSN, they are associated with an increase in precipitation, which highlights the enhanced role of evapotranspiration due to warming. For the rest of Canada, the decreasing DSN and increasing precipitation make these regions less vulnerable to dry conditions in the future (Sushama et al., 2010). In contrast, positive trends in WSD are observed over central Canada (Figure 5.4), which is consistent with the general wetting trend detected by Zhang *et al.* (2000) and Vincent *et al.* (2018). Moreover, the shortening of WSD in southern CP is closely related to the negative precipitation trends found in southern regions.

Results from various studies have revealed the importance of large-scale circulation patterns in affecting climate responses. Table 5.2 and 5.3 indicate that the stationarity has been compromised as more grids are found to be non-stationary under the impacts of ENSO and PNA. Similarly, using daily precipitation data, Tan and Gan (2017) reported that heavy precipitation in Canada has shown

strong non-stationarity, likely because of the influence of large-scale climate patterns given the strong correlation detected between extreme precipitation and climate indices.

The positive slope coefficients in Figure 5.9(a) suggest that dry spells tend to have longer durations with increasing MEI values. For western Canada, it has been shown that El Niño events are accompanied by the amplified western Canadian ridge and deepened Aleutian low. This could cause enhanced anticyclones and a northward-shifting mid-latitude jet stream, leading to below normal precipitation stretching from southern BC to the Great Lakes region (Gan et al., 2007; Shabbar et al., 1997). Tan and Gan (2017) investigated the frequency and intensity of Canadian heavy precipitation and found that heavy precipitation in eastern Canada tends to be lower in El Niño years than in La Niña years, a pattern which has also been captured by the negative slope at high quantiles in Figure 5.10(e). Additionally, our results reveal that a positive PNA phase is likely to lengthen drought durations at high quantiles in central Canada (Figure 5.9d), and this is further verified by the evidence that dry periods in the CP are usually characterized by a persistently positive PNA pattern (ridging over western Canada) and anomalously warm temperatures (Hryciw et al., 2013). Meanwhile, using wavelet analysis, Asong *et al.* (2018) found that PNA has shown a strong in-phase relationship with dry conditions over Canada, and this finding again agrees with the generally positive slope coefficients for PNA in Figure 5.9.

Furthermore, North American monsoon precipitation is strongly linked to local land temperatures attributed to evaporative cooling and radiation changes driven by varying cloud cover. To examine extreme dry and wet spell characteristics in the South Asian monsoon region, Singh *et al.* (2014) reported that increases in the frequency of dry spells and the intensity of wet spells are related to

increases in the convective available potential energy (CAPE) and low-level moisture convergence in response to atmospheric warming. In the meantime, the spatial and temporal evolutions of the relationships between large-scale climate patterns and dry/wet spells are greatly affected by hydro-climatic complexities within individual watersheds, especially in Canada's Cordillera region (Bonsal and Shabbar, 2008). Therefore, the role of local temperature and CAPE in persisting long-term dry and wet spells in Canada is still needed for further investigation.

5.4 Summary and conclusions

The observed changes in wet and dry spells have great significance in mitigating climate-related hazards, especially for water resources, agriculture, and infrastructure planning (Li and Babovic, 2018; Singh et al., 2014). By discretizing the precipitation time series into two states “dry” and “wet”, the present study aims to assess the spatial and temporal variations in dry and wet spells, and the influences of large-scale climate patterns in Canada. The identification of spatial distribution of dry and wet spell return periods across Canada has also been undertaken for hazard mitigation and strategy planning.

The main findings of the paper are summarized as follows:

1. There is a mixing trend of DSN: positive trends dominate over northern Ontario and western Quebec, while most negative trends are confined to the northwest and southwest. Moreover, both DSN and DSD have displayed an upward trend in the southern CP, which indicates that dry spells have been aggravated from 1979 to 2018.

2. Wet spells in western BC and eastern Canada have occurred more frequently in these areas compared with other parts of Canada. Meanwhile, there is an overall wetting trend in central Canada except for in the southern CP, which further suggests the deteriorating drying condition in the southern CP.

3. The stationarity has been compromised as more regions are found to be non-stationary under the impacts of ENSO and PNA. The PNA has stronger effects on MDSD than the MEI, especially in the central CP and eastern Ontario. In contrast, the MEI has a greater impact on wet spells than on dry spells in eastern NT and western Ontario.

4. The quantile relationships between large-scale climate patterns and precipitation spells have exhibited significant differences in different regions. For western Canada, the influences of ENSO on dry spells are stronger for high quantiles than low quantiles, indicating that high (low) DSD quantiles in El Niño years (with larger MEI values) tend to be higher (lower) than those in La Niña years, which is a result associated with the moisture deficit caused by El Niño events. Meanwhile, as the PNA value increases, WSD at 0.2-0.8 quantiles is anticipated to increase; however, WSD at the 0.9 quantile is expected to decline. For central Canada, both MEI and PNA have shown a negative (positive) slope at low (high) quantiles, implying the opposite behavior in low and high WSD and further demonstrating the weakness of traditional linear regression. For eastern Canada, the PNA index is positively correlated to DSD, and its effect is largest at the medium. As MEI increases (towards El Niño-like conditions), WSD at all quantile levels tends to decrease.

Chapter 6. Summary, Conclusions, and Recommendations for Future Work

6.1 Summary and Conclusions

Climate change is likely one of the most significant, global scale challenge to mankind in the 21st century, and the impact of global warming on the spatial and temporal variability of climate extremes has worsened, with devastating effects on the environment, society, and economy across the world. A major concern to climate change is the occurrences of extreme events is expected to increase (Easterling, 2000). In this research, a rigorous statistical analysis of the long-term precipitation and temperature data across Canada was performed to analyze the climate dynamics, and to quantify the possible impacts of climate change on climatic regimes of Canada, with an emphasis on climate extremes since the mid-twentieth century. The results of this study provide a better understanding of the dynamics of climate extremes in Canada, which is essential for policymakers and practitioners to improve the risk management and the implementation of more effective strategies to mitigate the impact of climatic extremes.

In Chapter 2, trend analysis, probability distribution function, principal component analysis, and wavelet analysis were used to investigate the spatial and temporal patterns of extreme precipitation of Canada. Ten extreme precipitation indices were calculated using long-term daily precipitation data (1950-2012) from 164 Canadian gauging stations. Several large-scale climate patterns such as El Niño–Southern Oscillation (ENSO), Pacific Decadal Oscillation (PDO), Pacific-North American (PNA), and North Atlantic Oscillation (NAO) were selected to analyze the relationships between extreme precipitation and climate indices. In addition, Convective Available Potential Energy (CAPE), specific humidity, and surface temperature were employed to investigate potential causes of trends in extreme precipitation. The results reveal statistically significant positive trends

for most extreme precipitation indices, which means that extreme precipitation of Canada has generally become more severe since the mid-twentieth century. Majority of indices display more increasing trends along the southern border of Canada while decreasing trends dominated the central Canadian Prairies (CP). In addition, strong teleconnections are found between extreme precipitation and climate indices, but the effects of climate patterns differ from region to region. Furthermore, complex interactions of climate patterns with synoptic atmospheric circulations can also affect precipitation variability, and changes to the summer and winter extreme precipitation could be explained more by the thermodynamic impact, and the combined thermodynamic and dynamic effects, respectively. The seasonal CAPE, specific humidity, and temperature are correlated to Canadian extreme precipitation, but the correlations are season-dependent, which could be either positive or negative.

In Chapter 3, trends of monthly CAPE and of event extreme precipitation indices, namely RX1day, RX5day, and R20mm, were analyzed for the summer of 1979-2013 over the United States (US) and southern Canada. A homogeneity test in CAPE data using the Wilcoxon-rank-sum test showed that statistically significant change points mainly occurred between 2000 and 2003 probably due to changes in humidity sensors during this period. Therefore, the trend analysis was split into two categories: 1979-2013 for regions where no statistically significant change points in CAPE were detected and 1979-2001 and 2002-2013 for regions where statistically significant change points in CAPE were detected. The results show that increasing trends in CAPE and extreme precipitation indices dominate the eastern Atlantic coast of the US and some parts of the Great Lakes. Mixed increasing and decreasing trends were detected in the US mid-west while the western US and the Canadian Pacific coast had little trend in CAPE and extreme precipitation indices. Although both

increasing and decreasing trends were detected, the average trends in RX1day and RX5day were about 0.2 mm/decade and 0.5 mm/decade over 1979-2013. However, the average trend for 1979-2001 period was 0.2 mm/decade (RX1day) and 1.2 mm/decade (RX5day) as compared 1.2 mm/decade (RX1day) and 1.7mm/decade (RX5day) for 2002-2013 period. Temperatures also increased more during the 2002-2013 period (0.3˚C/decade) as compared to the 1979-2001 period (0.1˚C/decade). The recent higher increasing trends detected suggests that increasing temperatures could potentially lead to an overall increase in CAPE and extreme precipitation over the US and southern Canada.

In Chapter 4, drought characteristics in terms of duration, frequency, area, and severity are investigated using the Standardized Precipitation Evapotranspiration Index (SPEI) at seasonal (3-month) and annual (12-month) time scales for Canada over 1950-2016. Using k-means clustering, Canada is first divided into four sub-regions, each with distinct drought characteristics to facilitate the mitigation and management of regional droughts. Next, the time-dependent influences of large-scale climate drivers such as the ENSO, PDO, and PNA on regional drought variability were examined using a Bayesian Dynamic Linear (BDL) model. The results show that between 1950-2016 (1) there has been a prevalent drying trend in southwestern Canada during winter; (2) changes in maximum drought durations have occurred with certain dipolar patterns, i.e., northern Canada has experienced a longer drought duration than southern Canada; (3) drought frequency, area, and severity have predominantly experienced statistically significant decreasing trends, which means that droughts in Canada have generally become less severe; and (4) the relationships between climate patterns and drought variability have changed over time and they differed from region to region. Droughts are generally more negatively correlated to the ENSO and PDO after the 1970s,

while they are more positively correlated to the Atlantic Multi-decadal Oscillation (AMO) and Arctic Oscillation (AO) after the 1980s.

In Chapter 5, the spatial and temporal variations of dry and wet spells over Canada are investigated using daily precipitation over 1979-2018. Time-varying relationships between precipitation spells and large-scale atmospheric circulations are identified using the non-stationary generalized extreme value (GEV) distribution and the Bayesian quantile regression. The results reveal that dry and wet spells have displayed significant changes across Canada, particularly for the southern Canadian Prairies (CP), where both dry spell number and duration have displayed an increasing trend. Many regions are found to be non-stationary under the impacts of El Niño–Southern Oscillation (ENSO) and Pacific–North American pattern (PNA): the PNA has stronger effects on annual maximum dry spells than the ENSO, especially in the central CP and eastern Ontario. In addition, the quantile relationship is different from region to region. For western Canada, the influences of ENSO on dry spells are strong for high quantiles, a result which is associated with the moisture deficit caused by El Niño events. For central Canada, ENSO and PNA have shown a negative (positive) slope at low (high) wet spell duration quantiles. For eastern Canada, the PNA index is negatively correlated with wet spell duration and its effect is larger at higher quantiles.

6.2 Recommendations for Future work

(1) Copula-based risk assessment of drought in Canada

Droughts are closely associated with the stochastic nature of climate variables such as precipitation and temperature. A comprehensive probabilistic analysis of the frequency, duration, and severity of precipitation will have major contribution to the planning and management of our water

resources (Zhang et al., 2014). Estimating the risk of drought is often based on the probability that a specific duration or level of severity of drought will be surpassed, and the recurrence interval of droughts. Even though a simple probabilistic drought analysis method is effective, it does not account for the interactions and multi-dimensions of droughts which are complex. Since climatic variables responsible for the occurrence of drought are usually inter-related, a more comprehensive analysis of droughts should be done in a multivariate framework (Ayantobo et al., 2019; Requena et al., 2013). The copula method is an effective tool to model multivariate random variables in a probabilistic dependency structure, with independent marginal distributions, thus allowing multivariate random events to be described using different marginal distributions (Chen and Guo, 2019; Zhang et al., 2014).

(2) Attribution of human influence on precipitation extremes

To be able to identify effective mitigation policies and comprehensive adaptation strategies against climate change, it is crucial to understand how human activities have contributed to the occurrences of precipitation extremes. There has been a growing public demand for more thorough assessment of human contributions to extreme climate events (Easterling et al., 2016). Recent worldwide occurrences of climate extremes are clear evidence that in recent decades the global climate has changed as a result of human-induced rising concentrations of greenhouse gas emissions, but this does not imply that human influence has significantly altered the probability of every recently observed extreme weather or climate-related event (Stott et al., 2013). In addition, compelling evidence of anthropogenic fingerprints on regional climate extremes is obscured by observational and modeling uncertainties in spite of substantial ongoing improvements in models and new global reanalysis datasets (Sarojini et al., 2016).

In recent years, event attribution studies have been conducted to detect how anthropogenic forcings have altered the magnitude or probability of a particular type of extreme weather or climate-related event (Sarojini et al., 2016). In recent years efforts have been made to carry out such studies shortly after the events in question. For example, Tan et al. (2019) studied dynamic and thermodynamic changes conducive to the increased occurrence of extreme spring wildfires over western Canada. Mondal and Mujumdar (2015) performed a correlation-based detection and attribution analysis on extreme precipitation to investigate the presence of anthropogenic signals in observed precipitation changes in India.

(3) Nonstationary Intensity-Duration-Frequency (IDF) curves

Extreme climate events are likely to occur more frequently because of global warming, which is expected to result in additional stress over the life spans of critical infrastructures (Forzieri et al., 2018). However, current municipal infrastructure is designed using precipitation IDF curves assumed to be stationary (Cheng and Aghakouchak, 2014). To effectively mitigate the potential impact of future extreme precipitation events of Canada, the design of resilient infrastructure and resource management systems must account for the non-stationarity and the likelihood of future changes of extreme climate events (Diffenbaugh et al., 2017). For example, nonstationary precipitation IDF curves have been applied for urban infrastructure and drainage systems design (Agilan and Umamahesh, 2016; Kuo et al., 2015; Ouarda et al., 2019; Simonovic et al., 2016). More research on developing non-stationary IDF curves for Canadian municipalities are recommended.

Bibliography

Agilan, V., Umamahesh, N. V., 2016. Modelling nonlinear trend for developing non-stationary rainfall intensity-duration-frequency curve. Int. J. Climatol. 37, 1265–1281. https://doi.org/10.1002/joc.4774

Ahmed, K., Shahid, S., Harun, S. bin, Wang, X. jun, 2016. Characterization of seasonal droughts in Balochistan Province, Pakistan. Stoch. Environ. Res. Risk Assess. 30, 747–762. https://doi.org/10.1007/s00477-015-1117-2

Akaike, H., 1974. A new look at the statistical model identification. IEEE Trans. Automat. Contr. 19, 716–723. https://doi.org/10.1109/TAC.1974.1100705

Alexander, L. V., Zhang, X., Peterson, T.C., Caesar, J., Gleason, B., Klein Tank, A.M.G., Haylock, M., Collins, D., Trewin, B., Rahimzadeh, F., Tagipour, A., Rupa Kumar, K., Revadekar, J., Griffiths, G., Vincent, L., Stephenson, D.B., Burn, J., Aguilar, E., Brunet, M., Taylor, M., New, M., Zhai, P., Rusticucci, M., Vazquez-Aguirre, J.L., 2006. Global observed changes in daily climate extremes of temperature and precipitation. J. Geophys. Res. 111, D05109. https://doi.org/10.1029/2005JD006290

Allan, R.P., Soden, B.J., 2008. Atmospheric Warming and the Amplification of Precipitation Extremes. Science (80-.). 321, 1481–1484. https://doi.org/10.1126/science.1160787

Asong, Z.E., Khaliq, M.N., Wheater, H.S., 2016. Multisite multivariate modeling of daily precipitation and temperature in the Canadian Prairie Provinces using generalized linear models. Clim. Dyn. 47, 2901–2921. https://doi.org/10.1007/s00382-016-3004-z

Asong, Z.E., Wheater, H.S., Bonsal, B., Razavi, S., Kurkute, S., 2018. Historical drought patterns over Canada and their teleconnections with large-scale climate signals. Hydrol. Earth Syst. Sci. 22, 3105–3124. https://doi.org/10.5194/hess-22-3105-2018

Ayantobo, O.O., Li, Y., Song, S., 2019. Multivariate drought frequency analysis using four-variate symmetric and asymmetric Archimedean Copula functions. Water Resour. Manag. 33, 103–127. https://doi.org/10.1007/s11269-018-2090-6

Ayantobo, O.O., Li, Y., Song, S., Javed, T., Yao, N., 2018. Probabilistic modelling of drought events in China via 2-dimensional joint copula. J. Hydrol. 559, 373–391. https://doi.org/10.1016/j.jhydrol.2018.02.022

Baines, P.G., Folland, C.K., 2007. Evidence for a rapid global climate shift across the late 1960s. J. Clim. 20, 2721–2744. https://doi.org/10.1175/JCLI4177.1

Ban, N., Rajczak, J., Schmidli, J., Schär, C., 2018. Analysis of Alpine precipitation extremes using generalized extreme value theory in convection-resolving climate simulations. Clim. Dyn. 1–15. https://doi.org/10.1007/s00382-018-4339-4

Beguería, S., Vicente-Serrano, S.M., Reig, F., Latorre, B., 2014. Standardized precipitation evapotranspiration index (SPEI) revisited: Parameter fitting, evapotranspiration models, tools, datasets and drought monitoring. Int. J. Climatol. 34, 3001–3023. https://doi.org/10.1002/joc.3887

Beniston, M., Stephenson, D.B., 2004. Extreme climatic events and their evolution under changing climatic conditions. Glob. Planet. Change 44, 1–9. https://doi.org/10.1016/j.gloplacha.2004.06.001

Beniston, M., Stephenson, D.B., Christensen, O.B., Ferro, C.A.T., Frei, C., Goyette, S., Halsnaes, K., Holt, T., Jylhä, K., Koffi, B., Palutikof, J., Schöll, R., Semmler, T., Woth, K., 2007. Future extreme events in European climate: An exploration of regional climate model projections. Clim. Change 81, 71–95. https://doi.org/10.1007/s10584-006-9226-z

Benjamini, Y., Hochberg, Y., 1995. Controlling the False Discovery Rate: A Practical and Powerful Approach to Multiple Testing. J. R. Stat. Soc. Ser. B 57, 289–300. https://doi.org/10.2307/2346101

Benoit, D.F., Van den Poel, D., 2017. bayesQR: A Bayesian approach to quantile regression. J. Stat. Softw. 76, 1–32. https://doi.org/10.18637/jss.v076.i07

Benyahya, L., Gachon, P., St-Hilaire, A., Laprise, R., 2014. Frequency analysis of seasonal extreme precipitation in southern Quebec (Canada): an evaluation of regional climate model simulation with respect to two gridded datasets. Hydrol. Res. 45, 115. https://doi.org/10.2166/nh.2013.066

Berg, P., Moseley, C., Haerter, J.O., 2013. Strong increase in convective precipitation in response to higher temperatures. Nat. Geosci. 6, 181–185. https://doi.org/10.1038/ngeo1731

Bohlinger, P., Sorteberg, A., 2018. A comprehensive view on trends in extreme precipitation in Nepal and their spatial distribution. Int. J. Climatol. 38, 1833–1845. https://doi.org/10.1002/joc.5299

Bonsai, B.R., Wheaton, E.E., Bonsal, B.R., 2005. Atmospheric circulation comparisons between the 2001 and 2002 and the 1961 and 1988 Canadian Prairie droughts. Atmosphere-Ocean 43, 163–172. https://doi.org/10.3137/ao.430204

Bonsal, B., Regier, M., 2007. Historical comparison of the 2001/2002 drought in the Canadian Prairies. Clim. Res. 33, 229–242. https://doi.org/10.3354/cr033229

Bonsal, B., Shabbar, A., 2008. Impacts of Large-Scale Circulation Variability on Low Streamflows over Canada: A Review. Can. Water Resour. J. 33, 137–154. https://doi.org/10.4296/cwrj3302137

Bonsal, B.R., Aider, R., Gachon, P., Lapp, S., 2012. An assessment of Canadian prairie drought: past, present, and future. Clim. Dyn. 41, 501–516. https://doi.org/10.1007/s00382-012-1422-0

Bonsal, B.R., Chakravarti, A.K., Lawford, R.G., 1993. Teleconnections between North Pacific SST anomalies and growing season extended dry spells on the canadian prairies. Int. J. Climatol. 13, 865–878. https://doi.org/10.1002/joc.3370130805

Bonsal, B.R., Cuell, C., Wheaton, E., Sauchyn, D.J., Barrow, E., 2017. An assessment of historical and projected future hydro-climatic variability and extremes over southern watersheds in the Canadian Prairies. Int. J. Climatol. 37, 3934–3948. https://doi.org/10.1002/joc.4967

Bonsal, B.R., Lawford, R.G., 1999. Teleconnections between El Niño and La Niña events and summer extended dry spells on the Canadian Prairies. Int. J. Climatol. 19, 1445–1458.

Bonsal, B.R., Shabbar, A., Higuchi, K., 2001. Impacts of low frequency variability modes on Canadian winter temperature. Int. J. Climatol. 21, 95–108. https://doi.org/10.1002/joc.590

Bonsal, B.R., Wheaton, E.E., Chipanshi, A.C., Lin, C., Sauchyn, D.J., Wen, L., 2011. Drought Research in Canada: A Review. Atmosphere-Ocean 49, 303–319. https://doi.org/10.1080/07055900.2011.555103

Bracken, C., Rajagopalan, B., Alexander, M., Gangopadhyay, S., 2015. Spatial variability of seasonal extreme precipitation in the western United States. J. Geophys. Res. Atmos. 120, 4522–4533. https://doi.org/10.1002/2015JD023205

Brooks, H.E., Anderson, A.R., Riemann, K., Ebbers, I., Flachs, H., 2007. Climatological aspects of convective parameters from the NCAR/NCEP reanalysis. Atmos. Res. 83, 294–305. https://doi.org/10.1016/j.atmosres.2005.08.005

Brown, D.P., Comrie, A.C., 2004. A winter precipitation “dipole” in the western United States associated with multidecadal ENSO variability. Geophys. Res. Lett. 31, 1–4. https://doi.org/10.1029/2003GL018726

Bush, E., Lemmen, D.S., 2019. Canada’s changing climate report. Ottawa, ON.

Bush, E., Loder, J., James, T., Mortsch, L., Cohen, S., 2014. An overview of Canada’s changing climate, Canada in a Changing Climate: Sector Perspectives on Impacts and Adaptation, (ed.) FJ Warren and DS Lemmen. Ottawa, ON.

Canadian Meteorological and Oceanographic Society, 2016. Canada’s top ten weather stories for 2015 [WWW Document]. URL http://www.cmos.ca/site/top_ten?a=2015

Casanueva, A., Rodríguez-Puebla, C., Frías, M.D., González-Reviriego, N., 2014. Variability of extreme precipitation over Europe and its relationships with teleconnection patterns. Hydrol. Earth Syst. Sci. 18, 709–725. https://doi.org/10.5194/hess-18-709-2014

Cazelles, B., Chavez, M., Berteaux, D., Menard, F., Vik, J.O., Jenouvrier, S., Stenseth, N.C., 2008. Wavelet analysis of ecological time series. Oecologia 156, 287–304. https://doi.org/10.1007/s00442-008-0993-2

Chang, N. Bin, Vasquez, M.V., Chen, C.F., Imen, S., Mullon, L., 2015. Global nonlinear and nonstationary climate change effects on regional precipitation and forest phenology in Panama, Central America. Hydrol. Process. 29, 339–355. https://doi.org/10.1002/hyp.10151

Charrad, M., Ghazzali, N., Boiteau, V., Niknafs, A., 2014. NbClust: An R package for determining the relevant number of clusters in a data set. J. Stat. Softw. 61, 1–36. https://doi.org/10.18637/jss.v061.i06

Chen, L., Guo, S., 2019. Copulas and its applications in hydrology and water resources. Springer Water. https://doi.org/10.1007/978-981-13-0574-0_1

Chen, L., Singh, V.P., Guo, S., Zhou, J., Zhang, J., Liu, P., 2015. An objective method for partitioning the entire flood season into multiple sub-seasons. J. Hydrol. 528, 621–630. https://doi.org/10.1016/j.jhydrol.2015.07.003

Chen, M., Shi, W., Xie, P., Silva, V.B.S., Kousky, V.E., Higgins, R.W., Janowiak, J.E., 2008. Assessing objective techniques for gauge-based analyses of global daily precipitation. J. Geophys. Res. Atmos. 113, D04110. https://doi.org/10.1029/2007JD009132

Cheng, L., Aghakouchak, A., 2014. Nonstationary precipitation intensity-duration-frequency curves for infrastructure design in a changing climate. Sci. Rep. 4, 7093. https://doi.org/10.1038/srep07093

Choi, W., Kim, K., 2018. Physical mechanism of spring and early summer drought over North America associated with the boreal warming. Sci. Rep. 8, 1–8. https://doi.org/10.1038/s41598-018-25932-5

Cindrić, K., Pasarić, Z., Gajić-Čapka, M., 2010. Spatial and temporal analysis of dry spells in Croatia. Theor. Appl. Climatol. 102, 171–184. https://doi.org/10.1007/s00704-010-0250-6

Cioffi, F., Lall, U., Rus, E., Krishnamurthy, C.K.B., 2015. Space-time structure of extreme precipitation in Europe over the last century. Int. J. Climatol. 35, 1749–1760. https://doi.org/10.1002/joc.4116

Ciupak, M., Ozga-Zielinski, B., Adamowski, J., Quilty, J., Khalil, B., 2015. The application of Dynamic Linear Bayesian Models in hydrological forecasting: Varying Coefficient Regression and Discount Weighted Regression. J. Hydrol. 530, 762–784. https://doi.org/10.1016/j.jhydrol.2015.10.023

Coats, S., Smerdon, J.E., Cook, B.I., Seager, R., 2013. Stationarity of the tropical pacific teleconnection to North America in CMIP5/PMIP3 model simulations. Geophys. Res. Lett. 40, 4927–4932. https://doi.org/10.1002/grl.50938

Coles, S., 2001. An Introduction to Statistical Modeling of Extreme Values, Springer Series in Statistics. Springer London, London. https://doi.org/10.1007/978-1-4471-3675-0

Compo, G.P., Whitaker, J.S., Sardeshmukh, P.D., Matsui, N., Allan, R.J., Yin, X., Gleason, B.E., Vose, R.S., Rutledge, G., Bessemoulin, P., BroNnimann, S., Brunet, M., Crouthamel, R.I., Grant, A.N., Groisman, P.Y., Jones, P.D., Kruk, M.C., Kruger, A.C., Marshall, G.J., Maugeri, M., Mok, H.Y., Nordli, O., Ross, T.F., Trigo, R.M., Wang, X.L., Woodruff, S.D., Worley, S.J., 2011. The Twentieth Century Reanalysis Project. Q. J. R. Meteorol. Soc. 137, 1–28. https://doi.org/10.1002/qj.776

Cong, Z., Yang, D., Gao, B., Yang, H., Hu, H., 2009. Hydrological trend analysis in the Yellow River basin using a distributed hydrological model. Water Resour. Res. 45. https://doi.org/10.1029/2008WR006852

Cook, B.I., Smerdon, J.E., Seager, R., Coats, S., 2014. Global warming and 21st century drying. Clim. Dyn. 43, 2607–2627. https://doi.org/10.1007/s00382-014-2075-y

Costa, A.C., Soares, A., 2009. Trends in extreme precipitation indices derived from a daily rainfall database for the South of Portugal. Int. J. Climatol. 29, 1956–1975. https://doi.org/10.1002/joc.1834

Coulibaly, P., 2006. Spatial and temporal variability of Canadian seasonal precipitation (1900-2000). Adv. Water Resour. 29, 1846–1865. https://doi.org/10.1016/j.advwatres.2005.12.013

Cui, W., Dong, X., Xi, B., Kennedy, A., 2017. Evaluation of Reanalyzed Precipitation Variability and Trends Using the Gridded Gauge-Based Analysis over the CONUS. J. Hydrometeorol. 18, 2227–2248. https://doi.org/10.1175/JHM-D-17-0029.1

Dai, A., 2011a. Characteristics and trends in various forms of the Palmer Drought Severity Index during 1900-2008. J. Geophys. Res. Atmos. 116. https://doi.org/10.1029/2010JD015541

Dai, A., 2011b. Drought under global warming: A review. Wiley Interdiscip. Rev. Clim. Chang. 2, 45–65. https://doi.org/10.1002/wcc.81

Dai, A., 2008. Temperature and pressure dependence of the rain-snow phase transition over land and ocean. Geophys. Res. Lett. 35, n/a-n/a. https://doi.org/10.1029/2008GL033295

Dai, A., Trenberth, K.E., Karl, T.R., 1998. Global variations in droughts and wet spells: 1900-1995. Geophys. Res. Lett. 25, 3367–3370. https://doi.org/10.1029/98GL52511

Dai, A.G., 2013. Increasing drought under global warming in observations and models. Nat. Clim. Chang. 3, 52–58. https://doi.org/10.1038/nclimate1633

Daufresne, M., Lengfellner, K., Sommer, U., 2009. Global warming benefits the small in aquatic ecosystems. Proc. Natl. Acad. Sci. 106, 12788–12793. https://doi.org/10.1073/pnas.0902080106

DeMott, C.A., Randall, D.A., 2004. Observed variations of tropical convective available potential energy. J. Geophys. Res. 109, D02102. https://doi.org/10.1029/2003JD003784

Dhakal, N., Tharu, B., 2018. Spatio-temporal trends in daily precipitation extremes and their connection with North Atlantic tropical cyclones for the southeastern United States. Int. J. Climatol. https://doi.org/10.1002/joc.5535

Di Lorenzo, E., Schneider, N., Cobb, K.M., Franks, P.J.S., Chhak, K., Miller, A.J., McWilliams, J.C., Bograd, S.J., Arango, H., Curchitser, E., Powell, T.M., Rivière, P., 2008. North Pacific Gyre Oscillation links ocean climate and ecosystem change. Geophys. Res. Lett. 35. https://doi.org/10.1029/2007GL032838

Diffenbaugh, N.S., Singh, D., Mankin, J.S., Horton, D.E., Swain, D.L., Touma, D., Charland, A., Liu, Y., Haugen, M., Tsiang, M., Rajaratnam, B., 2017. Quantifying the influence of global warming on unprecedented extreme climate events. Proc. Natl. Acad. Sci. 114, 4881–4886. https://doi.org/10.1073/pnas.1618082114

Dominguez, F., Rivera, E., Lettenmaier, D.P., Castro, C.L., 2012. Changes in winter precipitation extremes for the western United States under a warmer climate as simulated by regional climate models. Geophys. Res. Lett. 39, n/a-n/a. https://doi.org/10.1029/2011GL050762

Dong, W., Lin, Y., Wright, J.S., Xie, Y., Yin, X., Guo, J., 2018. Precipitable water and CAPE dependence of rainfall intensities in China. Clim. Dyn. 1–12. https://doi.org/10.1007/s00382-018-4327-8

Doswell, C.A., Evans, J.S., 2003. Proximity sounding analysis for derechos and supercells: An assessment of similarities and differences. Atmos. Res. 67–68, 117–133. https://doi.org/10.1016/S0169-8095(03)00047-4

Duan, W., He, B., Takara, K., Luo, P., Hu, M., Alias, N.E., Nover, D., 2015. Changes of precipitation amounts and extremes over Japan between 1901 and 2012 and their connection to climate indices. Clim. Dyn. 45, 2273–2292. https://doi.org/10.1007/s00382-015-2778-8

Easterling, D.R., 2000. Climate Extremes: Observations, Modeling, and Impacts. Science (80-.). 289, 2068–2074. https://doi.org/10.1126/science.289.5487.2068

Easterling, D.R., Evans, J.L., Groisman, P.Y., Karl, T.R., Kunkel, K.E., Ambenje, P., 2000. Observed variability and trends in extreme climate events: A brief review. Bull. Am. Meteorol. Soc. 81, 417–425. https://doi.org/10.1175/1520-0477(2000)081<0417:OVATIE>2.3.CO;2

Easterling, D.R., Kunkel, K.E., Wehner, M.F., Sun, L., 2016. Detection and attribution of climate extremes in the observed record. Weather Clim. Extrem. 11, 17–27. https://doi.org/10.1016/j.wace.2016.01.001

Elewa, H.H., Ramadan, E.-S.M., Nosair, A.M., 2016. Spatial-based hydro-morphometric watershed modeling for the assessment of flooding potentialities. Environ. Earth Sci. 75, 927. https://doi.org/10.1007/s12665-016-5692-4

Escalante-Sandoval, C., Nuñez-Garcia, P., 2017. Meteorological drought features in northern and northwestern parts of Mexico under different climate change scenarios. J. Arid Land 9, 65–75. https://doi.org/10.1007/s40333-016-0022-y

Fang, W., Huang, S., Huang, G., Huang, Q., Wang, H., Wang, L., Zhang, Y., Li, P., Ma, L., 2018. Copulas-based risk analysis for inter-seasonal combinations of wet and dry conditions under a changing climate. Int. J. Climatol. https://doi.org/10.1002/joc.5929

Faustin Katchele, O., Ma, Z.-G., Yang, Q., Batebana, K., 2017. Comparison of trends and frequencies of drought in central North China and sub-Saharan Africa from 1901 to 2010. Atmos. Ocean. Sci. Lett. 1–9. https://doi.org/10.1080/16742834.2017.1392825

Fay, P.A., Carlisle, J.D., Knapp, A.K., Blair, J.M., Collins, S.L., 2003. Productivity responses to altered rainfall patterns in a C 4-dominated grassland. Oecologia 137, 245–251. https://doi.org/10.1007/s00442-003-1331-3

Ficklin, D.L., Maxwell, J.T., Letsinger, S.L., Gholizadeh, H., 2015. A climatic deconstruction of recent drought trends in the United States. Environ. Res. Lett. 10, 044009. https://doi.org/10.1088/1748-9326/10/4/044009

Field, C.B., Barros, V., Stocker, T.F., Dahe, Q., Dokken, D.J., Ebi, K.L., Mastrandrea, M.D., Mach, K.J., Plattner, G.-K., Allen, S.K., Tignor, M., Midgley, P.M., 2012. Managing the risks of extreme events and disasters to advance climate change adaptation: Special report of the Intergovernmental Panel on Climate Change. Cambridge, UK, and New York, NY, USA.

Fischer, A.M., Keller, D.E., Liniger, M.A., Rajczak, J., Schär, C., Appenzeller, C., 2015. Projected changes in precipitation intensity and frequency in Switzerland: A multi-model perspective. Int. J. Climatol. 35, 3204–3219. https://doi.org/10.1002/joc.4162

Fischer, E.M., Knutti, R., 2016. Observed heavy precipitation increase confirms theory and early models. Nat. Clim. Chang. 6, 986–991. https://doi.org/10.1038/nclimate3110

Forzieri, G., Bianchi, A., Silva, F.B. e., Marin Herrera, M.A., Leblois, A., Lavalle, C., Aerts, J.C.J.H., Feyen, L., 2018. Escalating impacts of climate extremes on critical infrastructures in Europe. Glob. Environ. Chang. 48, 97–107. https://doi.org/10.1016/j.gloenvcha.2017.11.007

Frazier, A.G., Giambelluca, T.W., 2016. Spatial trend analysis of Hawaiian rainfall from 1920 to 2012. Int. J. Climatol. https://doi.org/10.1002/joc.4862

Fu, C., James, A.L., Wachowiak, M.P., 2012. Analyzing the combined influence of solar activity and El Niño on streamflow across southern Canada. Water Resour. Res. 48. https://doi.org/10.1029/2011WR011507

Fu, X., Kuo, C.C., Gan, T.Y., 2014. Change point analysis of precipitation indices of Western Canada. Int. J. Climatol. 35, 2592–2607. https://doi.org/10.1002/joc.4144

Gan, T.Y., 1998. Hydroclimatic trends and possible climatic warming in the Canadian Prairies. Water Resour. Res. 34, 3009–3015. https://doi.org/10.1029/98WR01265

Gan, T.Y., Barry, R.G., Gizaw, M., Gobena, A., Balaji, R., 2013. Changes in North American snowpacks for 1979-2007 detected from the snow water equivalent data of SMMR and SSM/I passive microwave and related climatic factors. J. Geophys. Res. Atmos. 118, 7682–7697. https://doi.org/10.1002/jgrd.50507

Gan, T.Y., Gobena, A.K., Wang, Q., 2007. Precipitation of southwestern Canada: Wavelet, scaling, multifractal analysis, and teleconnection to climate anomalies. J. Geophys. Res. Atmos. 112. https://doi.org/10.1029/2006JD007157

Gan, T.Y., Ito, M., Huelsmann, S., Qin, X., Lu, X., Liong, S.Y., Rutschman, P., Disse, M., Koivosalo, H., 2016. Possible climate change/variability and human impacts, vulnerability of African drought prone regions, its water resources and capacity building. Hydrol. Sci. J. 61, 1209–1226. https://doi.org/10.1080/02626667.2015.1057143

Gao, L., Huang, J., Chen, X., Chen, Y., Liu, M., 2017. Risk of Extreme Precipitation under Nonstationarity Conditions during the Second Flood Season in the Southeastern Coastal Region of China. J. Hydrometeorol. 18, 669–681. https://doi.org/10.1175/JHM-D-16-0119.1

Gao, T., Wang, H.J., Zhou, T., 2017. Changes of extreme precipitation and nonlinear influence of climate variables over monsoon region in China. Atmos. Res. 197, 379–389. https://doi.org/10.1016/j.atmosres.2017.07.017

Ge, Y., Apurv, T., Cai, X., 2016. Spatial and temporal patterns of drought in the Continental U.S. during the past century. Geophys. Res. Lett. https://doi.org/10.1002/2016GL069660

Gibbons, J.D., Chakraborti, S., 2011. Nonparametric statistical inference, 5th Editio. ed. Chapman & Hall/Taylor & Francis.

Gilleland, E., Katz, R.W., 2016. extRemes 2.0: An Extreme Value Analysis Package in R. J. Stat. Softw. 72, 1–39. https://doi.org/10.18637/jss.v072.i08

Girardin, M.P., Tardif, J., Flannigan, M.D., Bergeron, Y., 2004a. Multicentury reconstruction of the Canadian Drought Code from eastern Canada and its relationship with paleoclimatic indices of atmospheric circulation. Clim. Dyn. 23, 99–115. https://doi.org/10.1007/s00382-004-0417-x

Girardin, M.P., Tardif, J., Flannigan, M.D., Wotton, B.M., Bergeron, Y., 2004b. Trends and periodicities in the Canadian Drought Code and their relationships with atmospheric circulation for the southern Canadian boreal forest. Can. J. For. Res. 34, 103–119. https://doi.org/10.1139/x03-195

Gizaw, M.S., Gan, T.Y., 2016a. Possible impact of climate change on future extreme precipitation of the Oldman, Bow and Red Deer River Basins of Alberta. Int. J. Climatol. 36, 208–224. https://doi.org/10.1002/joc.4338

Gizaw, M.S., Gan, T.Y., 2016b. Regional Flood Frequency Analysis using Support Vector Regression under historical and future climate. J. Hydrol. 538, 387–398. https://doi.org/10.1016/j.jhydrol.2016.04.041

Gobena, A.K., Gan, T.Y., 2013. Assessment of trends and possible climate change impacts on summer moisture availability in western canada based on metrics of the palmer drought severity index. J. Clim. 26, 4583–4595. https://doi.org/10.1175/JCLI-D-12-00421.1

Gocic, M., Trajkovic, S., 2015. Water surplus variability index as an indicator of drought. J. Hydrol. Eng. 20, 04014038. https://doi.org/10.1061/(ASCE)HE.1943-5584.0001008

Gong, X., Richman, M.B., 1995. On the application of cluster analysis to growing season precipitation data in North America east of the Rockies. J. Clim. 8, 897–931. https://doi.org/10.1175/1520-0442(1995)008<0897:OTAOCA>2.0.CO;2

Greene, H., Leighton, H.G., Stewart, R.E., 2011. Drought and associated cloud fields over the canadian prairie provinces. Atmos. - Ocean 49, 356–365. https://doi.org/10.1080/07055900.2011.559771

Gregersen, I.B., Madsen, H., Rosbjerg, D., Arnbjerg-Nielsen, K., 2015. Long term variations of extreme rainfall in Denmark and southern Sweden. Clim. Dyn. 44, 3155–3169. https://doi.org/10.1007/s00382-014-2276-4

Gregersen, I.B., Sørup, H.J.D., Madsen, H., Rosbjerg, D., Mikkelsen, P.S., Arnbjerg-Nielsen, K., 2013. Assessing future climatic changes of rainfall extremes at small spatio-temporal scales. Clim. Change 118, 783–797. https://doi.org/10.1007/s10584-012-0669-0

Grinsted, A., Moore, J.C., Jevrejeva, S., 2004. Application of the cross wavelet transform and wavelet coherence to geophysical time series. Nonlinear Process. Geophys. 11, 561–566. https://doi.org/10.5194/npg-11-561-2004

Groisman, P.Y., Knight, R.W., Karl, T.R., Easterling, D.R., Sun, B., Lawrimore, J.H., 2004. Contemporary changes of the hydrological cycle over the Contiguous United States: Trends derived from in situ observations. J. Hydrometeorol. 5, 64–85. https://doi.org/10.1175/1525-7541(2004)005<0064:CCOTHC>2.0.CO;2

Guenang, G.M., Mkankam Kamga, F., 2014. Computation of the standardized precipitation index (SPI) and its use to assess drought occurrences in Cameroon over recent decades. J. Appl. Meteorol. Climatol. 53, 2310–2324. https://doi.org/10.1175/JAMC-D-14-0032.1

Guichard, F., Petch, J.C., Redelsperger, J.L., Bechtold, P., Chaboureau, J.P., Cheinet, S., Grabowski, W., Grenier, H., Jones, C.G., Köhler, M., Piriou, J.M., Tailleux, R., Tomasini, M., 2004. Modelling the diurnal cycle of deep precipitating convection over land with cloud-resolving models and single-column models. Q. J. R. Meteorol. Soc. 130 C, 3139–3172. https://doi.org/10.1256/qj.03.145

Guo, H., Bao, A., Liu, T., Jiapaer, G., Ndayisaba, F., Jiang, L., Kurban, A., De Maeyer, P., 2018. Spatial and temporal characteristics of droughts in Central Asia during 1966–2015. Sci. Total Environ. 624, 1523–1538. https://doi.org/10.1016/j.scitotenv.2017.12.120

Gutowski, W.J., Hegerl, G.C., Holland, G.J., Knutson, T.R., Mearns, L.O., Stouffer, R.J., Webster, P.J., Wehner, M.F., Zwiers, F.W., 2008. Causes of observed changes in extremes and projections of future changes. Weather Clim. Extrem. a Chang. Clim. Reg. Focus. North Am. Hawaii, Caribbean, U.S. Pacific Islands T.R. Karl, G.A. Meehl, C.D. Miller, S.J. Hassol, A.M. Waple, W.L. Murray.

Hales, S., Edwards, S.J., Kovats, R.S., 2003. Impacts on health of climate extremes, in: Climate Change and Human Health: Risks and Responses. pp. 79–102.

Hamed, K.H., Rao, A.R., 1998. A modified Mann-Kendall trend test for autocorrelated data. J. Hydrol. 204, 182–196. https://doi.org/10.1016/S0022-1694(97)00125-X

Hanesiak, J.M., Stewart, R.E., Bonsal, B.R., Harder, P., Lawford, R., Aider, R., Amiro, B.D., Atallah, E., Barr, A.G., Black, T.A., Bullock, P., Brimelow, J.C., Brown, R., Carmichael, H., Derksen, C., Flanagan, L.B., Gachon, P., Greene, H., Gyakum, J., Henson, W., Hogg, E.H., Kochtubajda, B., Leighton, H., Lin, C., Luo, Y., McCaughey, J.H., Meinert, A., Shabbar, A., Snelgrove, K., Szeto, K., Trishchenko, A., Van Der Kamp, G., Wang, S., Wen, L., Wheaton, E., Wielki, C., Yang, Y., Yirdaw, S., Zha, T., 2011. Characterization and summary of the

1999-2005 Canadian Prairie drought. Atmos. - Ocean 49, 421–452. https://doi.org/10.1080/07055900.2011.626757

Hansen, J., Sato, M., Ruedy, R., 2012. Perception of climate change. Proc. Natl. Acad. Sci. 109, E2415–E2423. https://doi.org/10.1073/pnas.1205276109

Hao, Z., Singh, V.P., Xia, Y., 2018. Seasonal drought prediction: advances, challenges, and future prospects. Rev. Geophys. https://doi.org/10.1002/2016RG000549

Harris, I., Jones, P.D., Osborn, T.J., Lister, D.H., 2014. Updated high-resolution grids of monthly climatic observations - the CRU TS3.10 Dataset. Int. J. Climatol. 34, 623–642. https://doi.org/10.1002/joc.3711

Hartmann, D.L., Klein Tank, A.M.G., Rusticucci, M., Alexander, L.V., Brönnimann, S., Charabi, Y., Dentener, F.J., Dlugokencky, E.J., Easterling, D.R., Kaplan, A., Soden, B.J., Thorne, P.W., Wild, M., Zhai, P.M., 2013. Observations: Atmosphere and Surface, in: Climate Change 2013: The Physical Science Basis. Contribution of Working Group I to the Fifth Assessment Report of the Intergovernmental Panel on Climate Change. Cambridge University Press, Cambridge, United Kingdom and New York, NY, USA.

He, Y., Ye, J., Yang, X., 2015. Analysis of the spatio-temporal patterns of dry and wet conditions in the Huai River Basin using the standardized precipitation index. Atmos. Res. 166, 120–128. https://doi.org/10.1016/j.atmosres.2015.06.022

Held, I.M., Soden, B.J., 2006. Robust responses of the hydrological cycle to global warming. J. Clim. 19, 5686–5699. https://doi.org/10.1175/2010JCLI4045.1

Hirsch, R.M., Slack, J.R., Smith, R.A., 1982. Techniques of trend analysis for monthly water quality data. Water Resour. Res. 18, 107–121. https://doi.org/10.1029/WR018i001p00107

Hou, D., Charles, M., Luo, Y., Toth, Z., Zhu, Y., Krzysztofowicz, R., Lin, Y., Xie, P., Seo, D.-J., Pena, M., Cui, B., 2014. Climatology-Calibrated Precipitation Analysis at Fine Scales: Statistical Adjustment of Stage IV toward CPC Gauge-Based Analysis. J. Hydrometeorol. 15, 2542–2557. https://doi.org/10.1175/JHM-D-11-0140.1

Hryciw, L.M., Atallah, E.H., Milrad, S.M., Gyakum, J.R., 2013. A meteorological analysis of important contributors to the 1999–2005 Canadian Prairie drought. Mon. Weather Rev. 141, 3593–3609. https://doi.org/10.1175/MWR-D-12-00261.1

Hu, Z., Zhou, Q., Chen, X., Li, J., Li, Q., Chen, D., Liu, W., Yin, G., 2018. Evaluation of three global gridded precipitation data sets in central Asia based on rain gauge observations. Int. J. Climatol. https://doi.org/10.1002/joc.5510

Huang, H., Winter, J.M., Osterberg, E.C., Horton, R.M., Beckage, B., 2017. Total and Extreme Precipitation Changes over the Northeastern United States. J. Hydrometeorol. 18, 1783–1798. https://doi.org/10.1175/JHM-D-16-0195.1

Hurrell, J.W., Kushnir, Y., Visbeck, M.H., 2001. The North Atlantic Oscillation. Science (80-.). 291, 603–5. https://doi.org/10.1126/science.1058761

Ionita, M., Boroneant, C., Chelcea, S., 2015. Seasonal modes of dryness and wetness variability over Europe and their connections with large scale atmospheric circulation and global sea surface temperature. Clim. Dyn. 45, 2803–2829. https://doi.org/10.1007/s00382-015-2508-2

IPCC, 2018. Summary for policymakers, in: Global Warming of 1.5°C. An IPCC Special Report on the Impacts of Global Warming of 1.5°C above Pre-Industrial Levels and Related Global Greenhouse Gas Emission Pathways, in the Context of Strengthening the Global Response to the Threat of Climate Change,.

IPCC, 2014. Climate Change 2014: Synthesis Report. Contribution of Working Groups I, II and III to the Fifth Assessment Report of the Intergovernmental Panel on Climate Change. Geneva, Switzerland.

Islam, Z., Gan, T.Y., 2015. Potential combined hydrologic impacts of climate change and El Niño Southern Oscillation to South Saskatchewan River Basin. J. Hydrol. 523, 34–48. https://doi.org/10.1016/j.jhydrol.2015.01.043

Jacques-Coper, M., Garreaud, R.D., 2015. Characterization of the 1970s climate shift in South America. Int. J. Climatol. 35, 2164–2179. https://doi.org/10.1002/joc.4120

Jiang, P., Yu, Z., Gautam, M.R., Acharya, K., 2016. The Spatiotemporal Characteristics of Extreme Precipitation Events in the Western United States. Water Resour. Manag. 1–15. https://doi.org/10.1007/s11269-016-1454-z

Jiang, R., Gan, T.Y., Xie, J., Wang, N., 2014a. Spatiotemporal variability of Alberta's seasonal precipitation, their teleconnection with large-scale climate anomalies and sea surface temperature. Int. J. Climatol. 34, 2899–2917. https://doi.org/10.1002/joc.3883

Jiang, R., Gan, T.Y., Xie, J., Wang, N., Kuo, C.C., 2015. Historical and potential changes of precipitation and temperature of Alberta subjected to climate change impact: 1900–2100. Theor. Appl. Climatol. 127, 725–739. https://doi.org/10.1007/s00704-015-1664-y

Jiang, R., Xie, J., He, H., Luo, J., Zhu, J., 2014b. Use of four drought indices for evaluating drought characteristics under climate change in Shaanxi, China: 1951-2012. Nat. Hazards 75, 2885–2903. https://doi.org/10.1007/s11069-014-1468-x

Jiang, R., Xie, J., Zhao, Y., He, H., He, G., 2016. Spatiotemporal variability of extreme precipitation in Shaanxi province under climate change. Theor. Appl. Climatol. 1–15. https://doi.org/10.1007/s00704-016-1910-y

Jiang, R., Yu, X., Xie, J., Zhao, Y., Li, F., Yang, M., 2017. Recent changes in daily climate extremes in a serious water shortage metropolitan region, a case study in Jing-Jin-Ji of China. Theor. Appl. Climatol. https://doi.org/10.1007/s00704-017-2293-4

Jolliffe, I.T., 2002. Principal Component Analysis, 2nd ed, Springer Series in Statistics. Springer-Verlag, New York. https://doi.org/10.1007/b98835

Joshi, N., Gupta, D., Suryavanshi, S., Adamowski, J., Madramootoo, C.A., 2016. Analysis of trends and dominant periodicities in drought variables in India: A wavelet transform based approach. Atmos. Res. 182, 200–220. https://doi.org/10.1016/j.atmosres.2016.07.030

Kanamitsu, M., Ebisuzaki, W., Woollen, J., Yang, S.K., Hnilo, J.J., Fiorino, M., Potter, G.L., 2002. NCEP-DOE AMIP-II reanalysis (R-2). Bull. Am. Meteorol. Soc. 83, 1631-1643+1559. https://doi.org/10.1175/BAMS-83-11-1631(2002)083<1631:NAR>2.3.CO;2

Karl, T.R., Koss, W.J., 1984. Regional and national monthly, seasonal, and annual temperature weighted by area, 1895-1983. Hist. Climatol. Ser. 3-3.

Kendall, M.G., 1948. Rank correlation methods, Griffin: London.

Khaliq, M.N., Ouarda, T.B.M.J., Ondo, J.C., Gachon, P., Bobée, B., 2006. Frequency analysis of a sequence of dependent and/or non-stationary hydro-meteorological observations: A review. J. Hydrol. 329, 534–552. https://doi.org/10.1016/j.jhydrol.2006.03.004

Kim, H., Kim, S., Shin, H., Heo, J.H., 2017. Appropriate model selection methods for nonstationary generalized extreme value models. J. Hydrol. 547, 557–574. https://doi.org/10.1016/j.jhydrol.2017.02.005

Kishtawal, C.M., Niyogi, D., Tewari, M., Pielke, R.A., Shepherd, J.M., 2010. Urbanization signature in the observed heavy rainfall climatology over India. Int. J. Climatol. 30, 1908–1916. https://doi.org/10.1002/joc.2044

Koenker, R., Bassett, G., 1978. Regression quantiles. Econometrica 46, 33. https://doi.org/10.2307/1913643

Koenker, R., Hallock, K.F., 2001. Quantile regression. J. Econ. Perspect. 15, 143–156. https://doi.org/10.1257/jep.15.4.143

Krichak, S.O., Barkan, J., Breitgand, J.S., Gualdi, S., Feldstein, S.B., 2015. The role of the export of tropical moisture into midlatitudes for extreme precipitation events in the Mediterranean region. Theor. Appl. Climatol. 121, 499–515. https://doi.org/10.1007/s00704-014-1244-6

Kunkel, K.E., 2003. North American trends in extreme precipitation. Nat. Hazards 29, 291–305. https://doi.org/10.1023/A:1023694115864

Kunkel, K.E., Andsager, K., Easterling, D.D.R., 1999. Long-Term Trends in Extreme Precipitation Events over the Conterminous United States and Canada. J. Clim. 12, 2515–2527. https://doi.org/http://dx.doi.org/10.1175/1520-0442(1999)012<2515:LTTIEP>2.0.CO;2

Kunkel, K.E., Robinson, D.A., Champion, S., Yin, X., Estilow, T., Frankson, R.M., 2016. Trends and extremes in Northern Hemisphere snow characteristics. Curr. Clim. Chang. Reports 2, 65–73. https://doi.org/10.1007/s40641-016-0036-8

Kuo, C.-C., Gan, T.Y., Gizaw, M., 2015. Potential impact of climate change on intensity duration frequency curves of central Alberta. Clim. Change 130, 115–129. https://doi.org/10.1007/s10584-015-1347-9

Kutiel, H., Türkeş, M., 2017. Spatial and temporal variability of dryness characteristics in Turkey. Int. J. Climatol. 37, 818–828. https://doi.org/10.1002/joc.5040

Lana, X., Burgueño, A., Martínez, M.D., Serra, C., 2006. Statistical distributions and sampling strategies for the analysis of extreme dry spells in Catalonia (NE Spain). J. Hydrol. 324, 94–114. https://doi.org/10.1016/j.jhydrol.2005.09.013

Larsen, S.H., 2005. Solar variability, dimethyl sulphide, clouds, and climate. Global Biogeochem. Cycles 19, 1–12. https://doi.org/10.1029/2004GB002333

Lemmen, D.S., Warren, F.J., 2004. Climate change impacts and adaptation: a Canadian perspective. Ottawa, Ontario.

Lenderink, G., Van Meijgaard, E., 2008. Increase in hourly precipitation extremes beyond expectations from temperature changes. Nat. Geosci. 1, 511–514. https://doi.org/10.1038/ngeo262

Lepore, C., Veneziano, D., Molini, A., 2015. Temperature and CAPE dependence of rainfall extremes in the eastern United States. Geophys. Res. Lett. 42, 74–83. https://doi.org/10.1002/2014GL062247

Li, J., Chen, Y.D., Gan, T.Y., Lau, N.-C., 2018. Elevated increases in human-perceived temperature under climate warming. Nat. Clim. Chang. 8, 43–47. https://doi.org/10.1038/s41558-017-0036-2

Li, X., Babovic, V., 2018. A new scheme for multivariate, multisite weather generator with inter-variable, inter-site dependence and inter-annual variability based on empirical copula approach. Clim. Dyn. 1–21. https://doi.org/10.1007/s00382-018-4249-5

Li, X., Meshgi, A., Babovic, V., 2016. Spatio-temporal variation of wet and dry spell characteristics of tropical precipitation in Singapore and its association with ENSO. Int. J. Climatol. 36, 4831–4846. https://doi.org/10.1002/joc.4672

Limsakul, A., Singhruck, P., 2016. Long-term trends and variability of total and extreme precipitation in Thailand. Atmos. Res. 169, 301–317. https://doi.org/10.1016/j.atmosres.2015.10.015

Liu, B., Chen, Xiuhong, Li, Y., Chen, Xiaohong, 2018. Long-term change of potential evapotranspiration over southwest China and teleconnections with large-scale climate anomalies. Int. J. Climatol. 38, 1964–1975. https://doi.org/10.1002/joc.5309

Lolis, C., Türkeş, M., 2016. Atmospheric circulation characteristics favouring extreme precipitation in Turkey. Clim. Res. 71, 139–153. https://doi.org/10.3354/cr01433

Lovino, M.A., Müller, O. V., Berbery, E.H., Müller, G. V., 2018. How have daily climate extremes changed in the recent past over northeastern Argentina? Glob. Planet. Change 168, 78–97. https://doi.org/10.1016/j.gloplacha.2018.06.008

Mann, H.B., 1945. Nonparametric tests against trend. Econometrica 13, 245–259.

Mantua, N.J., Hare, S.R., 2002. The Pacific Decadal Oscillation. J. Oceanogr. 58, 35–44. https://doi.org/10.1023/A:1015820616384

Mascaro, G., 2018. On the distributions of annual and seasonal daily rainfall extremes in central Arizona and their spatial variability. J. Hydrol. 559, 266–281. https://doi.org/10.1016/j.jhydrol.2018.02.011

Mass, C., Skalenakis, A., Warner, M., 2011. Extreme Precipitation over the West Coast of North America: Is There a Trend? J. Hydrometeorol. 12, 310–318. https://doi.org/10.1175/2010JHM1341.1

May, W., 2008. Potential future changes in the characteristics of daily precipitation in Europe simulated by the HIRHAM regional climate model. Clim. Dyn. 30, 581–603. https://doi.org/10.1007/s00382-007-0309-y

Mckee, T.B., Doesken, N.J., Kleist, J., 1993. The relationship of drought frequency and duration to time scales. AMS 8th Conf. Appl. Climatol. 179–184. https://doi.org/citeulike-article-id:10490403

McKee, T.B., Doesken, N.J., Kleist, J., 1995. Drought monitoring with multiple Time scales. Proc. 9th AMS Conf. Appl. Climatol. 233–236.

McMillen, D.P., 2013. Quantile regression for spatial data, SpringerBriefs in Regional Science. Springer Berlin Heidelberg, Berlin, Heidelberg. https://doi.org/10.1007/978-3-642-31815-3

Meehl, G. a, Washington, W.M., Wigley, T.M.L., Arblaster, J.M., Dai, A., 2002. Solar and greenhouse gas forcing and climate response in the twentieth century. J. Clim. 16, 426–444. https://doi.org/10.1175/1520-0442(2003)016<0426:SAGGFA>2.0.CO;2

Meehl, G.A., Hu, A., Santer, B.D., 2009. The mid-1970s climate shift in the pacific and the relative roles of forced versus inherent decadal variability. J. Clim. 22, 780–792. https://doi.org/10.1175/2008JCLI2552.1

Mekis, É., Vincent, L.A., 2011. An overview of the Second Generation Adjusted Daily Precipitation Dataset for trend analysis in Canada. Atmosphere-Ocean 49, 163–177. https://doi.org/10.1080/07055900.2011.583910

Menne, M.J., Durre, I., Vose, R.S., Gleason, B.E., Houston, T.G., 2012. An overview of the global historical climatology network-daily database. J. Atmos. Ocean. Technol. 29, 897–910. https://doi.org/10.1175/JTECH-D-11-00103.1

Mesinger, F., DiMego, G., Kalnay, E., Mitchell, K., Shafran, P.C., Ebisuzaki, W., Jović, D., Woollen, J., Rogers, E., Berbery, E.H., Ek, M.B., Fan, Y., Grumbine, R., Higgins, W., Li, H.,

Lin, Y., Manikin, G., Parrish, D., Shi, W., 2006. North American regional reanalysis. Bull. Am. Meteorol. Soc. 87, 343–360. https://doi.org/10.1175/BAMS-87-3-343

Meukaleuni, C., Lenouo, A., Monkam, D., 2016. Climatology of convective available potential energy (CAPE) in ERA-Interim reanalysis over West Africa. Atmos. Sci. Lett. 17, 65–70. https://doi.org/10.1002/asl.601

Meyn, A., Schmidtlein, S., Taylor, S.W., Girardin, M.P., Thonicke, K., Cramer, W., 2010. Spatial variation of trends in wildfire and summer drought in British Columbia, Canada, 1920-2000. Int. J. Wildl. Fire 19, 272–283. https://doi.org/10.1071/WF09055

Miao, C., Ashouri, H., Hsu, K.-L., Sorooshian, S., Duan, Q., 2015. Evaluation of the PERSIANN-CDR Daily Rainfall Estimates in Capturing the Behavior of Extreme Precipitation Events over China. J. Hydrometeorol. 16, 1387–1396. https://doi.org/10.1175/JHM-D-14-0174.1

Miller, A., Cayan, D., Barnett, T., Graham, N., Oberhuber, J., 1994. The 1976-77 climate shift of the Pacific Ocean. Oceanography. https://doi.org/10.5670/oceanog.1994.11

Milly, P.C.D., Betancourt, J., Falkenmark, M., Hirsch, R.M., Kundzewicz, Z.W., Lettenmaier, D.P., Stouffer, R.J., 2008. Stationarity is dead: Whither water management? Science (80-.). 319, 573–574. https://doi.org/10.1126/science.1151915

Milrad, S.M., Gyakum, J.R., Atallah, E.H., 2015. A Meteorological Analysis of the 2013 Alberta Flood: Antecedent Large-Scale Flow Pattern and Synoptic–Dynamic Characteristics. Mon. Weather Rev. 143, 2817–2841. https://doi.org/10.1175/MWR-D-14-00236.1

Mishra, A.K., Singh, V.P., 2010. A review of drought concepts. J. Hydrol. 391, 202–216. https://doi.org/10.1016/j.jhydrol.2010.07.012

Mitchell, K.E., 2004. The multi-institution North American Land Data Assimilation System (NLDAS): Utilizing multiple GCIP products and partners in a continental distributed hydrological modeling system. J. Geophys. Res. 109, D07S90. https://doi.org/10.1029/2003jd003823

Mladjic, B., Sushama, L., Khaliq, M.N., Laprise, R., Caya, D., Roy, R., 2011. Canadian RCM Projected Changes to Extreme Precipitation Characteristics over Canada. J. Clim. 24, 2565–2584. https://doi.org/10.1175/2010JCLI3937.1

Mondal, A., Mujumdar, P.P., 2015. On the detection of human influence in extreme precipitation over India. J. Hydrol. 529, 1161–1172. https://doi.org/10.1016/j.jhydrol.2015.09.030

Monkam, D., 2002. Convective available potential energy (CAPE) in Northern Africa and tropical Atlantic and study of its connections with rainfall in Central and West Africa during summer 1985. Atmos. Res. 62, 125–147. https://doi.org/10.1016/S0169-8095(02)00006-6

Murugavel, P., Pawar, S.D., Gopalakrishnan, V., 2012. Trends of Convective Available Potential Energy over the Indian region and its effect on rainfall. Int. J. Climatol. 32, 1362–1372. https://doi.org/10.1002/joc.2359

Mwale, D., Gan, T.Y., Devito, K., Mendoza, C., Silins, U., Petrone, R., 2009. Precipitation variability and its relationship to hydrologic variability in Alberta. Hydrol. Process. 23, 3040–3056. https://doi.org/10.1002/hyp.7415

Naumann, G., Alfieri, L., Wyser, K., Mentaschi, L., Betts, R.A., Carrao, H., Spinoni, J., Vogt, J., Feyen, L., 2018. Global changes in drought conditions under different levels of warming. Geophys. Res. Lett. https://doi.org/10.1002/2017GL076521

Neena, J.M., Goswami, B.N., 2010. Extension of potential predictability of Indian summer monsoon dry and wet spells in recent decades. Q. J. R. Meteorol. Soc. 136, 583–592. https://doi.org/10.1002/qj.595

Nguyen, H.T.T., Galelli, S., 2018. A Linear Dynamical Systems Approach to Streamflow Reconstruction Reveals History of Regime Shifts in Northern Thailand. Water Resour. Res. https://doi.org/10.1002/2017WR022114

Ntale, H.K., Gan, T.Y., 2004. East African Rainfall Anomaly Patterns in Association with El Niño/Southern Oscillation. J. Hydrol. Eng. 9, 257–268. https://doi.org/10.1061/(ASCE)1084-0699(2004)9:4(257)

O'Gorman, P.A., 2014. Contrasting responses of mean and extreme snowfall to climate change. Nature 512, 416–418. https://doi.org/10.1038/nature13625

O'Gorman, P.A., Schneider, T., 2009. The physical basis for increases in precipitation extremes in simulations of 21st-century climate change. Proc. Natl. Acad. Sci. 106, 14773–14777. https://doi.org/10.1073/pnas.0907610106

O'Kane, T.J., Matear, R.J., Chamberlain, M.A., Oke, P.R., 2014. ENSO regimes and the late 1970's climate shift: The role of synoptic weather and South Pacific ocean spiciness. J. Comput. Phys. 271, 19–38. https://doi.org/10.1016/j.jcp.2013.10.058

Okonkwo, C., 2014. An Advanced Review of the Relationships between Sahel Precipitation and Climate Indices: A Wavelet Approach. Int. J. Atmos. Sci. 2014, 1–11. https://doi.org/10.1155/2014/759067

Orgeville, M., Peltier, W.R., Erler, A.R., Gula, J., 2014. Climate change impacts on Great Lakes Basin precipitation extremes. J. Geophys. Res. Atmos. 119, 10799–10812. https://doi.org/10.1002/2014JD021855.Received

Ouarda, T.B.M.J., Yousef, L.A., Charron, C., 2019. Non-stationary intensity-duration-frequency curves integrating information concerning teleconnections and climate change. Int. J. Climatol. 39, 2306–2323. https://doi.org/10.1002/joc.5953

Pachauri, R.K., Allen, M.R., Barros, V.R., Broome, J., Cramer, W., Christ, R., Church, J.A., Clarke, L., Dahe, Q.D., Dasqupta, P., Dubash, N.K., Edenhofer, O., Elgizouli, I., Field, C.B., Forster, P., Friedlingstein, P., Fuglestvedt, J., Gomez-Echeverri, L., Hallegatte, S., Hegerl, G., Howden, M., Jiang, K., Jimenez Cisneros, B., Kattsov, V., Lee, H., Mach, K.J., Marotzke, J., Mastrandrea, M.D., Meyer, L., Minx, J., Mulugetta, Y., O'Brien, K., Oppenheimer, M., Pereira, J.J., Pichs-Madruga, R., Plattner, G.-K., Pörtner, H.-O., Power, S.B., Preston, B., Ravindranath, N.H., Reisinger, A., Riahi, K., Rusticucci, M., Scholes, R., Seyboth, K., Sokona, Y., Stavins, R., Stocker, T.F., Tschakert, P., van Vuuren, D., van Ypersele, J.-P., 2014. Climate change 2014 synthesis report. contribution of working groups I, II, and III to the fifth assessment report of the Intergovernmental Panel on Climate Change. IPCC.

PaiMazumder, D., Sushama, L., Laprise, R., Khaliq, M.N., Sauchyn, D., 2013. Canadian RCM projected changes to short- and long-term drought characteristics over the Canadian Prairies. Int. J. Climatol. 33, 1409–1423. https://doi.org/10.1002/joc.3521

Palmer, W.C., 1968. Keeping track of crop moisture conditions, nationwide: The new crop moisture index. Weatherwise 21, 156–161. https://doi.org/10.1080/00431672.1968.9932814

Palmer, W.C., 1965. Meteorological Drought, Washington, DC: US Department of Commerce, Weather Bureau.

Panda, D.K., Kumar, A., 2014. The changing characteristics of monsoon rainfall in India during 1971-2005 and links with large scale circulation. Int. J. Climatol. 34, 3881–3899. https://doi.org/10.1002/joc.3948

Pedron, I.T., Silva Dias, M.A.F., de Paula Dias, S., Carvalho, L.M. V., Freitas, E.D., 2016. Trends and variability in extremes of precipitation in Curitiba - Southern Brazil. Int. J. Climatol. https://doi.org/10.1002/joc.4773

Petris, G., 2010. An R Package for Dynamic Linear Models. J. Stat. Softw. 36, 1–16. https://doi.org/10.1007/BF02887432

Petris, G., Petrone, S., Campagnoli, P., 2013. Dynamic Linear Models with R. Springer-Verlag. https://doi.org/10.1111/j.1751-5823.2010.00109_26.x

Pettitt, A.N., 1979. A Non-Parametric Approach to the Change-Point Problem. Appl. Stat. 28, 126. https://doi.org/10.2307/2346729

Philippon, N., Camberlin, P., Moron, V., Boyard-Micheau, J., 2015. Anomalously wet and dry rainy seasons in Equatorial East Africa and associated differences in intra-seasonal characteristics. Clim. Dyn. 45, 2101–2121. https://doi.org/10.1007/s00382-014-2460-6

Plummer, D.A., Caya, D., Frigon, A., Côté, H., Giguère, M., Paquin, D., Biner, S., Harvey, R., De Elia, R., 2006. Climate and climate change over North America as simulated by the Canadian RCM. J. Clim. 19, 3112–3132. https://doi.org/10.1175/JCLI3769.1

Polade, S.D., Pierce, D.W., Cayan, D.R., Gershunov, A., Dettinger, M.D., 2014. The key role of dry days in changing regional climate and precipitation regimes. Sci. Rep. 4, 4364. https://doi.org/10.1038/srep04364

Prokoph, A., Adamowski, J., Adamowski, K., 2012. Influence of the 11 year solar cycle on annual streamflow maxima in Southern Canada. J. Hydrol. 442–443, 55–62. https://doi.org/10.1016/j.jhydrol.2012.03.038

Quiring, S.M., Papakryiakou, T.N., 2003. An evaluation of agricultural drought indices for the Canadian prairies. Agric. For. Meteorol. 118, 49–62. https://doi.org/10.1016/S0168-1923(03)00072-8

Rajagopalan, B., Cook, E., Lall, U., Ray, B.K., 2000. Spatiotemporal variability of ENSO and SST teleconnections to summer drought over the United States during the twentieth century. J. Clim. 13, 4244–4255. https://doi.org/10.1175/1520-0442(2000)013<4244:SVOEAS>2.0.CO;2

Rapaić, M., Brown, R., Markovic, M., Chaumont, D., 2015. An Evaluation of Temperature and Precipitation Surface-Based and Reanalysis Datasets for the Canadian Arctic, 1950-2010. Atmos. - Ocean 53, 283–303. https://doi.org/10.1080/07055900.2015.1045825

Rasmussen, E.N., Blanchard, D.O., 1998. A Baseline Climatology of Sounding-Derived Supercell and Tornado Forecast Parameters. Weather Forecast. 13, 1148–1164. https://doi.org/10.1175/1520-0434(1998)013<1148:ABCOSD>2.0.CO;2

Rasmusson, E.M., Wallace, J.M., 1983. Meteorological aspects of the El Nino/southern oscillation. Science 222, 1195–202. https://doi.org/10.1126/science.222.4629.1195

Raymond, F., Drobinski, P., Ullmann, A., Camberlin, P., 2018. Extreme dry spells over the Mediterranean Basin during the wet season: Assessment of HyMeX/Med-CORDEX regional climate simulations (1979-2009). Int. J. Climatol. https://doi.org/10.1002/joc.5487

Requena, A.I., Mediero, L., Garrote, L., 2013. A bivariate return period based on copulas for hydrologic dam design: Accounting for reservoir routing in risk estimation. Hydrol. Earth Syst. Sci. 17, 3023–3038. https://doi.org/10.5194/hess-17-3023-2013

Riemann-Campe, K., Fraedrich, K., Lunkeit, F., 2009. Global climatology of Convective Available Potential Energy (CAPE) and Convective Inhibition (CIN) in ERA-40 reanalysis. Atmos. Res. 93, 534–545. https://doi.org/10.1016/j.atmosres.2008.09.037

Roque-Malo, S., Kumar, P., 2017. Patterns of change in high frequency precipitation variability over North America. Sci. Rep. 7, 10853. https://doi.org/10.1038/s41598-017-10827-8

Sadri, S., Burn, D.H., 2014. Copula-based pooled frequency analysis of droughts in the Canadian Prairies. J. Hydrol. Eng. 19, 277–289. https://doi.org/10.1061/(ASCE)HE.1943-5584.0000603

Santos, J.F., Portela, M.M., Pulido-Calvo, I., 2011. Regional Frequency Analysis of Droughts in Portugal. Water Resour. Manag. 25, 3537–3558. https://doi.org/10.1007/s11269-011-9869-z

Santos, J.F., Pulido-Calvo, I., Portela, M.M., 2010. Spatial and temporal variability of droughts in Portugal. Water Resour. Res. 46, n/a-n/a. https://doi.org/10.1029/2009WR008071

Sarojini, B.B., Stott, P.A., Black, E., 2016. Detection and attribution of human influence on regional precipitation. Nat. Clim. Chang. https://doi.org/10.1038/NCLIMATE2976

Seeley, J.T., Romps, D.M., 2015. Why does tropical convective available potential energy (CAPE) increase with warming? Geophys. Res. Lett. 42, 10429–10437. https://doi.org/10.1002/2015GL066199

Sen, P.K., 1968. Estimates of the Regression Coefficient Based on Kendall's Tau. J. Am. Stat. Assoc. 63, 1379–1389. https://doi.org/10.2307/2285891

Shabbar, A., Bonsal, B., Khandekar, M., 1997. Canadian precipitation patterns associated with the Southern Oscillation. J. Clim. 10, 3016–3027. https://doi.org/10.1175/1520-0442(1997)010<3016:CPPAWT>2.0.CO;2

Shabbar, A., Skinner, W., 2004. Summer drought patterns in Canada and the relationship to global sea surface temperatures. J. Clim. 17, 2866–2880. https://doi.org/10.1175/1520-0442(2004)017<2866:SDPICA>2.0.CO;2

Shadmani, M., Marofi, S., Roknian, M., 2011. Trend Analysis in Reference Evapotranspiration Using Mann-Kendall and Spearman's Rho Tests in Arid Regions of Iran. Water Resour. Manag. 26, 211–224. https://doi.org/10.1007/s11269-011-9913-z

Sheffield, J., Camargo, S.J., Fu, R., Hu, Q., Jiang, X., Johnson, N., Karnauskas, K.B., Kim, S.T., Kinter, J., Kumar, S., Langenbrunner, B., Maloney, E., Mariotti, A., Meyerson, J.E., Neelin, J.D., Nigam, S., Pan, Z., Ruiz-Barradas, A., Seager, R., Serra, Y.L., Sun, D.-Z., Wang, C., Xie, S.-P., Yu, J.-Y., Zhang, T., Zhao, M., Sheffield, J., Camargo, S.J., Fu, R., Hu, Q., Jiang, X., Johnson, N., Karnauskas, K.B., Kim, S.T., Kinter, J., Kumar, S., Langenbrunner, B., Maloney, E., Mariotti, A., Meyerson, J.E., Neelin, J.D., Nigam, S., Pan, Z., Ruiz-Barradas, A., Seager, R., Serra, Y.L., Sun, D.-Z., Wang, C., Xie, S.-P., Yu, J.-Y., Zhang, T., Zhao, M., 2013. North American climate in CMIP5 experiments. Part II: Evaluation of historical simulations of intraseasonal to decadal variability. J. Clim. 26, 9247–9290. https://doi.org/10.1175/JCLI-D-12-00593.1

Shephard, M.W., Mekis, E., Morris, R.J., Feng, Y., Zhang, X., Kilcup, K., Fleetwood, R., 2014. Trends in canadian short-duration extreme rainfall: Including an intensity-duration-frequency perspective. Atmos. - Ocean 52, 398–417. https://doi.org/10.1080/07055900.2014.969677

Simonovic, S.P., Schardong, A., Sandink, D., 2016. Mapping Extreme Rainfall Statistics for Canada under Climate Change Using Updated Intensity-Duration-Frequency Curves. J. Water Resour. Plan. Manag. 04016078. https://doi.org/10.1061/(ASCE)WR.1943-5452.0000725

Singh, D., Tsiang, M., Rajaratnam, B., Diffenbaugh, N.S., 2014. Observed changes in extreme wet and dry spells during the South Asian summer monsoon season. Nat. Clim. Chang. 4, 456–461. https://doi.org/10.1038/nclimate2208

Singh, N., Ranade, A., 2010. The Wet and Dry Spells across India during 1951–2007. J. Hydrometeorol. 11, 26–45. https://doi.org/10.1175/2009JHM1161.1

Song, X., Song, S., Sun, W., Mu, X., Wang, S., Li, J., Li, Y., 2015. Recent changes in extreme precipitation and drought over the Songhua River Basin, China, during 1960-2013. Atmos. Res. 157, 137–152. https://doi.org/10.1016/j.atmosres.2015.01.022

Spearman, C., 1904. The Proof and Measurement of Association between Two Things. Am. J. Psychol. 15, 72–101. https://doi.org/10.2307/1412159

Spinoni, J., Naumann, G., Carrao, H., Barbosa, P., Vogt, J., 2014. World drought frequency, duration, and severity for 1951-2010. Int. J. Climatol. 34, 2792–2804. https://doi.org/10.1002/joc.3875

St. George, S., 2007. Streamflow in the Winnipeg River basin, Canada: Trends, extremes and climate linkages. J. Hydrol. 332, 396–411. https://doi.org/10.1016/j.jhydrol.2006.07.014

Stott, P.A., Allen, M., Christidis, N., Dole, R., Hoerling, M., Huntingford, C., Pall, P., Perlwitz, J., Stone, D., 2013. Attribution of weather and climate-related events, in: Climate Science for Serving Society. Springer Netherlands. Springer Netherlands, Dordrecht, pp. 307–337. https://doi.org/10.1007/978-94-007-6692-1

Sushama, L., Khaliq, N., Laprise, R., 2010. Dry spell characteristics over Canada in a changing climate as simulated by the Canadian RCM. Glob. Planet. Change 74, 1–14. https://doi.org/10.1016/j.gloplacha.2010.07.004

Swain, S., Hayhoe, K., 2015. CMIP5 projected changes in spring and summer drought and wet conditions over North America. Clim. Dyn. 44, 2737–2750. https://doi.org/10.1007/s00382-014-2255-9

Szeto, K., Zhang, X., White, R.E., Brimelow, J., 2016. The 2015 extreme drought in western Canada. Bull. Am. Meteorol. Soc. 97, S42–S46. https://doi.org/10.1175/BAMS-D-16-0147.1

Tan, X., Chen, S., Gan, T.Y., Liu, B., Chen, X., 2019. Dynamic and thermodynamic changes conducive to the increased occurrence of extreme spring fire weather over western Canada under possible anthropogenic climate change. Agric. For. Meteorol. 265, 269–279. https://doi.org/10.1016/j.agrformet.2018.11.026

Tan, X., Gan, T.Y., 2017. Non-stationary analysis of the frequency and intensity of heavy precipitation over Canada and their relations to large-scale climate patterns. Clim. Dyn. 1–19. https://doi.org/10.1007/s00382-016-3246-9

Tan, X., Gan, T.Y., 2015. Nonstationary analysis of annual maximum streamflow of Canada. J. Clim. 28, 1788–1805. https://doi.org/10.1175/JCLI-D-14-00538.1

Tan, X., Gan, T.Y., Chen, S., Liu, B., 2018a. Modeling distributional changes in winter precipitation of Canada using Bayesian spatiotemporal quantile regression subjected to different teleconnections. Clim. Dyn. 1–20. https://doi.org/10.1007/s00382-018-4241-0

Tan, X., Gan, T.Y., Chen, Y.D., 2018b. Moisture sources and pathways associated with the spatial variability of seasonal extreme precipitation over Canada. Clim. Dyn. 50, 629–640. https://doi.org/10.1007/s00382-017-3630-0

Tan, X., Gan, T.Y., Chen, Y.D., 2018c. Synoptic moisture pathways associated with mean and extreme precipitation over Canada for summer and fall. Clim. Dyn. 1–21. https://doi.org/10.1007/s00382-018-4300-6

Tan, X., Gan, T.Y., Horton, D.E., 2018d. Projected timing of perceivable changes in climate extremes for terrestrial and marine ecosystems. Glob. Chang. Biol. https://doi.org/10.1111/gcb.14329

Tan, X., Gan, T.Y., Shao, D., 2017. Effects of persistence and large-scale climate anomalies on trends and change points in extreme precipitation of Canada. J. Hydrol. https://doi.org/10.1016/j.jhydrol.2017.05.028

Tan, X., Gan, T.Y., Shao, D., 2016. Wavelet analysis of precipitation extremes over Canadian ecoregions and teleconnections to large-scale climate anomalies. J. Geophys. Res. Atmos. https://doi.org/10.1002/2016JD025533

Tandon, N.F., Zhang, X., Sobel, A.H., 2018. Understanding the dynamics of future changes in extreme precipitation intensity. Geophys. Res. Lett. 45, 2870–2878. https://doi.org/10.1002/2017GL076361

Tebaldi, C., Hayhoe, K., Arblaster, J.M., Meehl, G.A., 2006. Going to the extremes: An intercomparison of model-simulated historical and future changes in extreme events. Clim. Change 79, 185–211. https://doi.org/10.1007/s10584-006-9051-4

Theil, H., 1992. A rank-invariant method of linear and polynomial regression analysis. Springer, Dordrecht, pp. 345–381. https://doi.org/10.1007/978-94-011-2546-8_20

Theobald, A., Mcgowan, H., Speirs, J., 2018. Teleconnection influence of precipitation-bearing synoptic types over the Snowy Mountains region of south-east Australia. Int. J. Climatol. 38, 2743–2759. https://doi.org/10.1002/joc.5457

Torrence, C., Compo, G.P., 1998. A Practical Guide to Wavelet Analysis. Bull. Am. Meteorol. Soc. 79, 61–78. https://doi.org/10.1175/1520-0477(1998)079<0061:APGTWA>2.0.CO;2

Tramblay, Y., Hertig, E., 2018. Modelling extreme dry spells in the Mediterranean region in connection with atmospheric circulation. Atmos. Res. 202, 40–48. https://doi.org/10.1016/j.atmosres.2017.11.015

Trenberth, K.E., Dai, A., Van Der Schrier, G., Jones, P.D., Barichivich, J., Briffa, K.R., Sheffield, J., 2014. Global warming and changes in drought. Nat. Clim. Chang. 4, 17–22. https://doi.org/10.1038/nclimate2067

Tsakiris, G., Pangalou, D., Vangelis, H., 2007. Regional Drought Assessment Based on the Reconnaissance Drought Index (RDI). Water Resour. Manag. 21, 821–833. https://doi.org/10.1007/s11269-006-9105-4

Utsumi, N., Seto, S., Kanae, S., Maeda, E.E., Oki, T., 2011. Does higher surface temperature intensify extreme precipitation? Geophys. Res. Lett. 38, n/a-n/a. https://doi.org/10.1029/2011GL048426

Van Der Schrier, G., Barichivich, J., Briffa, K.R., Jones, P.D., 2013. A scPDSI-based global data set of dry and wet spells for 1901-2009. J. Geophys. Res. Atmos. 118, 4025–4048. https://doi.org/10.1002/jgrd.50355

Ventura, V., Paciorek, C.J., Risbey, J.S., 2004. Controlling the Proportion of Falsely Rejected Hypotheses when Conducting Multiple Tests with Climatological Data. J. Clim. 17, 4343–4356. https://doi.org/10.1175/3199.1

Vicente-Serrano, S.M., Beguería, S., López-Moreno, J.I., 2010. A multiscalar drought index sensitive to global warming: The standardized precipitation evapotranspiration index. J. Clim. 23, 1696–1718. https://doi.org/10.1175/2009JCLI2909.1

Vincent, L. a., Mekis, É., 2006. Changes in Daily and Extreme Temperature and Precipitation Indices for Canada over the Twentieth Century. Atmosphere-Ocean 44, 177–193. https://doi.org/10.3137/ao.440205

Vincent, L.A., Milewska, E.J., 2007. Examination of potential biases in radiosonde temperature and humidity records in Canada, in: 14th Symposium on Meteorological Observation and Instrumentation. San Antonio, Texas.

Vincent, L.A., Zhang, X., Brown, R.D., Feng, Y., Mekis, E., Milewska, E.J., Wan, H., Wang, X.L., 2015. Observed trends in Canada's climate and influence of low-frequency variability modes. J. Clim. 28, 4545–4560. https://doi.org/10.1175/JCLI-D-14-00697.1

Vincent, L.A., Zhang, X., Mekis, E., Wan, H., Bush, E.J., 2018. Changes in Canada's climate: Trends in indices based on daily temperature and precipitation data. Atmosphere-Ocean 1–18. https://doi.org/10.1080/07055900.2018.1514579

Vinnarasi, R., Dhanya, C.T., 2016. Changing characteristics of extreme wet and dry spells of Indian monsoon rainfall. J. Geophys. Res. 121, 2146–2160. https://doi.org/10.1002/2015JD024310

Wang, B., Zhang, M., Wei, J., Wang, S., Li, S., Ma, Q., Li, X., Pan, S., 2013. Changes in extreme events of temperature and precipitation over Xinjiang, northwest China, during 1960–2009. Quat. Int. 298, 141–151. https://doi.org/10.1016/j.quaint.2012.09.010

Wang, J., Zhang, L., 2008. Systematic errors in global radiosonde precipitable water data from comparisons with groud-based GPS measurements. J. Clim. 21, 2218–2238. https://doi.org/10.1175/2007JCLI1944.1

Wang, Q., Wu, J., Lei, T., He, B., Wu, Z., Liu, M., Mo, X., Geng, G., Li, X., Zhou, H., Liu, D., 2014. Temporal-spatial characteristics of severe drought events and their impact on agriculture on a global scale. Quat. Int. 349, 10–21. https://doi.org/10.1016/j.quaint.2014.06.021

Wang, R., Chen, J., Chen, X., Wang, Y., 2017. Variability of precipitation extremes and dryness/wetness over the southeast coastal region of China, 1960-2014. Int. J. Climatol. https://doi.org/10.1002/joc.5113

Wang, X., Huang, G., Liu, J., 2014. Projected increases in intensity and frequency of rainfall extremes through a regional climate modeling approach. J. Geophys. Res. Atmos. 119, 13,271-13,286. https://doi.org/10.1002/2014JD022564

Wang, Y., McBean, E.A., Jarrett, P., 2015. Identification of changes in heavy rainfall events in Ontario, Canada. Stoch. Environ. Res. Risk Assess. 29, 1949–1962. https://doi.org/10.1007/s00477-015-1085-6

Wang, Y., Zhang, T., Chen, X., Li, J., Feng, P., 2017. Spatial and temporal characteristics of droughts in Luanhe River basin, China. Theor. Appl. Climatol. 1–17. https://doi.org/10.1007/s00704-017-2059-z

Wasko, C., Sharma, A., 2014. Quantile regression for investigating scaling of extreme precipitation with temperature. Water Resour. Res. 50, 3608–3614. https://doi.org/10.1002/2013WR015194

Wells, N., Goddard, S., Hayes, M.J., 2004. A self-calibrating Palmer Drought Severity Index. J. Clim. 17, 2335–2351. https://doi.org/10.1175/1520-0442(2004)017<2335:ASPDSI>2.0.CO;2

Wheaton, E., Kulshreshtha, S., Wittrock, V., Koshida, G., 2008. Dry times: Hard lessons from the Canadian drought of 2001 and 2002. Can. Geogr. 52, 241–262. https://doi.org/10.1111/j.1541-0064.2008.00211.x

Whitfield, P.H., Bodtker, K., Cannon, A.J., 2002. Recent variations in seasonality of temperature and precipitation in Canada, 1976-95. Int. J. Climatol. 22, 1617–1644. https://doi.org/10.1002/joc.813

Wilcox, C., Vischel, T., Panthou, G., Bodian, A., Blanchet, J., Descroix, L., Quantin, G., Cassé, C., Tanimoun, B., Kone, S., 2018. Trends in hydrological extremes in the Senegal and Niger Rivers. J. Hydrol. https://doi.org/10.1016/J.JHYDROL.2018.07.063

Wilcox, R.R., 1998. Simulations on the Theil-Sen regression estimator with right-censored data. Stat. Probab. Lett. 39, 43–47. https://doi.org/10.1016/S0167-7152(98)00022-4

Wilhite, D.A., 2000. Drought as a natural hazard: Concepts and definitions. Drought A Glob. Assess. 3–18.

Wilhite, D.A., Glantz, M.H., 1985. Understanding: the Drought Phenomenon: The Role of Definitions. Water Int. 10, 111–120. https://doi.org/10.1080/02508068508686328

Wolter, K., Timlin, M.S., 2011. El Niño/Southern Oscillation behaviour since 1871 as diagnosed in an extended multivariate ENSO index (MEI.ext). Int. J. Climatol. 31, 1074–1087. https://doi.org/10.1002/joc.2336

Wolter, K., Timlin, M.S., 1998. Measuring the strength of ENSO events: How does 1997/98 rank? Weather 53, 315–324. https://doi.org/10.1002/j.1477-8696.1998.tb06408.x

Wolter, K., Timlin, M.S., 1993. Monitoring ENSO in COADS with a seasonally adjusted principal component index, Proceedings of the 17th Climate Diagnostics Workshop,.

Wu, S., Liu, Z.-Y., Cheng, J., Li, C., 2018. Response of North Pacific and North Atlantic decadal variability to weak global warming. Adv. Clim. Chang. Res. https://doi.org/10.1016/J.ACCRE.2018.03.001

Xi, Y., Miao, C., Wu, J., Duan, Q., Lei, X., Li, H., 2018. Spatiotemporal changes in extreme temperature and precipitation events in the Three-Rivers Headwater region, China. J. Geophys. Res. Atmos. https://doi.org/10.1029/2017JD028226

Xia, Y., Mitchell, K., Ek, M., Cosgrove, B., Sheffield, J., Luo, L., Alonge, C., Wei, H., Meng, J., Livneh, B., Duan, Q., Lohmann, D., 2012. Continental-scale water and energy flux analysis and validation for North American Land Data Assimilation System project phase 2 (NLDAS-2): 2. Validation of model-simulated streamflow. J. Geophys. Res. Atmos. 117, n/a-n/a. https://doi.org/10.1029/2011JD016051

Xie, P., Chen, M., Shi, W., 2010. CPC unified gauge-based analysis of global daily precipitation, in: 24th Conference on Hydrology. Amer. Meteor. Soc, Atlanta.

Xie, P., Chen, M., Yang, S., Yatagai, A., Hayasaka, T., Fukushima, Y., Liu, C., 2007. A Gauge-Based Analysis of Daily Precipitation over East Asia. J. Hydrometeorol. 8, 607–626. https://doi.org/10.1175/JHM583.1

Yang, Y., Gan, T.Y., Tan, X., 2019. Spatiotemporal changes in precipitation extremes over Canada and their teleconnections to large-scale climate patterns. J. Hydrometeorol. 275–296. https://doi.org/10.1175/jhm-d-18-0004.1

Ye, B., Del Genio, A.D., Lo, K.K.W., 1998. CAPE variations in the current climate and in a climate change. J. Clim. 11, 1997–2015. https://doi.org/10.1175/1520-0442(1998)011<1997:CVITHCC>2.0.CO;2

Ye, H., 2018. Changes in duration of dry and wet spells associated with air temperatures in Russia. Environ. Res. Lett. https://doi.org/10.1088/1748-9326/aaae0d

Yevjevich, V., 1967. An objective approach to definitions and investigations of continental hydrologic droughts. Hydrol. Pap. (Colorado State Univ. 25. https://doi.org/10.1016/0022-1694(69)90110-3

Yu, K., Moyeed, R.A., 2001. Bayesian quantile regression. Stat. Probab. Lett. 54, 437–447. https://doi.org/10.1016/S0167-7152(01)00124-9

Yu, K., Zhang, J., 2005. A three-parameter asymmetric Laplace distribution and its extension. Commun. Stat. - Theory Methods 34, 1867–1879. https://doi.org/10.1080/03610920500199018

Yu, M., Li, Q., Hayes, M.J., Svoboda, M.D., Heim, R.R., 2014. Are droughts becoming more frequent or severe in China based on the Standardized Precipitation Evapotranspiration Index: 1951-2010? Int. J. Climatol. 34, 545–558. https://doi.org/10.1002/joc.3701

Zhai, P., Zhang, X., Wan, H., Pan, X., 2005. Trends in total precipitation and frequency of daily precipitation extremes over China. J. Clim. 18, 1096–1108. https://doi.org/10.1175/JCLI-3318.1

Zhang, D.D., Yan, D.H., Lu, F., Wang, Y.C., Feng, J., 2014. Copula-based risk assessment of drought in Yunnan province, China. Nat. Hazards 75, 2199–2220. https://doi.org/10.1007/s11069-014-1419-6

Zhang, J., Li, L., Wu, Z., Li, X., 2015. Prolonged dry spells in recent decades over north-central China and their association with a northward shift in planetary waves. Int. J. Climatol. 35, 4829–4842. https://doi.org/10.1002/joc.4337

Zhang, Q., 2012. Regional Evaluations of the Meteorological Drought Characteristics across the Pearl River Basin, China. Am. J. Clim. Chang. 01, 48–55. https://doi.org/10.4236/ajcc.2012.11005

Zhang, X., Alexander, L., Hegerl, G.C., Jones, P., Tank, A.K., Peterson, T.C., Trewin, B., Zwiers, F.W., 2011. Indices for monitoring changes in extremes based on daily temperature and precipitation data. Wiley Interdiscip. Rev. Clim. Chang. 2, 851–870. https://doi.org/10.1002/wcc.147

Zhang, X., Hogg, W.D., Mekis, É., 2001. Spatial and Temporal Characteristics of Heavy Precipitation Events over Canada. J. Clim. 14, 1923–1936. https://doi.org/10.1175/1520-0442(2001)014<1923:SATCOH>2.0.CO;2

Zhang, X., Vincent, L.A., Hogg, W.D., Niitsoo, A., 2000. Temperature and precipitation trends in Canada during the 20th century. Atmos. - Ocean 38, 395–429. https://doi.org/10.1080/07055900.2000.9649654

Zhang, X., Wang, J., Zwiers, F.W., Groisman, P.Y., 2010. The influence of large-scale climate variability on winter maximum daily precipitation over North America. J. Clim. 23, 2902–2915. https://doi.org/10.1175/2010JCLI3249.1

Zhao, H., Gao, G., An, W., Zou, X., Li, H., Hou, M., 2017. Timescale differences between SC-PDSI and SPEI for drought monitoring in China. Phys. Chem. Earth 102, 48–58. https://doi.org/10.1016/j.pce.2015.10.022

Zhou, X., Huang, G., Wang, X., Cheng, G., 2018. Future changes in precipitation extremes over Canada: driving factors and inherent mechanism. J. Geophys. Res. Atmos. 123, 5783–5803. https://doi.org/10.1029/2017JD027735

Zhu, J., Zhou, L., Huang, S., 2018. A hybrid drought index combining meteorological, hydrological, and agricultural information based on the entropy weight theory. Arab. J. Geosci. 11, 91. https://doi.org/10.1007/s12517-018-3438-1

Zilli, M.T., Carvalho, L.M. V., Liebmann, B., Silva Dias, M.A., 2017. A comprehensive analysis of trends in extreme precipitation over southeastern coast of Brazil. Int. J. Climatol. 37, 2269–2279. https://doi.org/10.1002/joc.4840